NASA CR-54004
ER-5623

THE PERMEATION OF HYDROGEN THROUGH MATERIALS FOR THE SUNFLOWER SYSTEM

by

E. A. Steigerwald

prepared for

NATIONAL AERONAUTICS AND SPACE ADMINISTRATION
CONTRACT NAS 5-462

TRW ELECTROMECHANICAL DIVISION
THOMPSON RAMO WOOLDRIDGE INC.
23555 EUCLID AVENUE ■ CLEVELAND, OHIO 44117

A

NASA CR-54004
ER-5623

FINAL REPORT

THE PERMEATION OF HYDROGEN THROUGH MATERIALS FOR THE SUNFLOWER SYSTEM

by

E. A. Steigerwald

prepared for

NATIONAL AERONAUTICS AND SPACE ADMINISTRATION

November 15, 1963

CONTRACT NAS 5-462

Technical Management
NASA Lewis Research Center
Cleveland, Ohio
Solar & Chemical Power Branch
J. A. Heller

TRW ELECTROMECHANICAL DIVISION
THOMPSON RAMO WOOLDRIDGE INC.
CLEVELAND, OHIO 44117

FOREWORD

This final report describes the results of a program designed to evaluate hydrogen permeability through constructional materials which have particular applicability to the Sunflower program. The investigation extended over the period 1 February 1961 to 30 October 1963 and was funded by NASA under Contract 5-462. During the course of the program the following technical reports which covered distinct phases of the work were published:

The Permeation of Hydrogen through Metals and Metal -Plus-Oxide Systems, TM 2865-67, March 31, 1961.

The Permeation of Hydrogen through Constructional Materials, ER-4776, June, 1962.

Applicability of Solaramic Coating as a Barrier to Hydrogen Permeation, TM 3404-67, April 30, 1962.

The Permeation of Hydrogen through Metallic Coatings, TM 3591-67, February 28, 1963.

The pertinent data previously presented in these reports are combined in this final report with the more recent permeability results to provide an integrated and consistent description of the overall program accomplishments.

ABSTRACT

23206

The permeability of hydrogen was studied in uncoated metals, metals coated with metallic coatings, metals coated with oxide coatings and metals coated with glasses. Particular emphasis was placed on conditions of time and temperature (1200 to 1600°F) which approximated the environment present in the Sunflower system.

Tungsten possessed the lowest permeability to hydrogen of any material evaluated. Metallic coatings which formed intermetallic coatings with the base metal were also effective hydrogen barriers. In the metal coated systems evaluated, a tungsten-silicon coating on a Haynes 25 base metal exhibited the lowest permeability. At the higher temperature, however, there was a general tendency for the intermetallic coatings to deteriorate as a result of gross diffusion into the base metal.

Oxide coatings produced, in situ, on the stainless steel or Haynes 25 base metal were effective hydrogen barriers at the lower temperatures but the barrier properties deteriorated at the higher temperatures due to chemical reduction of the oxide by the hydrogen.

Glass coatings had very low permeability to hydrogen, however, many of these barriers were susceptible to spalling. A Solaramic glass coating possessed the best overall properties of any coating tested on the basis of hydrogen permeability, ease of application, and long-time stability.

TABLE OF CONTENTS

LIST OF ILLUSTRATIONS

LIST OF ILLUSTRATIONS (Continued)

LIST OF ILLUSTRATIONS (Continued)

LIST OF TABLES

I INTRODUCTION

The permeability of hydrogen through constructional materials represents a critical design consideration in certain solar-powered systems such as Sunflower. The essential design features of these systems incorporate a heat storage medium such as lithium hydride to provide adequate heat availability from the sun to the shade cycle. Under the normal operating conditions (1200 to 1600°F), the lithium hydride has a strong tendency to dissociate. If the hydrogen generated by this disassociation diffuses through the container into space at a sufficiently rapid rate, an extensive conversion of the hydride to lithium occurs with an attendant loss in the efficiency of the power generating system. In addition to the loss into space, the hydrogen can also penetrate into the turbine and produce pump malfunction. The control of hydrogen permeation, therefore, represents a necessary condition for the effective utilization of the Sunflower system.

Although the permeability of gases through metals has been the subject of frequent investigations, there are still many questions and anomolies which exist in studying this phenomenon. In particular, the development of barriers to hydrogen flow generally involves the use of oxide or glass coatings to impede permeability (1)*. Under these conditions the problem of the chemical and mechanical stability of the coating significantly effects the results and no general rules are available to aid in the selection of materials for hydrogen containment.

The purpose of this program was to study the permeation of hydrogen through various metals and metal-plus-coating systems with particular reference to the materials which have possible application in Sunflower. Specific attempts were made to develop suitable hydrogen barriers by selected coating techniques. In certain cases attempts were also made to measure the chemical and mechanical stability of coatings by limited thermal cycling.

*Numbers in parentheses pertain to references in the Bibliography.

II APPARATUS AND PROCEDURE

The hydrogen permeability was measured with a modified Sieverts apparatus which is shown in Figures 1 and 2. In essence,the equipment consisted of a system to introduce relatively-pure hydrogen against a specimen diaphragm at a known pressure and temperature; and a system to measure the rate of hydrogen flow through the diaphragm.

The inlet section consisted of tank hydrogen which was purified by passing it through deoxo and drierite units and a titanium-filled getter furnace operating at approximately 1200°F. A gas burette and a mercury manometer were also employed on the inlet side for ballast and a method of measuring the inlet pressure. The measuring system was composed of a Toepler pump, which forced the permeating hydrogen into a suitably calibrated volume. The pressure rise on the outlet side was manually determined at periodic time intervals with a McLeod guage to obtain the desired permeability parameter.

With the exception of the tests involving the refractory metals, the test specimens, shown in Figure 3, consisted of a center chamber which contained a diaphragm of the material to be evaluated. The advantages of this particular specimen geometry have been previously described (2). In the majority of cases, this diaphragm was integrally machined from a suitable bar of the selected material, however, in certain cases where material in sheet form was to be tested, the diaphragm was TIG welded into a 304 stainless steel chamber. No significant difference in permeability was observed as a function of specimen type. End-caps with 1/2 inch diameter stainless steel tubes were welded to the center chamber and the whole assembly was mounted in the resistance-heated furnace through high-vacuum water-cooled seals. The furnace used to heat the test specimens was automatically controlled and maintained the desired temperature to within $\pm$ 5°F. During a given test,the temperature was continually monitored by a chromel-alumel thermocouple attached at the mid-point of the chamber.

In the case of tests conducted with the refractory metals such as tungsten, columbium and molybdenum which could not be easily incorporated into a specimen chamber by welding end caps to a diaphragm, a tube type specimen was employed. The exact tube geometry is shown in Figure 4. The disadvantage of this method is that the temperature is not constant along the entire tube length and a knowledge of the temperature gradient, coupled with an appropriate analytical technique, must be employed to determine the permeability. The temperature distribution along the tube specimen was determined in a separate test run which was conducted prior to the actual permeability test. The permeability was determined from the slope of the steady state pressure-time curve. Representative permeability calculations for both the diaphragm and tube specimens are presented in Appendices I and II.

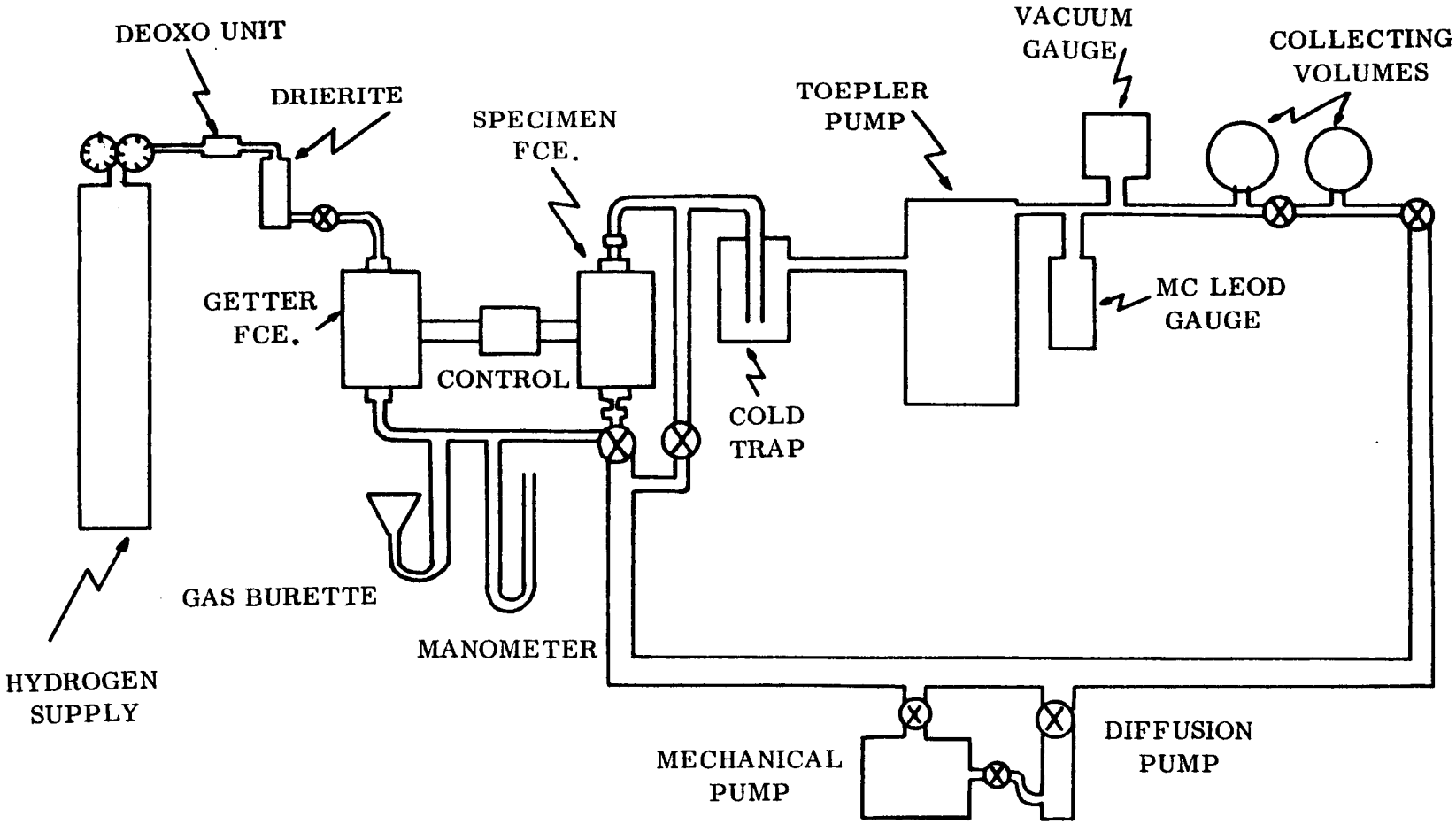

FIGURE 1

APPARATUS FOR STUDYING PERMEATION OF HYDROGEN THROUGH MATERIALS

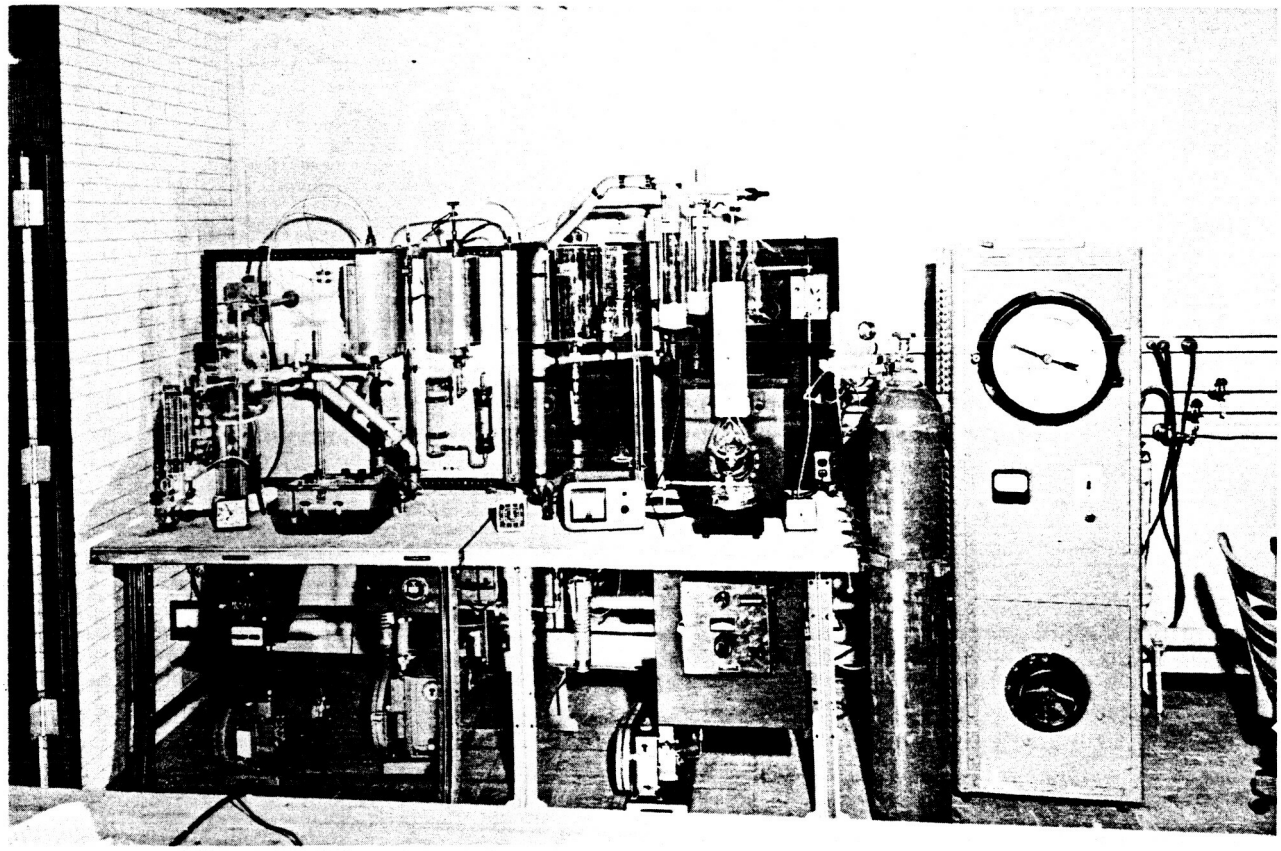

FIGURE 2

PICTURE OF TWO SIEVERTS TYPE STATIONS TO MEASURE HYDROGEN PERMEABILITY

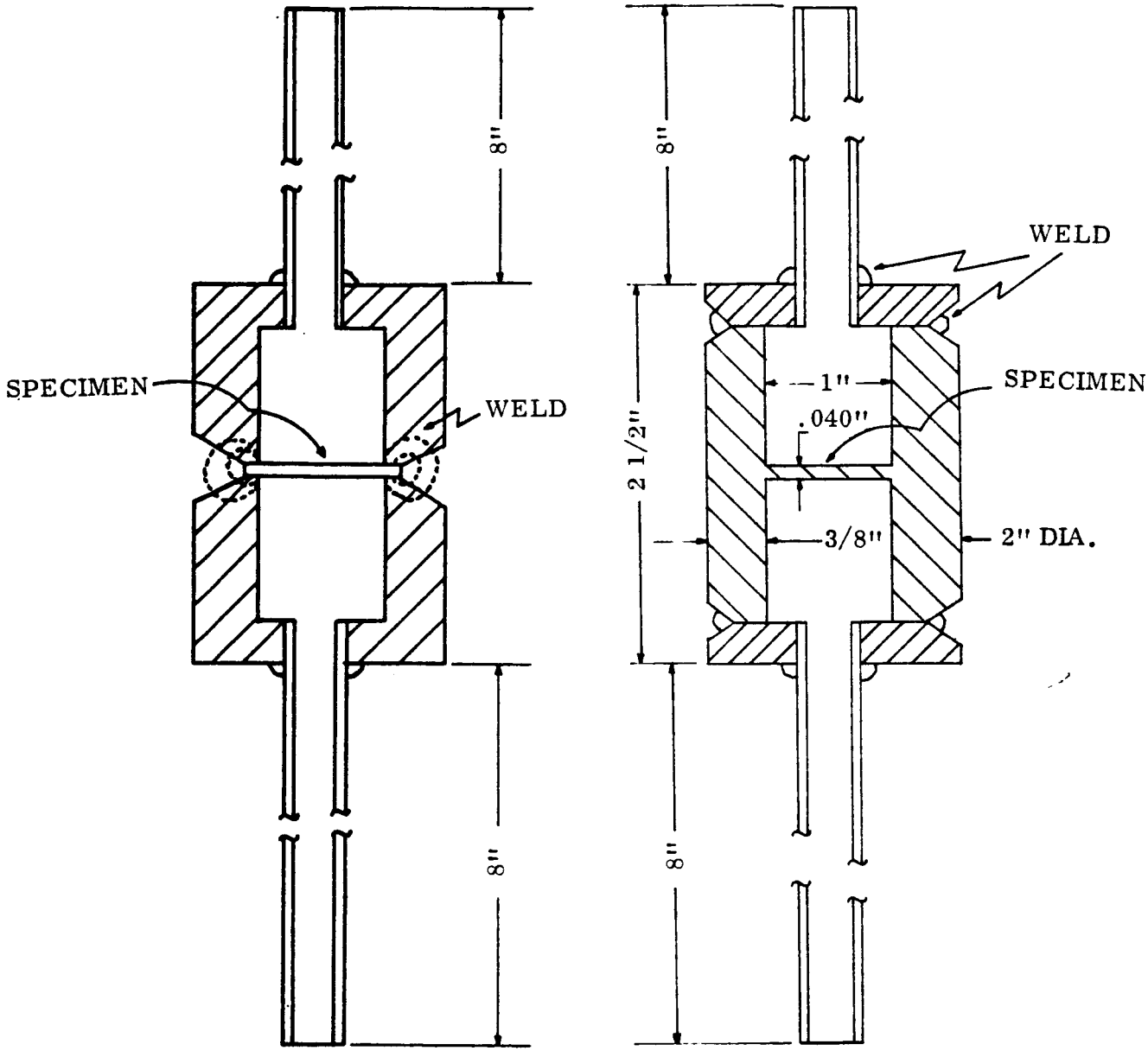

WELDED SPECIMEN INTEGRALLY-MACHINED SPECIMEN

FIGURE 3

GEOMETRY OF TEST SPECIMEN CHAMBERS

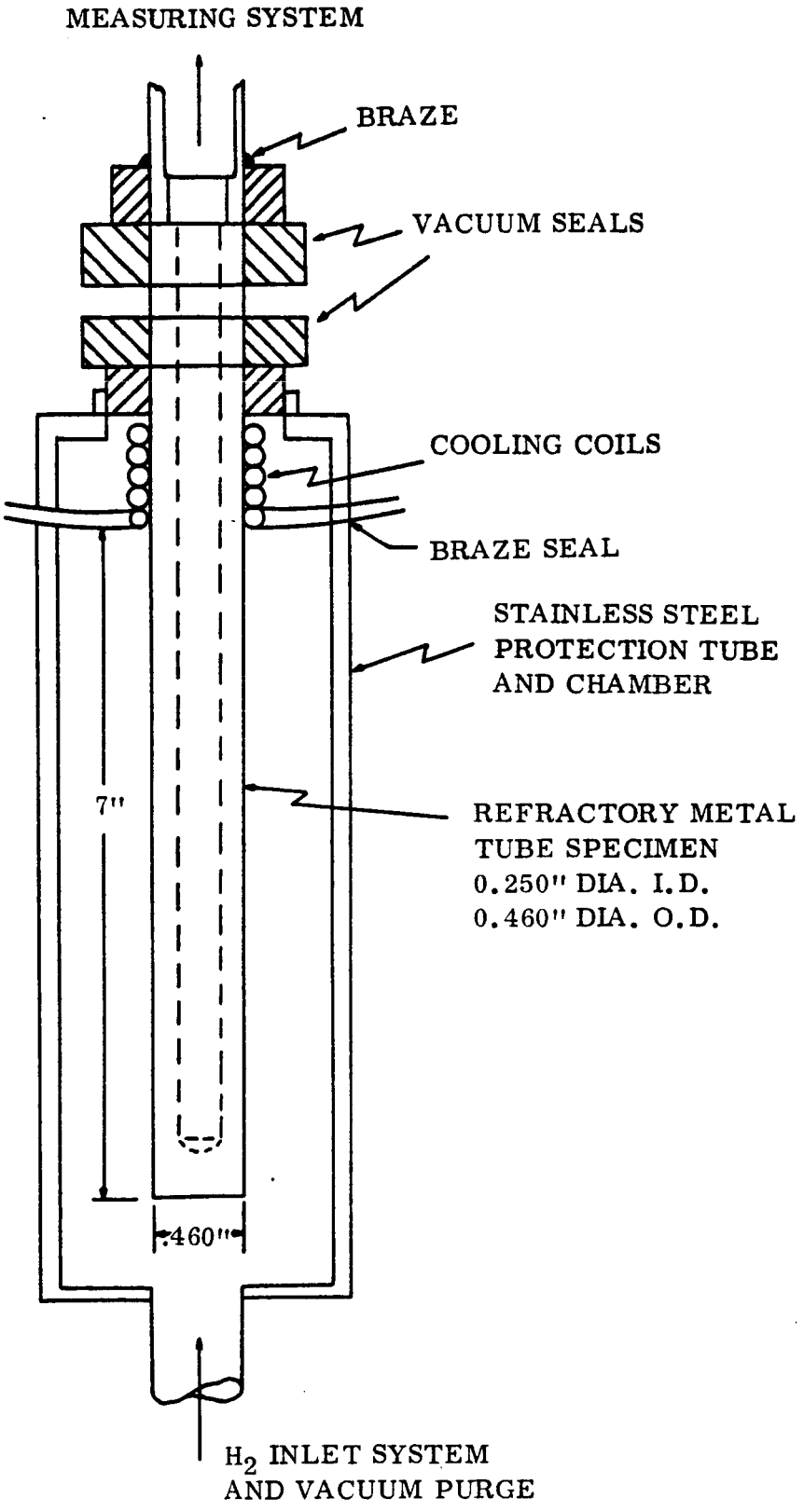

FIGURE 4

SPECIMEN AND EXPERIMENTAL SET-UP USED
TO TEST REFRACTORY METALS

After the specimen was mounted in the furnace, the experimental procedure consisted of evacuating the entire system to approximately 5×10^{-6} mm of mercury by means of the oil diffusion pump. The specimen furnace was set at 1600°F and the system was outgassed for 24 to 72 hours. The vacuum pumps were disconnected from the system and the "leak rate" was measured over a several hour period. When this "leak rate" was sufficiently low, hydrogen was introduced into the inlet side of the specimen chamber and the pressure rise on the outlet side was measured as a function of time. Although the majority of tests were conducted with an inlet pressure of one atmosphere, the pressure was systematically varied in selected materials from one-quarter to one atmosphere.

The hydrogen permeability* was measured at several temperatures and the data in this report are presented in an Arrhenius type plot which charts the logarithm of the permeability as a function of the reciprocal of the absolute temperature. Since the permeability can usually be expressed as:

$$P = P_o e^{-A/T}$$

where:

P is the permeability cm^3 of H_2 (S. T. P.)-mm/hr-cm^2-$atm^{1/2}$ at a pressure of one atmosphere on the inlet side and zero pressure on the outlet side.

T is the absolute temperature (°K) and,

Po and A are material constants.

The presentation of the data in this manner produces a linear relation between the permeability and temperature variables and simplifies necessary calculations or extrapolations.

---

*The permeability is the hydrogen flux under standard conditions, normalized in terms of unit area (cm^2) and thickness (mm) of the specimen and at a pressure of one atmosphere on the inlet side and zero atmosphere on the outlet side. When surface reactions are not rate controlling, the permeability represents the product of the diffusivity and the solubility of the gas in the metal.

III TEST MATERIALS

For purposes of discussion the test program can be classified as:

1) Tests on Uncoated Metals and Alloys, and

2) Tests on Coated Materials,

   a) metallic coatings,

   b) oxide coatings, and

   c) glass coatings.

The selection of uncoated metals for permeability studies was based on their ability to serve as structural materials in various Sunflower components. The composition of the metals is presented in Table I. The 300 series stainless steels were chosen as typical iron-base austenitic alloys while the Haynes No. 25 was selected as a respresentative cobalt-base, high-temperature material. The Croloy 9M, which is a ferritic iron-base alloy, was evaluated because of its potential applicability as a boiler tube material.

Three refractory metals--columbium, molybdenum, and tungsten--were tested for hydrogen permeability. At temperatures in the 1600°F range, molybdenum has an extremely-low permeability to hydrogen (3, 4) relative to other metals. Although no data are available concerning the flow of hydrogen through 100 percent dense tungsten, its similarity to molybdenum (VIA Group) suggests that it would also have a low permeability. Columbium, unlike the refractory metals in VIA Group of the periodic table, has an extremely high permeability to hydrogen above 1000°F. It was included in the program because of its possible application as a hydrogen "window" material in the mercury section of Sunflower. The columbium and tungsten specimens were generated by gun drilling blind holes into the bar stock while the molybdenum specimen was produced by electron beam welding a plug into one end of a tube.

The permeability of hydrogen through various metallic, metal oxide, and glass coatings was evaluated by applying the coatings to the austenitic stainless steel or Haynes Alloy No. 25 base metal. When a significant interaction appeared to be present between the base metal and the surface coating, more than one base metal was employed. In all cases, the coating was applied to the entire inside surface of the chamber and diaphragm to eliminate any significant flow through the chamber walls rather than the diaphragm (short-circuiting effects). The problem of defining a quantitative permeability parameter for composite systems such as coatings on metals has been previously discussed (5). The general results presented in this

TABLE I

NOMINAL COMPOSITIONS OF UNCOATED METALS USED IN THE HYDROGEN PERMEABILITY STUDIES

(WEIGHT PERCENT)

Material	Cr	Ni	W	Co	C	S	Mn	Mo	Fe	Other
303 Stainless Steel	18	9	-	-	.08	.28	.80	-	Bal.	
304 Stainless Steel	18	9	-	-	.06	.02	1.40	-	Bal.	
Haynes Alloy No. 25	20	10	15	Bal.	.10	-	1.0	-	2.0	
Croloy 9M	9	.10	0	-	.10	.02	.05	1.0	Bal.	
Columbium	electron beam melted									Cb
Molybdenum	pressed, sintered and worked to theoretical density									Mo
Tungsten	pressed, sintered and worked to theoretical density									W

investigation were obtained on 0.040 inch-thick diaphragms which were comparable to the thickness of the Sunflower lithium hydride boiler. The coating thicknesses were chosen to be representative of optimum adherence characteristics. In most cases, the effective permeability of the coating-base metal system was calculated on the basis of the total diaphragm thickness (i.e., base metal plus coating).

The general description of the coatings that were investigated is summarized in Tables II and III while the details of the coating methods are presented in Appendix III.

TABLE II

SUMMARY OF COATING SYSTEMS EVALUATED-METAL COATINGS

Base Metal	Coating	Method of Application	Total Diaphragm Thickness (In.)	Total Coating Thickness (In.)	
304 SS	Silver	Electroplate	0.053 to 0.030	0.003	Coating only on inlet side
304 SS	Copper	Electroplate	0.024	0.003	Coating only on inlet side
303 SS	Chromium	Pack Process	0.035	0.005	Coating on both sides
304 SS	Aluminum	Pack Process	0.045	0.008	Coating on both sides
304 SS	Aluminum	Spray and Diffusion Bond	0.052	0.006	Coating only on inlet side
304 SS	Tungsten	Vapor Plate	0.041	0.006-0.00	Coating only on inlet side
304 SS	Silicon	Pack Process	0.046	0.001	Coating only on inlet side
Haynes 25	Chromium	Pack Process	0.037	0.001	Coating on both sides
Haynes 25	Aluminum	Pack Process	0.050	0.006	Coating on both sides
Haynes 25	Aluminum	Spray and Diffusion Bond	0.042	0.006	Coating only on inlet side
Haynes 25	Silicon	Pack Process	0.050	0.0015	Coating on both sides
Haynes 25	Tungsten-Silicon	Pack Process	0.046	0.0025	Coating only on inlet side
Haynes 25	Molybdenum-Silicon	Pack Process	0.047	0.002	Coating only on inlet side
Haynes 25	Zirconium-Silicon	Pack Process	0.048	0.003	Coating only on inlet side
Haynes 25	Vanadium-Silicon	Pack Process	0.045	0.001	Coating only on inlet side.

TABLE III

SUMMARY OF COATING SYSTEMS EVALUATED

Base	Coating	Method of Application	Base Metal Thickness (In.)	Total Coating Thickness (In.)
	Oxide Coatings			
Haynes 25	Oxidized in wet H_2	Wet H_2 oxidation	0.040	0.0005
303 SS	Oxidized in wet H_2	Wet H_2 oxidation	0.048	0.0005
Haynes 25	Aluminized and oxidized	Pack alum., air oxidized	0.050	0.006
304 SS	Aluminized and oxidized	Pack alum., air oxidized	0.045	0.008
	Glass Coatings			
304 SS	Coating No. 3308	A. O. Smith	0.038	0.004
304 SS	Coating No. 3308	A. O. Smith	0.040	0.025
Haynes 24	Coating No. 3308	A. O. Smith	0.040	0.040
304 SS	Coating No. 3308	A. O. Smith	0.034	0.014
304 SS	Nucerite SC-30	Pfaudler Co.	0.040	0.019
304 SS	Nucerite SC-30	Pfaudler Co.	0.040	0.022 approx.
304 SS	Nucerite RD-30	Pfaudler Co.	0.042	0.020 approx.
304 SS	Nucerite Special	Pfaudler Co.	0.042	0.020 approx.
304 SS	Bettinger-Gray	Bettinger Corporation	0.043	0.015
304 SS	Bettinger-Green	Bettinger Corporation		
304 SS	Engineered Ceramics	Engineered Ceramics Corp.	0.041	0.004
304 SS	Solaramic	Ferro Corp. and TRW	Several specimens tested in this series	
Haynes 25	Solaramic	Ferro Corp. and TRW	diaphragm thickness approx. .040", coating thickness 0.008" to 0.012".	

IV RESULTS AND DISCUSSION

A. Uncoated Metals

The permeability of hydrogen through the 303 and 304 austenitic stainless steels, Haynes Alloy No. 25, and Croloy 9M is presented in Figure 5. The Haynes 25 had a permeability to hydrogen which was slightly less than the other alloys examined. The Croloy 9M exhibited a discontinuity in permeability at approximately 1500°F, presumably due to the $\alpha \rightarrow \gamma$ transformation (6). At a comparable temperature, the close-packed austenitic structure generally provides more resistance to hydrogen passage than the body-centered cubic ferrite. Above 1500°F, the Croloy 9M in the austenitic condition had a permeability which was directly comparable to the austenitic stainless steels.

The permeability of hydrogen through the refractory metals - molybdenum, tungsten, and columbium - is presented in Figures 6 and 7. The data obtained for the molybdenum specimen (Figure 6) were slightly below that previously reported (3, 4) and correspond to a permeability of approximately 8×10^{-2} cc-mm/hr-cm^2-atm.$^{1/2}$. The permeability of tungsten to hydrogen was extremely low. Over the 1200 and 1600°F temperature range, these values which represent the lowest reported for any currently-available metal, were almost two orders of magnitude below the results obtained for molybdenum.

The flow of hydrogen through columbium tubing was evaluated with particular reference to the temperature range (600 to 900°F) where the material may be applicable as a hydrogen window or vent. The results summarized in Figure 7 indicated that a discontinuity in the permeability curve existed at approximately 1000°F. Above this temperature,the permeability was essentially equal to the produce of diffusivity and solubility. Below 1000°F,the permeability decreased very rapidly, and at 600°F it was almost three orders of magnitude below that which would be predicted from an extrapolation of the high-temperature data. These results, coupled with desorption data presented in the literature, indicate that a surface reaction is probably rate controlling at temperatures below 1000°F (7). The practical implication is that columbium will not be an effective vent material unless heated to a suitable temperature (above 1000°F) where surface reactions do not predominate.

B. Coated Metals - Metallic Coatings

To simplify presentation and analysis, the permeation of hydrogen through metallic coatings will be discussed in terms of the following categories which describe the metallurgical interactions between the coating and base metal. These interactions are significant because they directly determine the ability of the coating to serve as a barrier to hydrogen flow.

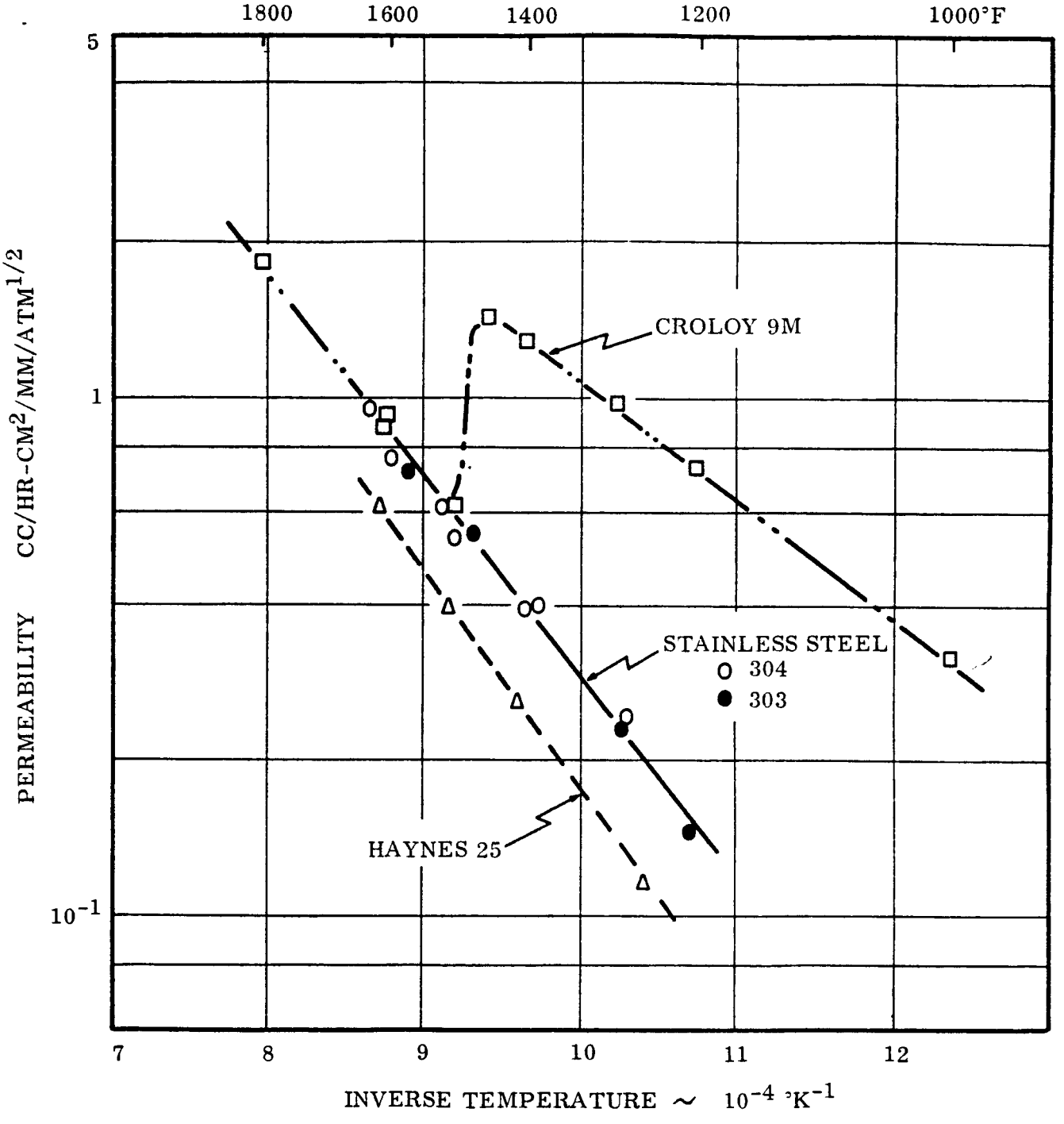

FIGURE 5

PERMEABILITY OF HYDROGEN THROUGH VARIOUS UNCOATED METALS

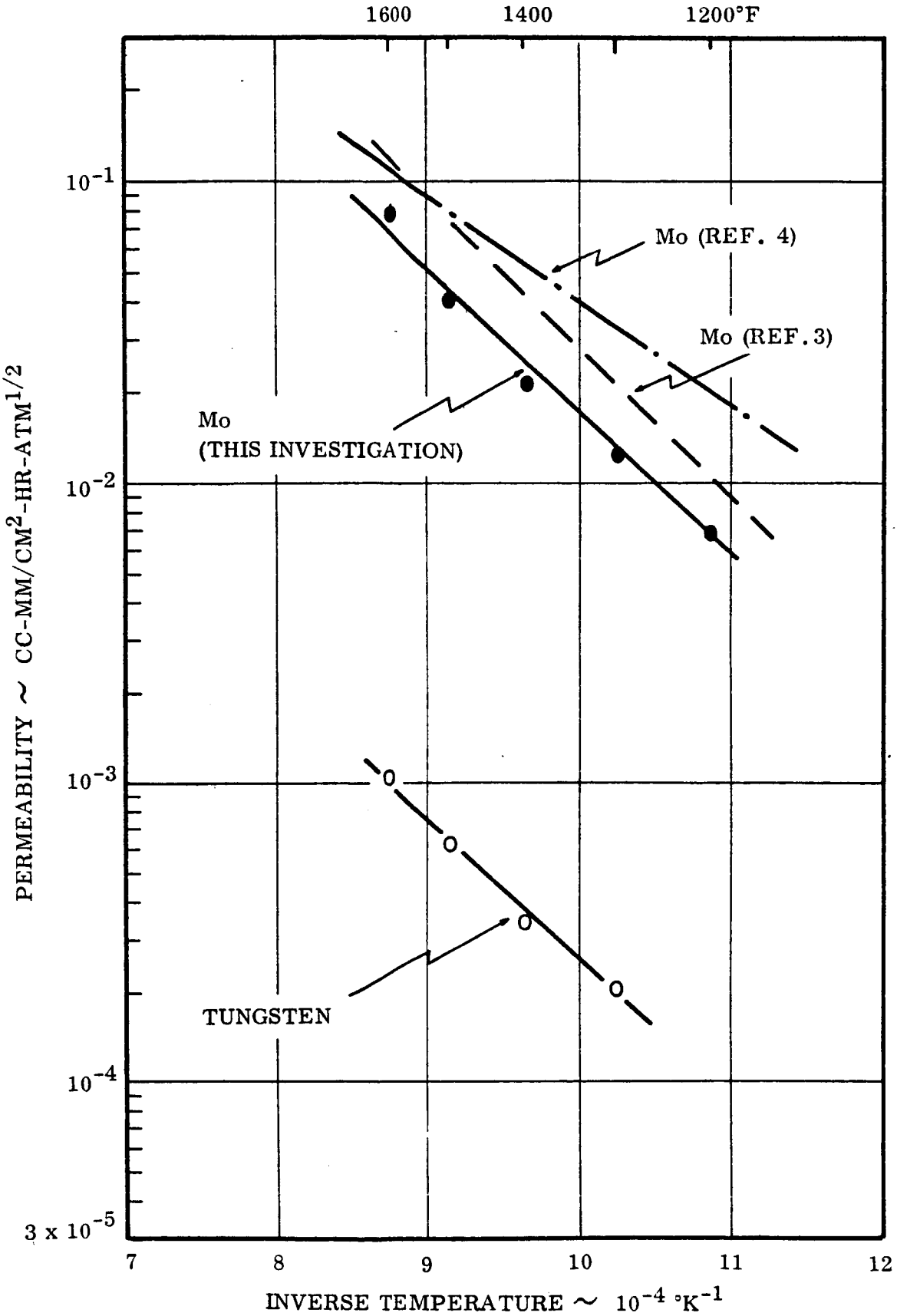

FIGURE 6

PERMEABILITY OF HYDROGEN THROUGH MOLYBDENUM AND TUNGSTEN

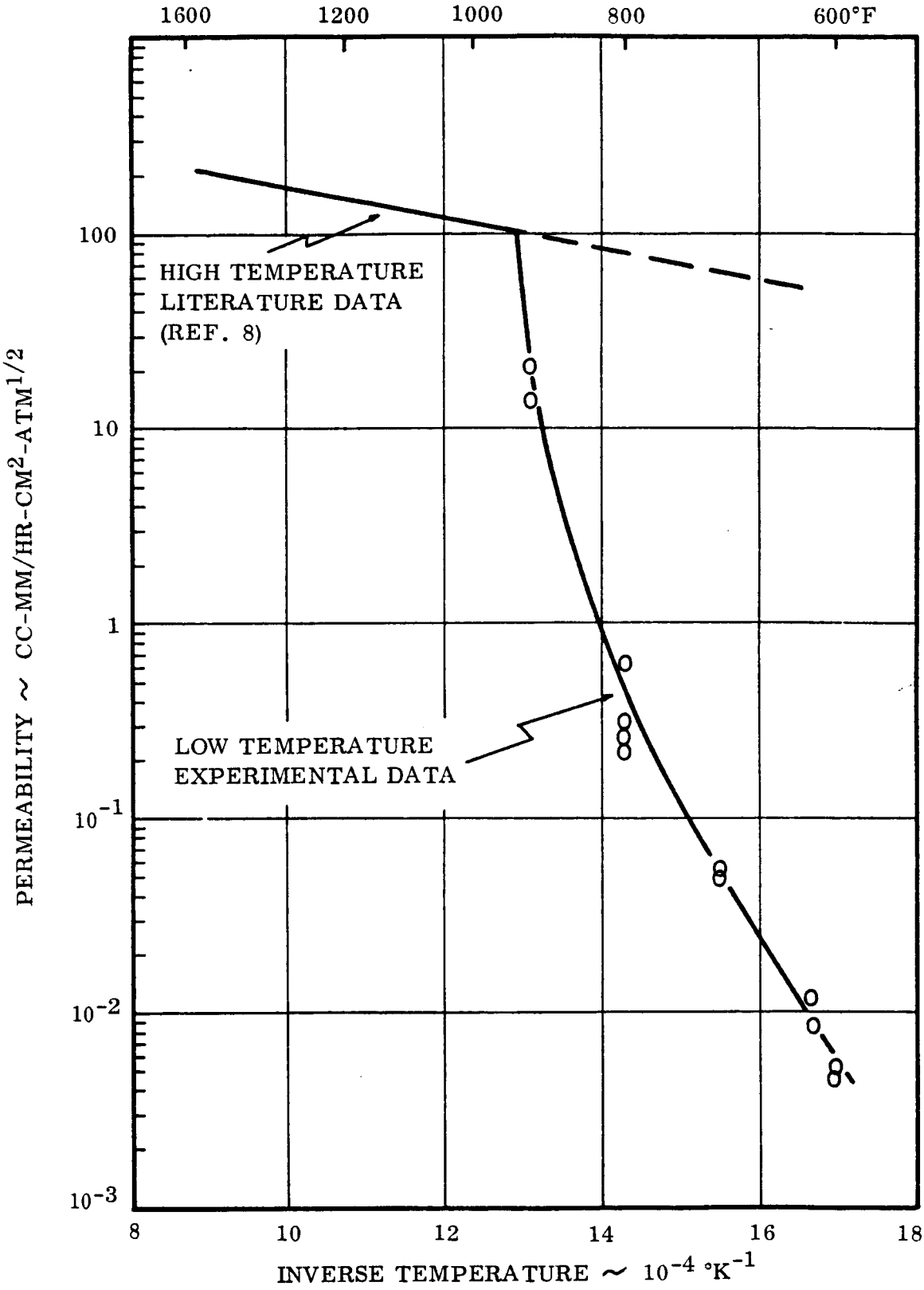

FIGURE 7

PERMEABILITY OF COLUMBIUM AS A FUNCTION OF TEMPERATURE

a. Coatings which do not appreciably interact with the base metal,

b. Coatings which are brittle and exhibit mechanical failure,

c. Coatings which form extensive solid solutions with the base metal, and

d. Coatings which form a series of intermetallic layers with the base metal.

a. Coatings Which Do Not Interact

The analysis of the flow of hydrogen through systems of this type can be quantitatively described by Ohm's Law in the same manner that an electric current flows through two resistors in series. In the case of gas permeability, the square root of pressure is equivalent to the electrical potential, the gas flux is comparable to the current flux, and the permeability is equivalent to the electrical conductivity. The analogy indicates that the rate of hydrogen flux through two metals which do not interact can be simply calculated from a knowledge of the thickness of the materials involved and the permeability of hydrogen through the individual components of the system.

$$Q = \frac{(\sqrt{P_1} - \sqrt{P_2})\ A}{(d_1/K_1 + d_2/K_2)} \qquad (1)$$

where:

Q = hydrogen flux cc (S. T. P.)/hour

P_1 = inlet pressure (atm)

P_2 = exit pressure (atm)

A = area (cm^2)

d_1 = thickness of coating (mm)

d_2 = thickness of base metal (mm)

K_1 = permeability of hydrogen through coating

K_2 = permeability of hydrogen through base metal

An example of the validity of this equation is shown in the system which involves electroplating copper on 304 stainless steel. Metallographic and X-ray diffraction

analysis conducted before and after permeability testing indicated that no significant interaction occurred at temperatures up to 1600°F for times approaching 200 hours. The experimentally-determined flow of hydrogen through a composite copper-stainless steel system is shown in Figure 8. The hydrogen flux calculated from the individual permeabilities of copper and stainless steel is also presented (dotted line in Figure 8). The agreement between calculated and observed flux values was excellent and supported the use of Ohm's Law to determine hydrogen flow values in this type of non-interacting composite system.

This method can also be used in certain instances to determine the permeability of hydrogen through relatively-small quantities of rare metals which are not amenable to conventional permeability measurements. Silver is a particularly interesting example since no data are available in the literature concerning hydrogen permeability and it can be easily plated on a more conventional base metal. Data obtained from silver-plated stainless steel are shown in Figure 9. The permeability of hydrogen through silver can be calculated from Equation 1 since the permeability of hydrogen through the uncoated base metal is known. The calculations performed on two separate ratios of coating-to-base metal thickness are in good agreement and indicate that silver has a permeability to hydrogen which is only slightly greater than molybdenum.

Although the permeability of hydrogen through a composite system can be reduced by a suitable metallic coating, in most practical cases the thickness ratio of coating to base metal is sufficiently low so that only a relatively small decrease is produced.

b. Metallic Coatings Which Exhibit Mechanical Failure

Coatings which experience mechanical failure such as spalling or cracking, are obviously not suitable hydrogen barriers. Typical metallic coatings which could be classified in this category were tungsten and chromium applied to either a 304 stainless steel or Haynes 25 base metal. Tungsten, due to its very low permeability to hydrogen and the ease with which it can be applied by gas plating techniques represents a particularly attractive barrier coating. In this investigation, tungsten coatings were applied to 304 stainless and Haynes 25 by both gas plating and vapor deposition techniques. In an effort to obtain good bonding characteristics, a diffusion anneal consisting of heating in vacuum at temperatures between 1870° and 2000°F was applied to specific specimens. During this treatment, considerable spalling and cracking occurred, possibly due to the difference in thermal expansion coefficients between the tungsten coating and the base metal. In the case of the 304 chamber, virtually no coating remained on the test piece, however, the Haynes 25 specimen retained a rather porous-appearing layer.

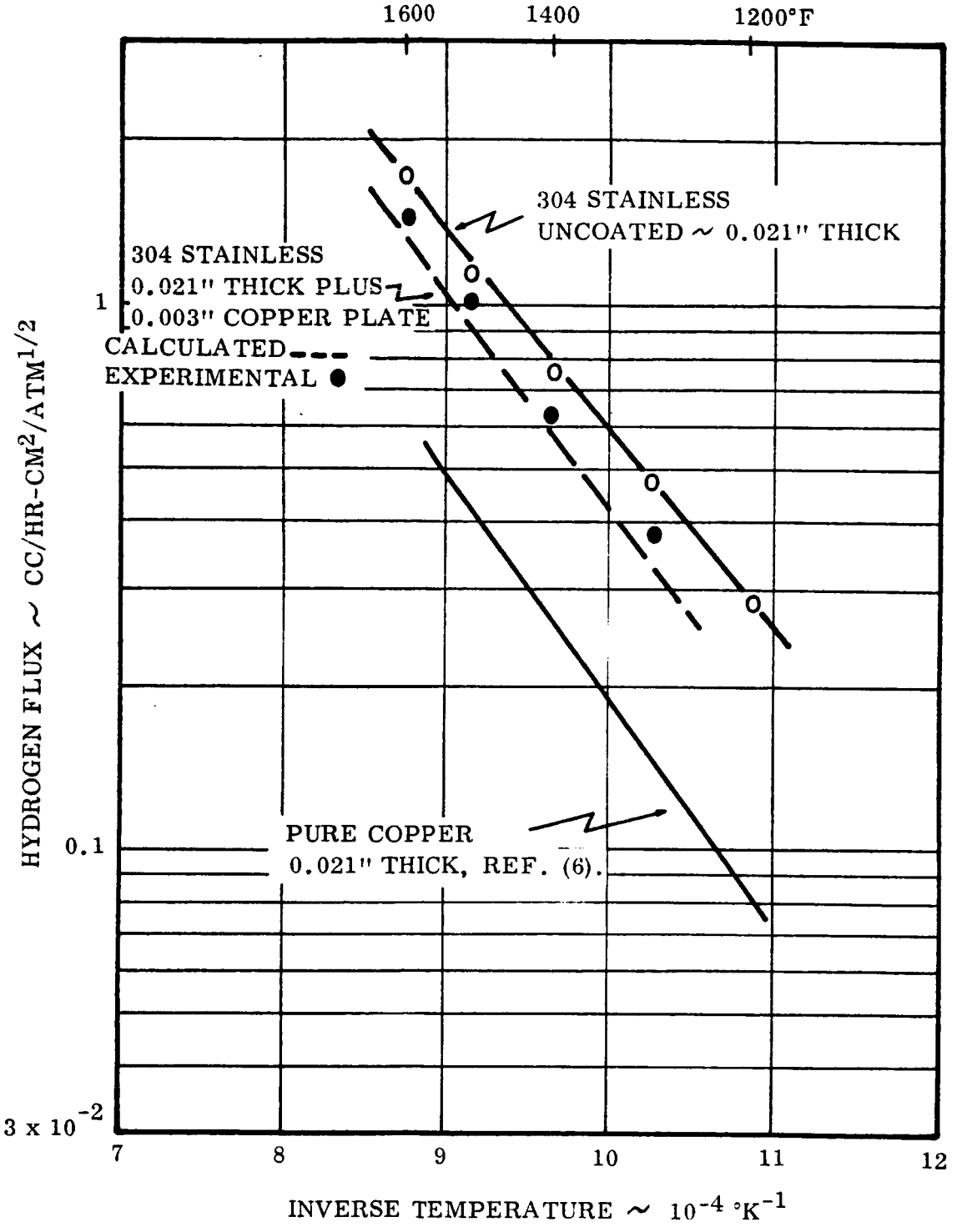

FIGURE 8

INFLUENCE OF COPPER PLATE ON THE FLOW OF HYDROGEN THROUGH STAINLESS STEEL

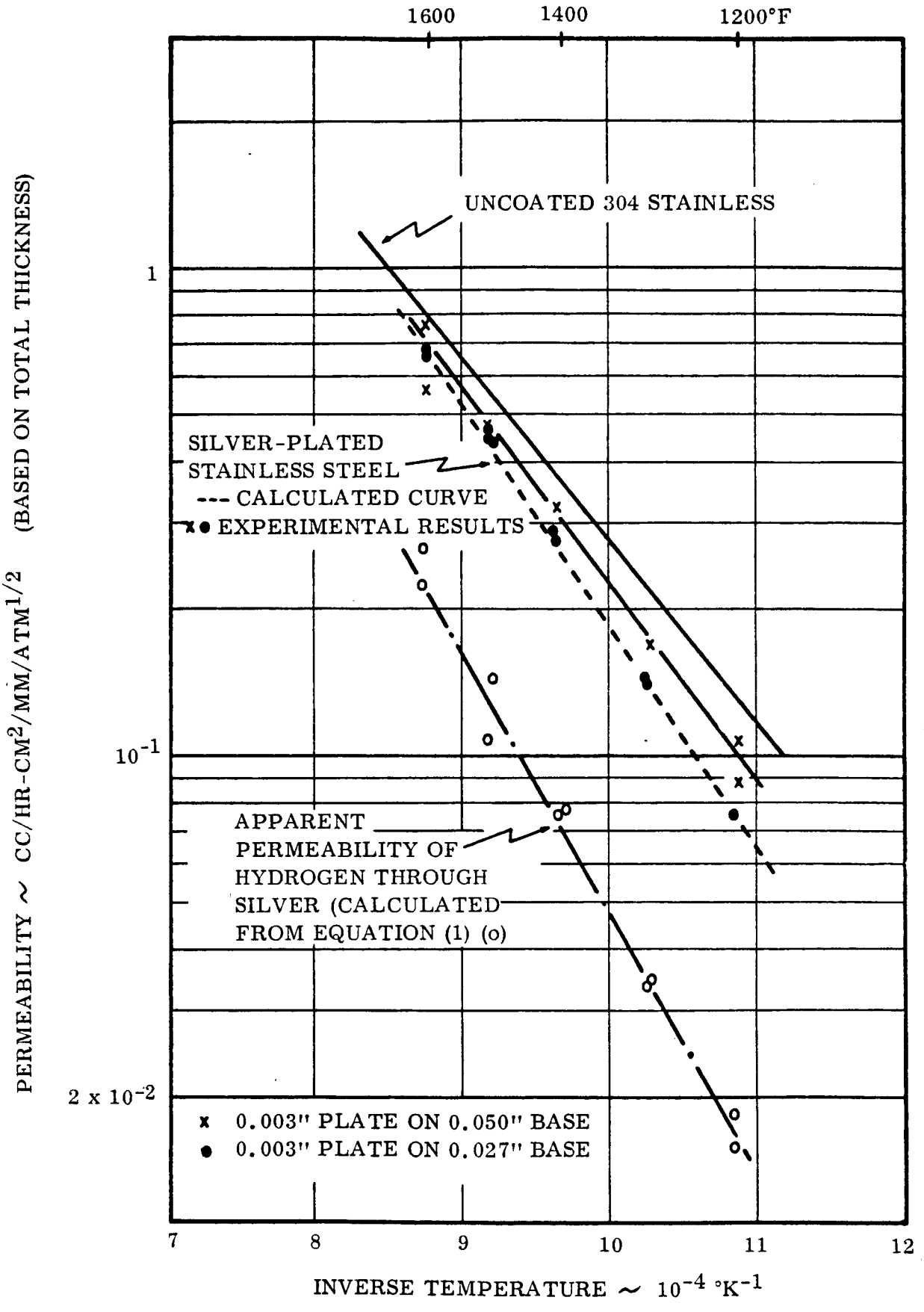

FIGURE 9

PERMEABILITY OF HYDROGEN THROUGH SILVER-PLATED STAINLESS STEEL

The permeability of hydrogen through the tungsten-coated diaphragms is presented in Figure 10. In no case did the tungsten produce any appreciable retardation in hydrogen flow. A flash nickel plate was placed on one Haynes 25 chamber prior to tungsten plating and annealing in an effort to increase the bonding of the coating. This treatment had no appreciable effect on the permeability of the specimen to hydrogen, but as shown in Figure 11,it did alter the microstructural characteristics of the coating. The tungsten coating appeared somewhat irregular, porous, and often cracked. The coating with the flash nickel plate had a thicker and more complex diffusion zone with an abundant quantity of non-continuous M_6C type carbides and a CO_2W type intermetallic.*

The results obtained with tungsten illustrate the point that brittle or porous coatings cannot be used satisfactorily as hydrogen barriers,and the rate of hydrogen permeability cannot be estimated from "Ohm's Law" when mechanical failure of the coating takes place. In addition, the tungsten-rich diffusion bond layer which was not cracked did not produce a significant retardation in permeability.

The chromium coatings which were evaluated as potential hydrogen barriers acted very similar to the tungsten coatings. As shown in Figure 12, the chromium layer on Haynes 25 had a high frequency of cracks,and the permeability through the composite-base metal coating system (see Figure 13) was slightly greater than through the uncoated Haynes 25. This result can be directly attributed to the fact that the cracked coating produced an increase in thickness of the diaphragm without an attendant decrease in hydrogen flux. Chromium coatings on 304 stainless steel were also ineffective hydrogen barriers. The chromium,itself,was partially spalled and cracked while the diffusion layer consisted of a rather complex duplex structure which was believed to be ferrite and sigma phase.

c. Coatings Which Form Extensive Solid Solutions

The permeability of hydrogen through a solid solution alloy which is composed of two metals is generally intermediate between the individual permeability values for the particular metals involved (5). On this basis,the coatings forming extensive solid solutions with the base would produce less of a barrier than that which would be predicted from a direct application of Ohm's Law which assumes no interaction effects. Since low permeability metallic coatings which experience no appreciable interaction with the base metal (e. g. silver and copper) provide very little practical barrier action, coatings which form extensive solid solutions will be even less effective and,therefore,should be avoided when selecting a base metal-coating system to produce optimum hydrogen retardation. Two base metal-coating systems were evaluated to further illustrate this point:

1) Silicon on 304 stainless steel,

2) Aluminum on 304 stainless steel.

*Determined from X-Ray diffraction analysis.

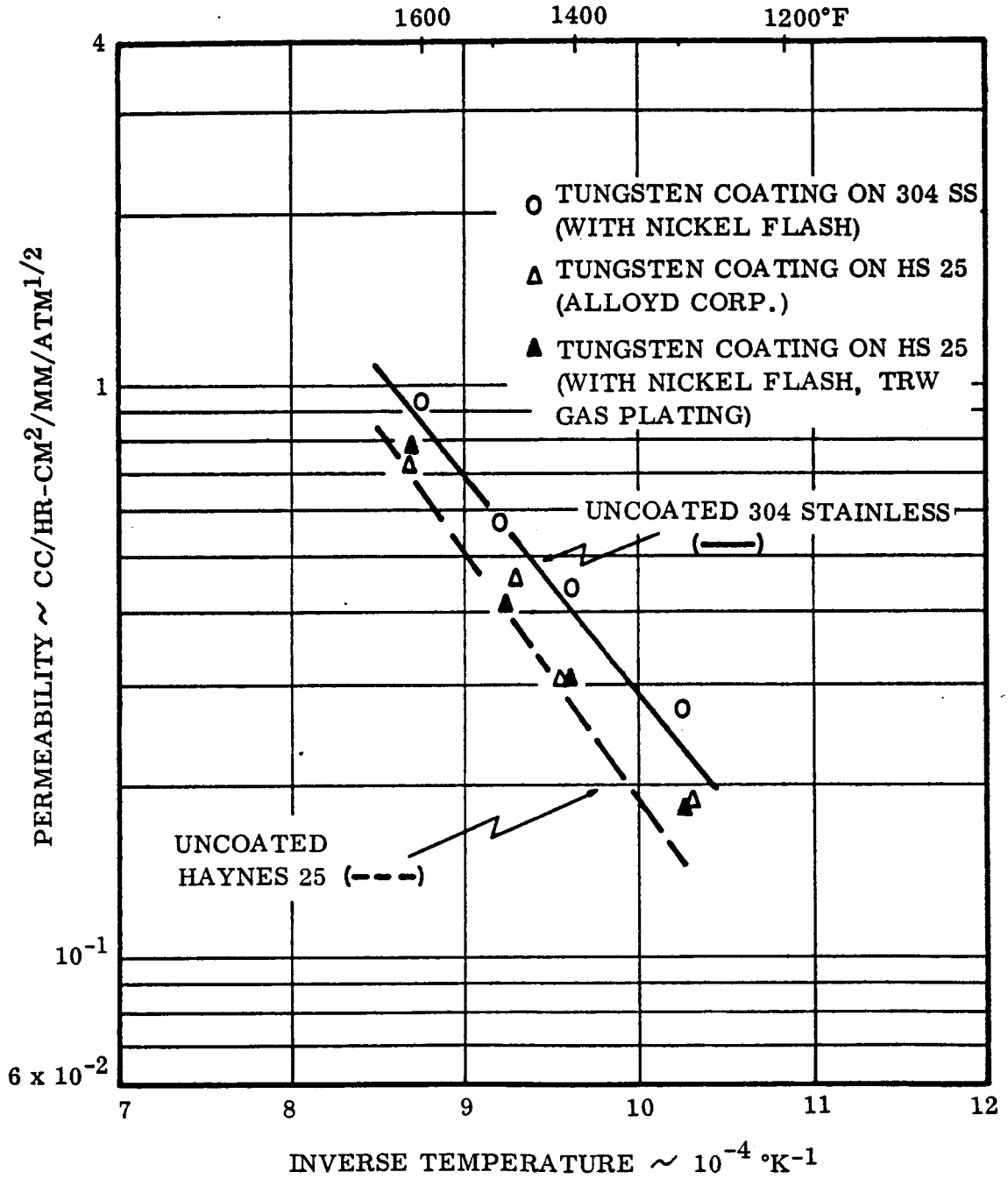

FIGURE 10

INFLUENCE OF TUNGSTEN COATINGS ON THE PERMEABILITY OF HYDROGEN THROUGH 304 STAINLESS STEEL AND HAYNES 25

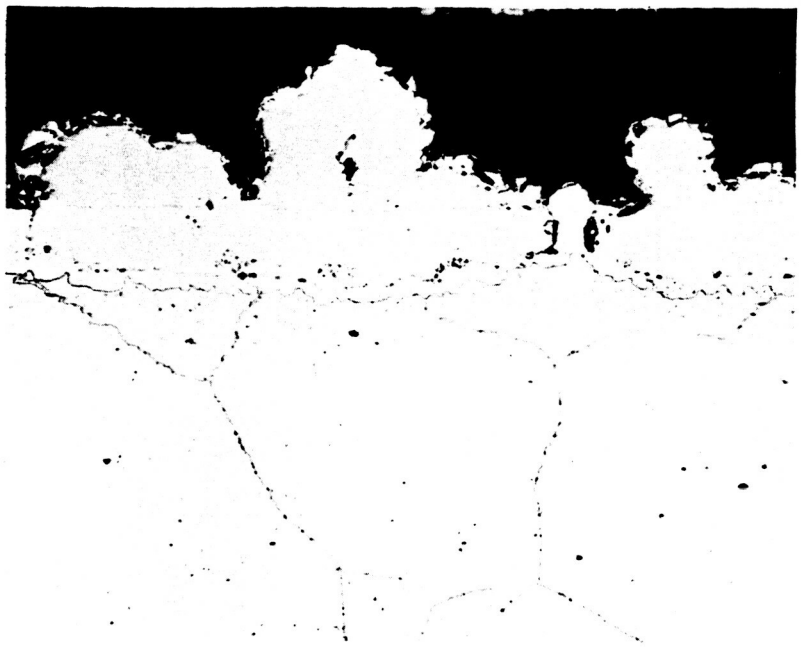

TUNGSTEN COATING

DIFFUSION LAYER

BASE METAL
HAYNES 25

RDM 4775

FIGURE 11 A

MICROSTRUCTURE OF TUNGSTEN COATING ON HAYNES 25 DIFFUSION ANNEALED 3 1/2 HOURS AT 2030°F IN VACUUM
ETCH: 15% HF, 15% H_2SO_4, 8% HNO_3, 62% H_2O; 250 X

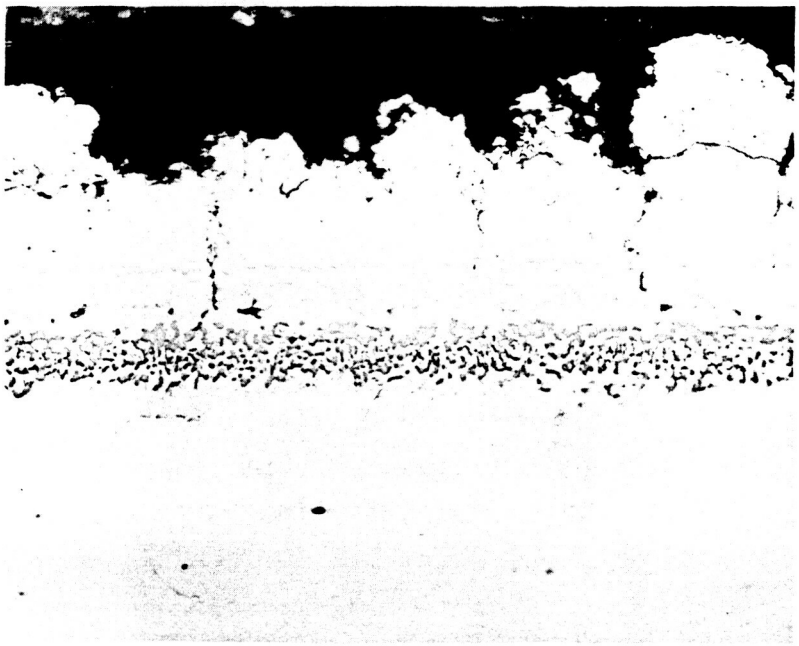

TUNGSTEN COATING

DIFFUSION LAYER

BASE METAL

RDM 4771

FIGURE 11 B

MICROSTRUCTURE OF TUNGSTEN COATING ON HAYNES 25 FLASH NICKEL PLATED PRIOR TO COATING DIFFUSION ANNEALED 3 1/2 HOURS AT 2030°F IN VACUUM
ETCH: 15% HF, 15% H_2SO_4, 8% HNO_3, 62% H_2O; 500 X

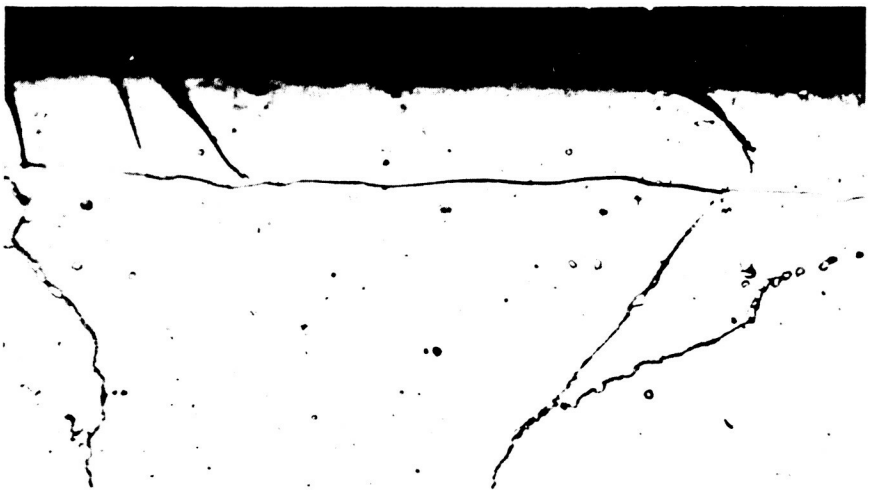

FIGURE 12

MICROSTRUCTURE OF CHROMIZED HAYNES 25 HCl-H_2O_2 ETCH, 500 X

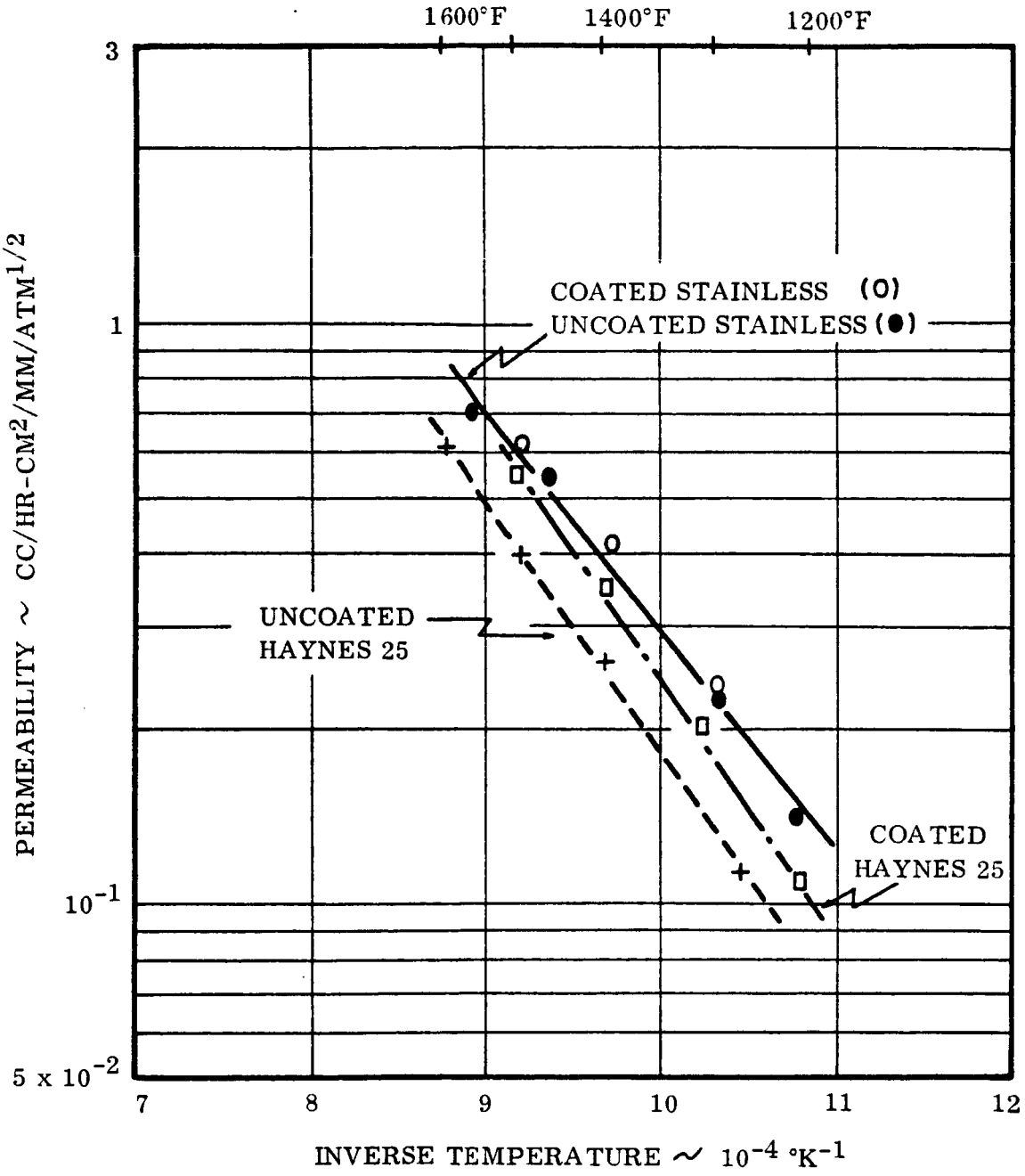

FIGURE 13

INFLUENCE OF CHROMIZING ON THE PERMEABILITY OF HYDROGEN THROUGH HAYNES 25 AND 304 STAINLESS STEEL

The results of permeability tests on siliconized 304 stainless steel are presented in Figure 14. The hydrogen flow was slightly greater through the coated specimen. Metallographic examination of the coating-base metal structure indicated that an appreciable coating existed, and X-ray diffraction analysis showed predominately body-centered cubic lines which had a lattice parameter comparable to α -iron. The addition of silicon to the stainless steel apparently stabilized the α phase and resulted in a complex solid solution of silicon in the base metal.

The presence of aluminum as a coating has been recognized as a substantial barrier to hydrogen (5, 9). Under the conditions of this investigation, which involved pack aluminizing 304 stainless steel with no subsequent oxidation treatment, the aluminum coating merely formed a solid solution with the base metal and no appreciable retardation in hydrogen permeability was observed (see Figure 14). The X-ray analysis of the aluminized diaphragm indicated that only body-centered cubic lines were present and, as in the case with siliconizing, the structure had a lattice parameter comparable to α iron. The addition of aluminum which is a potent ferrite stabilizer produced an extensive ferrite zone at the surface. The microstructural appearance of the aluminized stainless steel specimen substantiated the X-ray analysis and indicated an appreciable region of solid solution alloying.

d. Coatings Which Form a Series of Intermetallics with the Base Metal

As illustrated in the preceding two sections, metallic coatings which do not interact with the base metal and those which form extensive solid solutions do not produce significant variations in hydrogen permeability when the ratio of coating to base metal is relatively low. The most promising approach to generating effective barriers to hydrogen with metallic coatings appears to be through the formation of continuous intermetallic layers. The covalent bonding which characterizes the intermetallics should produce an unfavorable environment for hydrogen permeability and, in certain cases, result in a significant hydrogen barrier.

Permeability tests were initially conducted on two systems-aluminized Haynes 25 and siliconized Haynes 25 - which showed extensive intermetallic layers. The microstructure of the aluminized Haynes 25 is shown in Figure 15 along with microhardness values. The relatively-high hardness of certain layers indicates the presence of intermetallic phases. The results of X-ray diffraction analysis of two types of aluminized coatings are summarized in Tables IV and V. The results indicated the presence of AlNi, $AlNi_3$, type structures in the aluminized coating generated by the pack process, while the coating produced by the spray process showed lines with AlNi and Al_5Co_2 structures. This difference is believed to be due to the higher temperature employed in the pack method. The permeability of hydrogen through the aluminized Haynes 25 is presented in Figure 16. The presence of the aluminum coating significantly reduced the hydrogen flow. In addition, the coating generated by the pack process was more effective in this respect than the aluminized barrier produced by spraying. It should be noted, however, that the spray coating was somewhat thicker than that

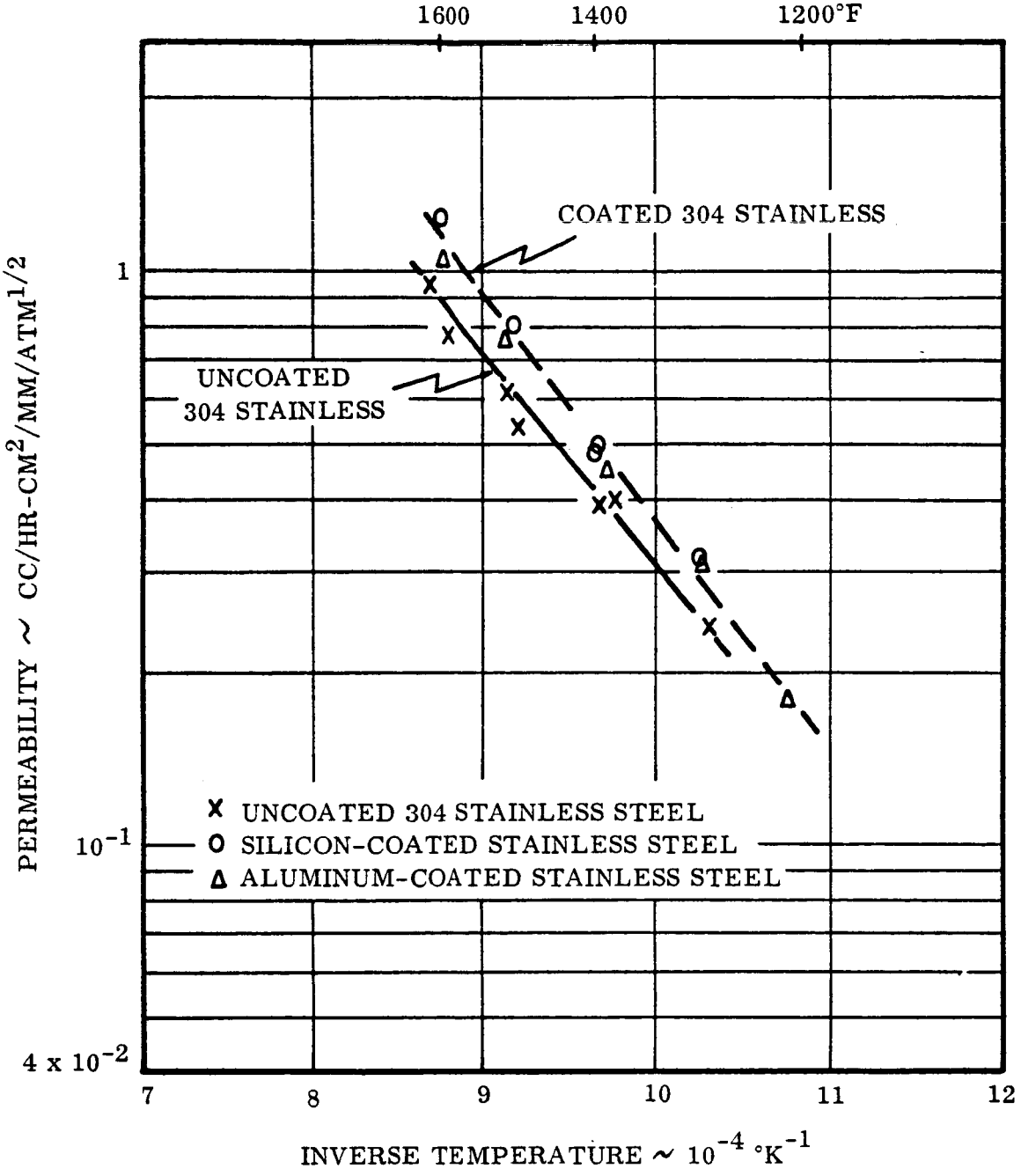

FIGURE 14

PERMEABILITY OF HYDROGEN THROUGH SILICONIZED AND ALUMINIZED 304 STAINLESS STEEL

BACKUP MATERIAL

HARDNESS R_c 53
HARDNESS R_c 68
} COATING

BASE METAL
HAYNES 25
HARDNESS R_c 44.5

RDM 6312

ALUMINIZED BY PACK PROCESS

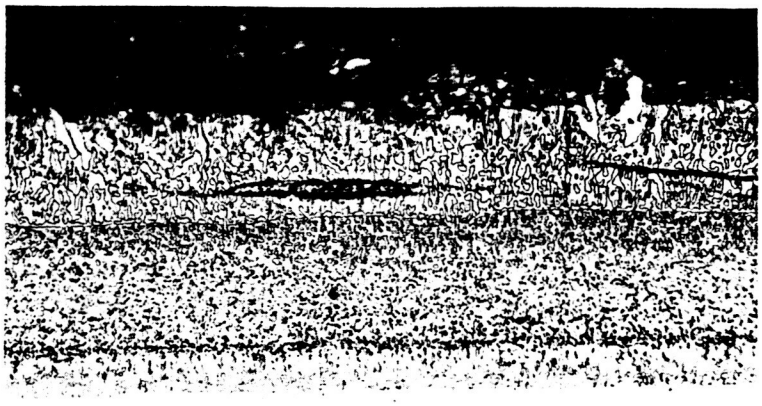

BACKUP MATERIAL

DPH 1050
R_c > 70
DPH 1210
R_c > 70
R_c 63.5
} COATING

BASE METAL
HAYNES 25
HARDNESS R_c 44.5

RDM 3999

ALUMINIZED BY SPRAY PROCESS

FIGURE 15

MICROSTRUCTURE OF ALUMINIZED HAYNES 25
ETCH: 15% HF, 15% H_2SO_4, 8% HNO_3, 62% H_2O; 250 X

TABLE IV

X-RAY DIFFRACTION RESULTS OF ALUMINIZED HAYNES 25 ALLOY

Aluminized By Spray Process		Ni Al		Ni_3Al		Al_5Co_2	
d (A°)	Intensity	d (A°)	Intensity	d (A°)	Intensity	d (A°)	Intensity
3.859	VS					3.82	60
3.560	W			3.60	40		
2.867	VW	2.87	40	2.547	40		
2.221	W					2.22	30
2.157	W						
2.133	W					2.13	
2.029	MS	2.02	100	2.074	100	2.02	80
1.934	VS					1.92	100
1.769	W					1.91	90
1.658	W	1.655	20				
1.435	VW	1.43	20	1.46	20		
1.305	VW	1.285	10				
1.289	S	1.17	70				
1.172		1.015	20				

TABLE V

X-RAY DIFFRACTION RESULTS OF ALUMINIZED HAYNES 25 ALLOY

ALUMINIZED BY PACK PROCESS

		NiAl		Ni_3Al	
d (A°)	Intensity	d (A°)	Intensity	d(A°)	Intensity
3.587	W			3.60	40
2.881	MS	2.87	40		
2.554	W			2.547	40
2.227	W				
2.078	M			2.074	100
2.032	VS	2.02	100		
1.878	W				
1.658	MS	1.655	20		
1.572	W				
1.480	VW			1.46	20
1.438	MS	1.43	20		
1.285	W	1.285	10		
1.170	S	1.170	70		
1.020	MS	1.015	20		

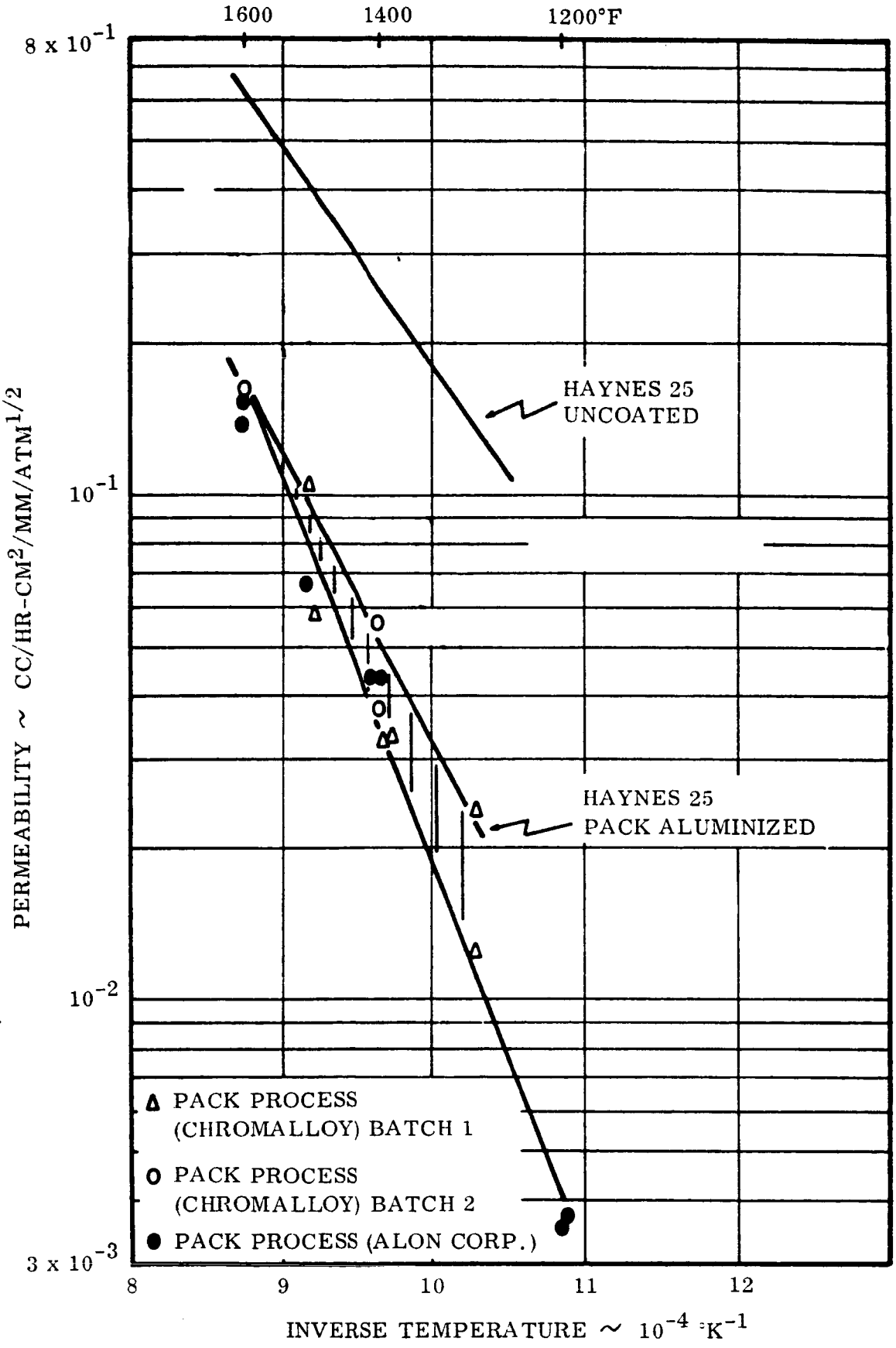

FIGURE 16

PERMEABILITY OF HYDROGEN THROUGH ALUMINIZED HAYNES 25

produced by packing and, as a result, the spray barrier had some craze-type cracks present which may have reduced the effectiveness of the coating. The other possibility for the difference is that the AlNi plus $AlNi_3$ intermetallic system generated in the pack process was a more effective barrier than the AlNi plus Al_5Co_2 type of intermetallic present after spray aluminizing.

When discussing aluminizing, some comment is necessary concerning the influence of the oxide barrier which is formed on the aluminized surface and which is known to have a significant effect on permeability (9, 10). Under the experimental conditions employed in this series of tests, variations in surface treatments had virtually no effect on hydrogen permeability. This point is illustrated in Figure 17 for surface treatments which involved oxidizing in air and wet hydrogen and treating in helium. A possible explanation for this lack of sensitivity to surface conditions is that the oxide film is formed during the processing operation and subsequent treatments have little additional influence. Conventional X-ray and metallographic techniques were incapable of detecting the oxide film, however, previously-published work using electrical measurements indicate that the film is approximately 10^{-7} cm thick (10). An alternative possibility is that at the test temperatures employed (1200 to 1600°F) the rate controlling step in the permeability process is not the passage of the hydrogen through the oxide but rather the permeability through the intermetallic layers. This would also explain the lack of sensitivity of permeability to surface treatments.

The microstructure of the siliconized Haynes 25 prior to permeability testing is shown in Figure 18. The microhardness traverse indicates the presence of the relatively hard intermetallic layers and clearly delineates the zone interfaces. The results of X-ray diffraction analysis, also performed prior to permeability testing, are summarized in Table VI and, although the coating is complex, the results indicate the presence of $CoSi_2$ and CoSi type intermetallics. The tests of hydrogen permeability through the siliconized Haynes 25 diaphragm (see Figure 19) are particularly interesting since they showed an initially-low permeability at 1600°F which progressively increased from 0.143 cc-mm/cm^2-hr-$atm^{1/2}$ to 0.245 cc-mm/cm^2-hr-$atm^{1/2}$ after 200 hours of testing. Post test examination indicated that a gross change in microstructure occurred during permeability testing (compare Figures 18 and 20). X-ray diffraction analysis summarized in Table VII showed that the coating was altered from a $CoSi_2$ and CoSi type microstructure to a $CoSi_2$ type intermetallic. The degradation in barrier properties of the coating could, therefore, be qualitatively accounted for by the diffusion of silicon into the base metal and the breakdown of the higher silicon intermetallic. Although this correlation exists between the conversion of the intermetallic compounds and the hydrogen permeability, there is still some question concerning why certain intermetallic compounds are more effective hydrogen barriers than others. One possibility is that an increase in the covalent bonding of various intermetallics increases their resistance to hydrogen permeation.

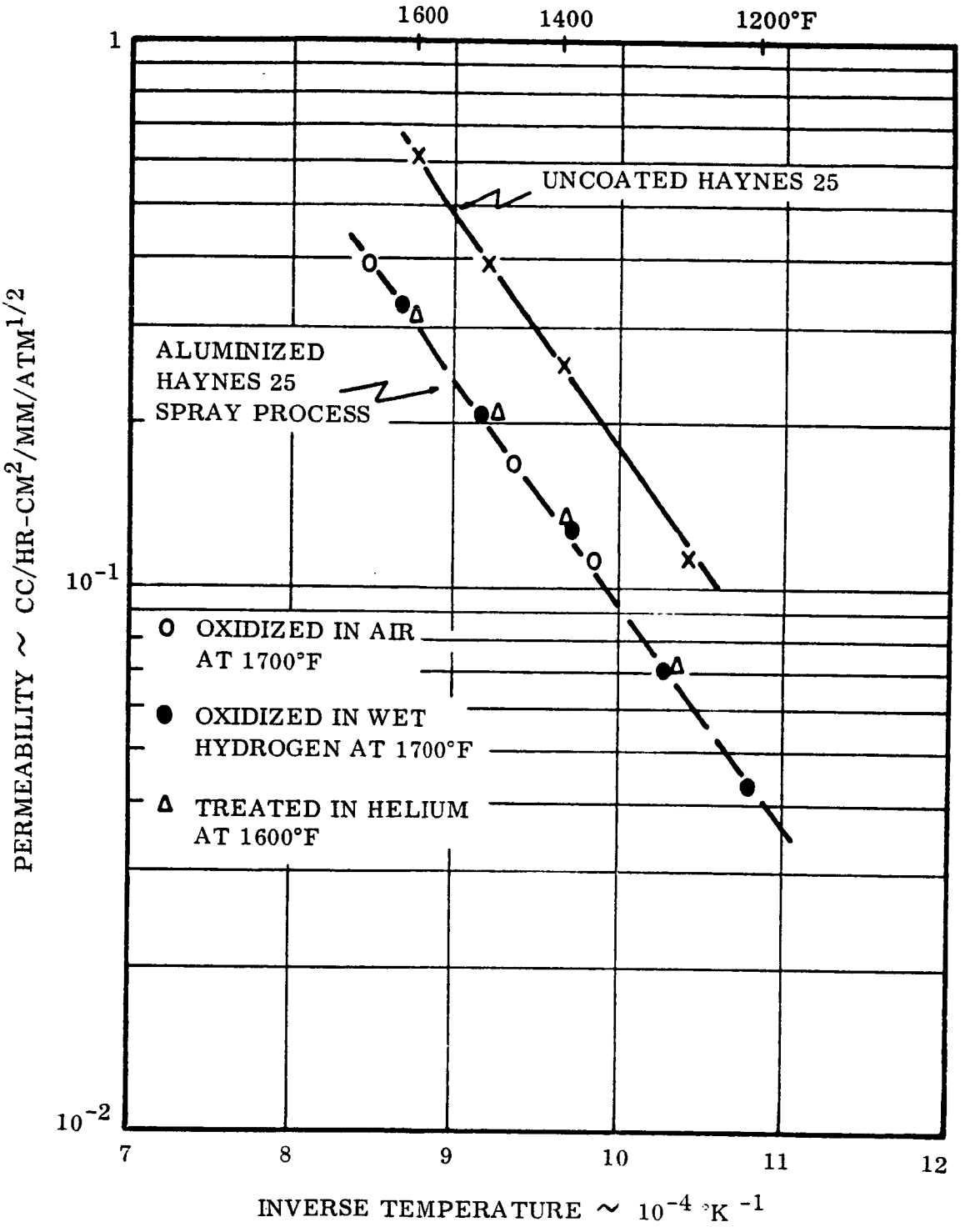

FIGURE 17

INFLUENCE OF SURFACE TREATMENT ON THE PERMEABILITY OF HYDROGEN THROUGH ALUMINIZED HAYNES 25

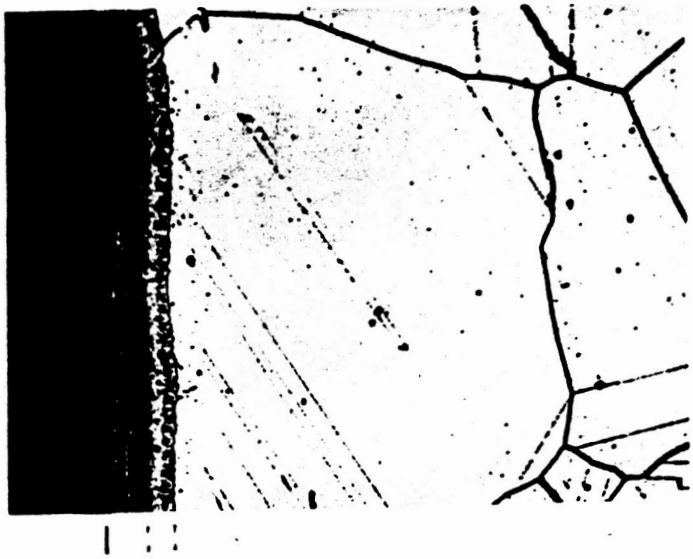

RDM 6012

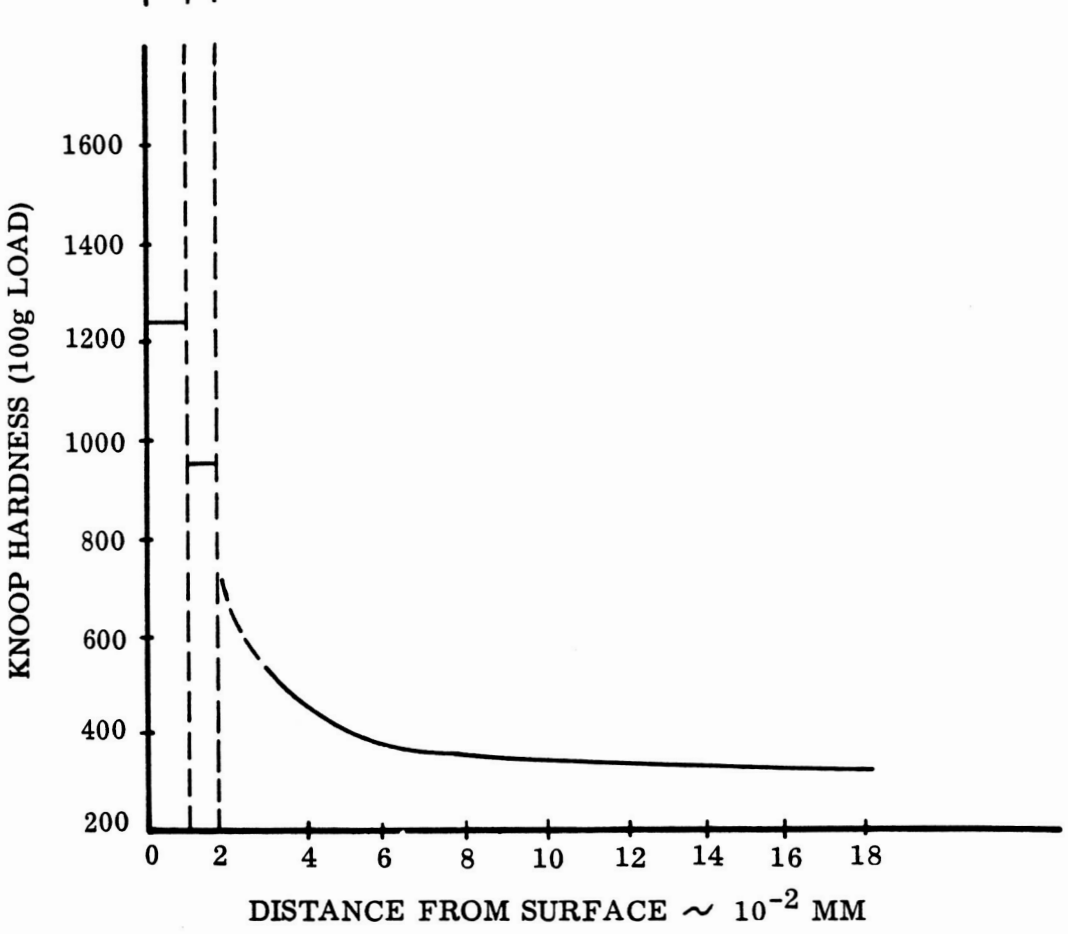

FIGURE 18

MICROSTRUCTURE OF SILICONIZED HAYNES 25 PRIOR TO PERMEABILITY TESTING, REFRACTORY
ETCH: 15% HF, 15% H_2SO_4, 8% HNO_3, 62% H_2O, 500 X

TABLE VI

X-RAY DIFFRACTION DATA ON SILICONIZED HAYNES 25

PRIOR TO PERMEABILITY TESTING

Pattern		CoSi			$CoSi_2$		
d (A°)	Intensity	d (A°)	Intensity	hK1	d (A°)	Intensity	hK1
3.15	W	3.13	60	110			
3.09	VS				3.08	60	111
2.59	W	2.57	50	111			
2.22	W	2.21	40	200			
2.12	VW						
2.09	W						
1.99	VS	1.98	100	210			
1.90	VS				1.89	80	220
1.82	S	1.81	90	211			
1.62	S				1.61	40	311
1.34	W	1.33	60	311	1.34	20	400
1.23	VW	1.22	40	320			
1.19	W	1.18	70	321			

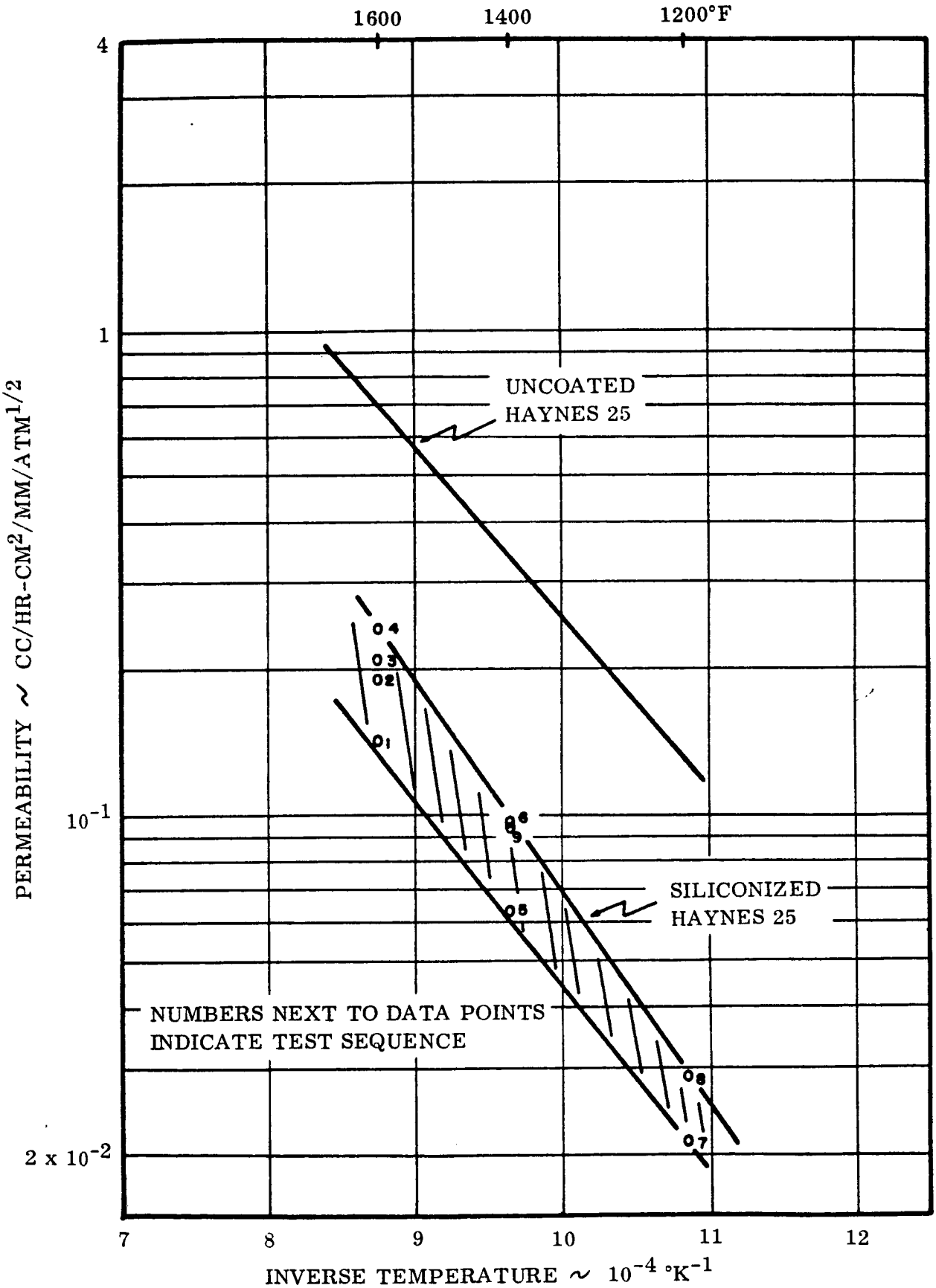

FIGURE 19

PERMEABILITY OF HYDROGEN THROUGH SILICONIZED HAYNES 25

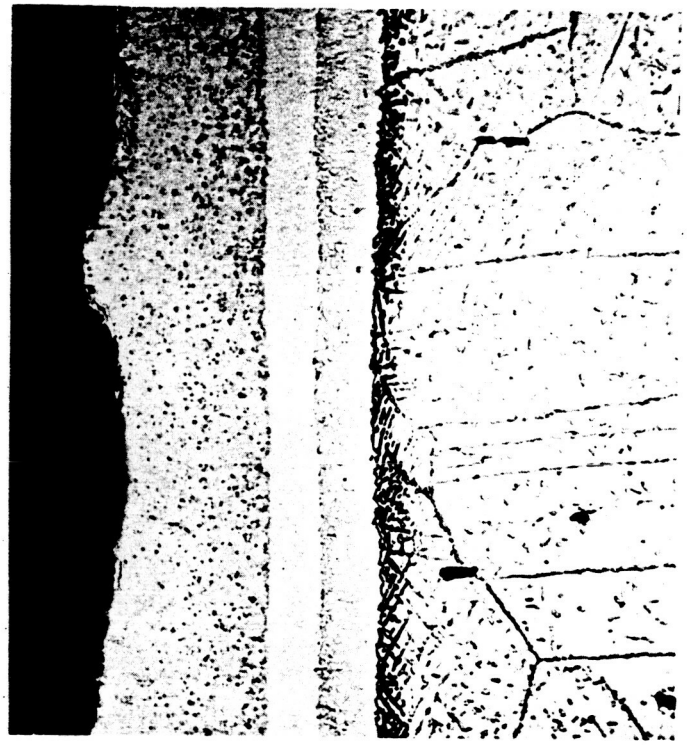

RDM 6011-2

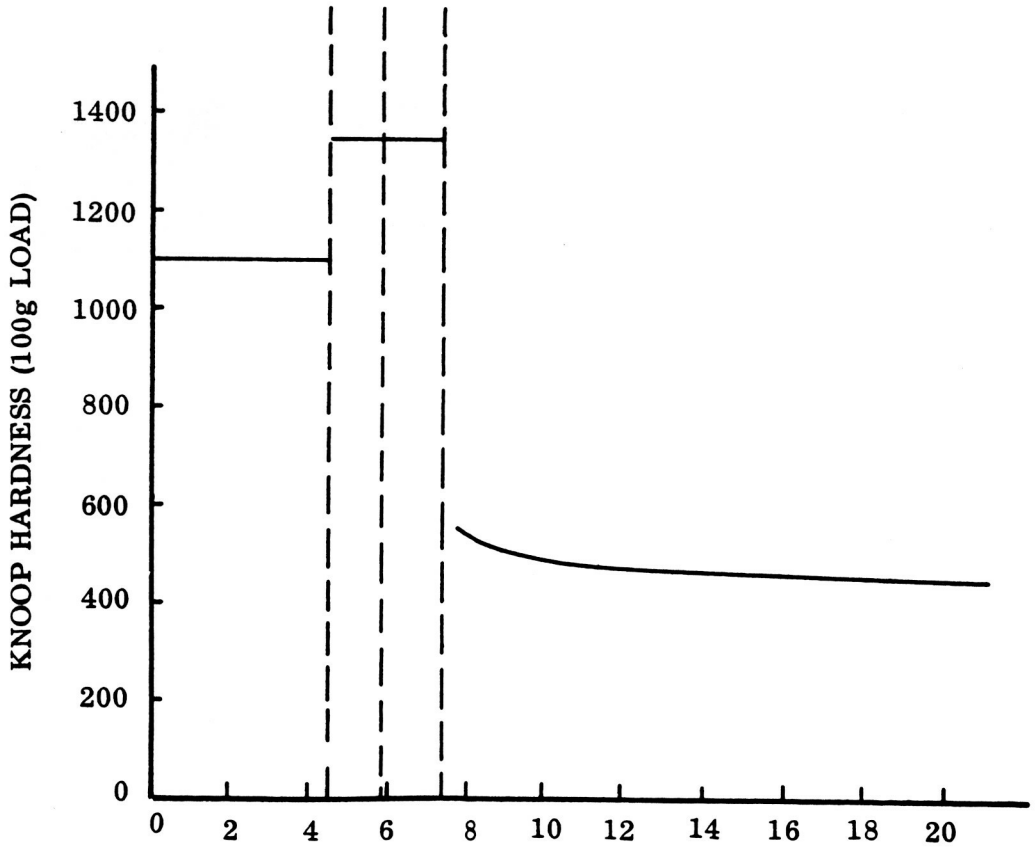

FIGURE 20

MICROSTRUCTURE OF SILICONIZED HAYNES 25 SUBSEQUENT TO PERMEABILITY TESTING (APPROX. 350 HOURS BETWEEN 1200°F AND 1600°F)
ETCH: 15% HF, 15% H_2SO_4, 8% HNO_3, 62% H_2O; 500 X

TABLE VII

X-RAY DIFFRACTION DATA ON SILICONIZED HAYNES 25

SUBSEQUENT TO PERMEABILITY TESTING

Pattern			Co_2Si		
d (A°)	Intensity		d (A°)	Intensity	hKl
3.305	W		3.31	30	101
2.879	W		2.88	30	210
2.754	M		2.75	70	111
2.323	W				
2.285	M		2.28	50	211
2.186	M				
2.133	S		2.13	50	310
2.066	S		2.05	100	021
2.026	S		2.02	70	220
1.998	VS		2.00	100	301
1.964	M		1.97	100	121
1.921	M				
1.875	S		1.87	100	002
1.854	M		1.85	100	311
1.714	M	Numerous Peaks Approx. 30-50 Intensity	1.71	100	320
1.380	M		1.37	70	222
1.260	M		1.26	70	322

The correlation between the conversion of an intermetallic and the increase in permeability suggests that it may be possible to select very stable intermetallics to avoid the degradation in barrier properties. To examine this possibility, the permeability of hydrogen through the following silicides was examined using a Haynes 25 base metal: vanadium silicide, zirconium silicide, molybdenum silicide, and tungsten silicide. These silicides possessed a wide range in melting points and bonding energies. In general, the application technique (see Appendix III) consisted of a duplex pack process which involved the initial formation of a very thin coating of the V, Zr, Mo, or W, followed by a siliconizing treatment in an activated mixture of the original coating powder and silicon. The final treatment was performed at a relatively-low temperature (approximately 1700°F) to avoid any chance of forming a nickel-silicon eutectic.

The permeability of the hydrogen through the various silicide coatings is shown in Figure 21. There was a considerable range in the barrier properties of the silicides with the tungsten-silicon coating providing the largest decrease in permeability. The microstructure of each of the coatings* along with the microhardness measurements are shown in Figures 22 to 25. The relationship between the melting points of the duplex silicide coatings** and their permeability to hydrogen is presented in Figure 26. For a given system, the melting point might be expected to exert some control over permeability since the coatings with higher melting points generally tend to resist breakdown due to gross diffusion, and there is also some degree of correlation between the bonding energy of the structure and the melting point (11). In general, the duplex coatings with higher melting points produce a greater retardation to hydrogen flow.

The results indicate that selected intermetallic coatings can significantly decrease hydrogen permeation, and these barriers represent potentially-useable systems for times and temperatures which do not involve gross diffusion of the coating into the base metal.

C. Coated Metals - Oxide Coatings

In an effort to determine the applicability of simple metal oxides as barriers to hydrogen flow, 303 stainless steel and Haynes 25 were oxidized in wet hydrogen at 1700°F for four hours. This treatment produced a continuous thin oxide film over the entire specimen area. The results of permeability tests conducted on 303 stainless steel are presented in Figure 27. During the initial tests at relatively low temperatures (1200 to 1400°F), the oxide barrier reduced the permeability of hydrogen through

*The microstructure was developed by etching in a solution of 15% HF, 15% H_2SO_4, 8% HNO_3 and 62% water. The etch time which varied for each specimen was selected to develop the most definitive structure in the coating, and, therefore, often did not produce suitable etching of the base metal.

**The melting points were obtained as handbook values for the ideal composition of the silicides, i.e., no dilution effects due to the base metal were taken into account.

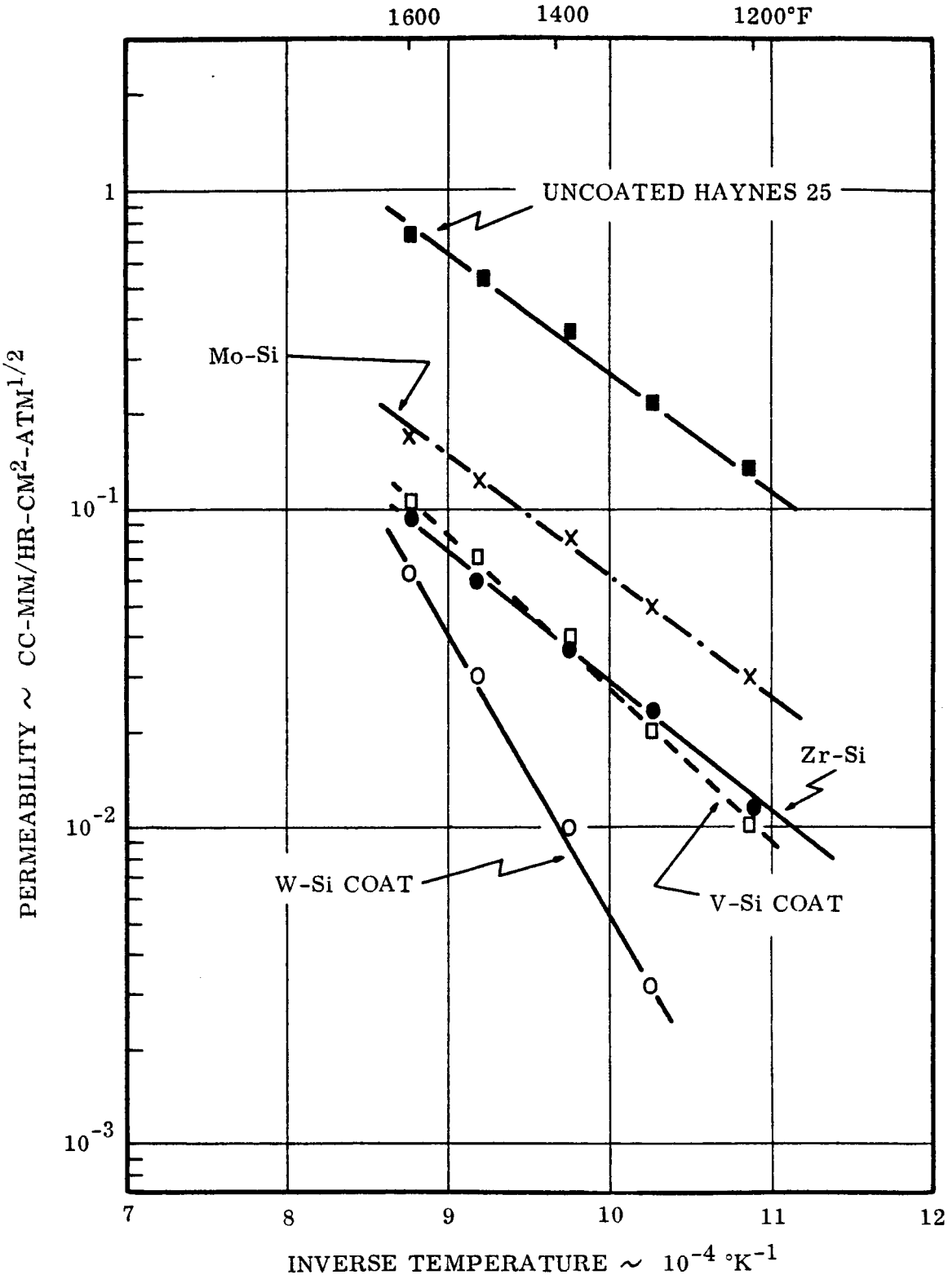

FIGURE 21

PERMEABILITY OF HYDROGEN THROUGH HAYNES 25 COATED WITH VARIOUS METAL-SILICON BARRIERS

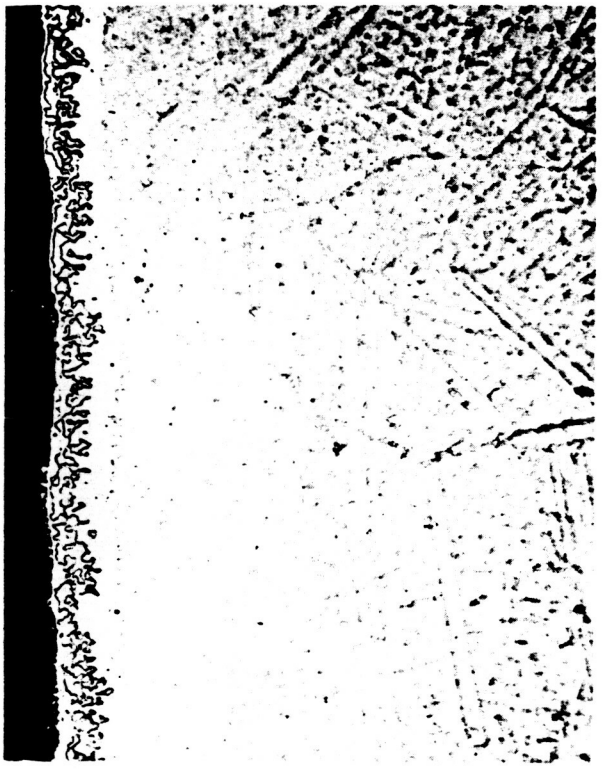

RDM 8038

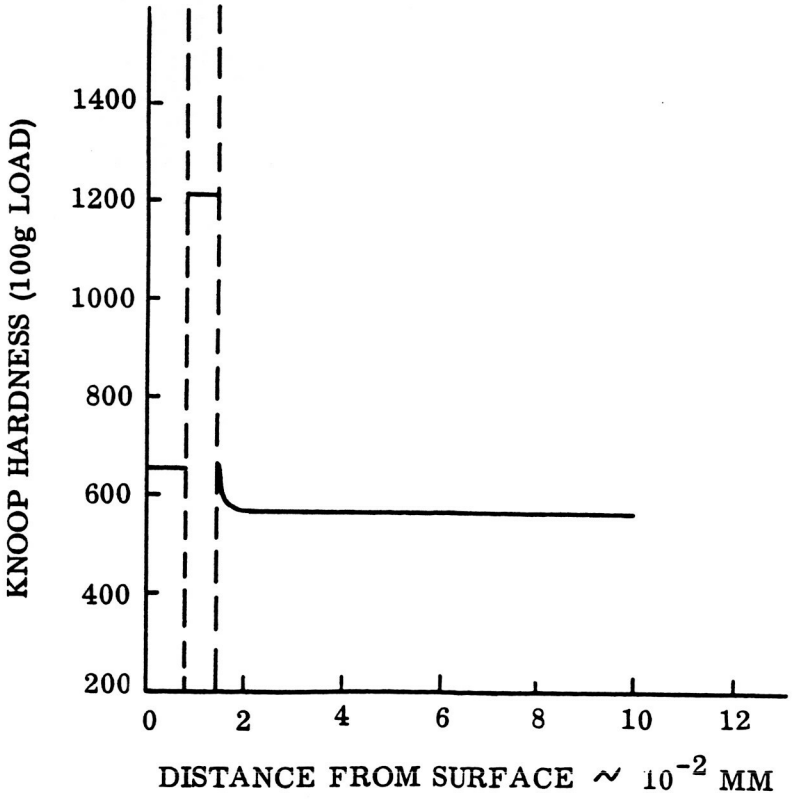

FIGURE 22

MICROSTRUCTURE OF HAYNES 25 COATED WITH VANADIUM-SILICON, AFTER PERMEABILITY TESTING
ETCH: 15% HF, 15% H_2SO_4, 8% HNO_3, 62% H_2O; 500 X

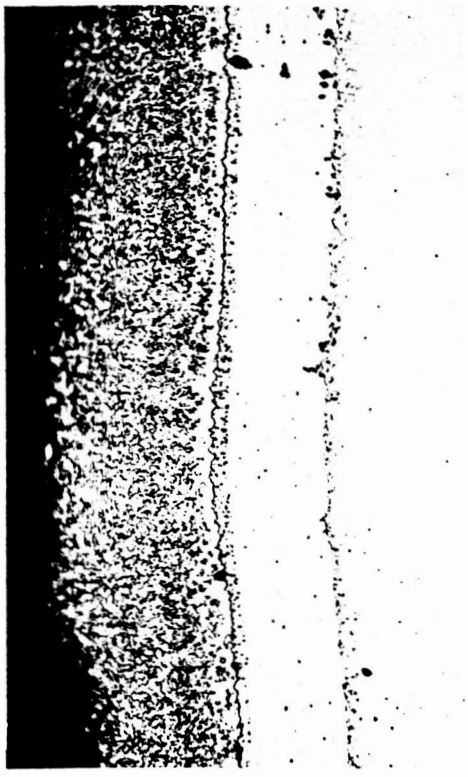

RDM 8039

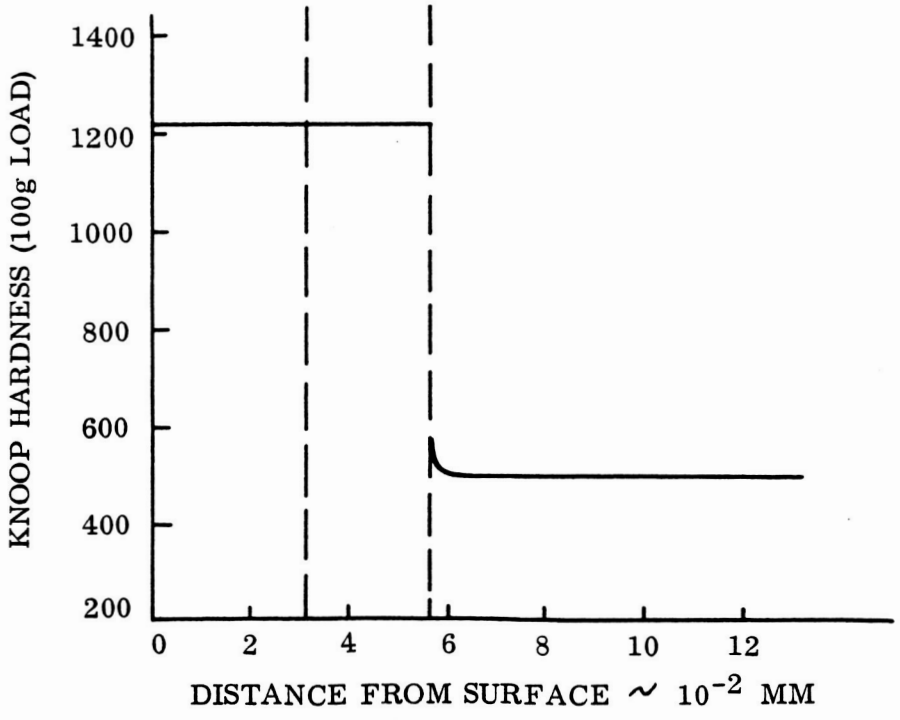

FIGURE 23

MICROSTRUCTURE OF HAYNES 25 COATED WITH ZIRCONIUM-SILICON, AFTER PERMEABILITY TESTING, REFRACTORY METAL ETCH: 15% HF, 15% H_2SO_4, 8% HNO_3, 62% H_2O; 500 X

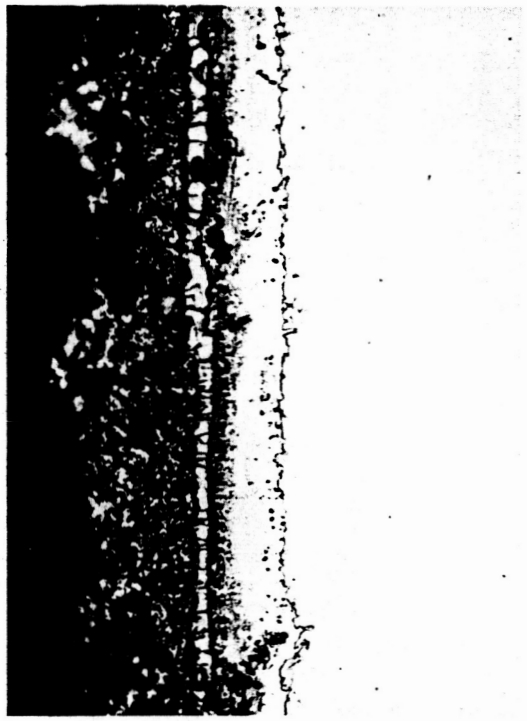

RDM 8629

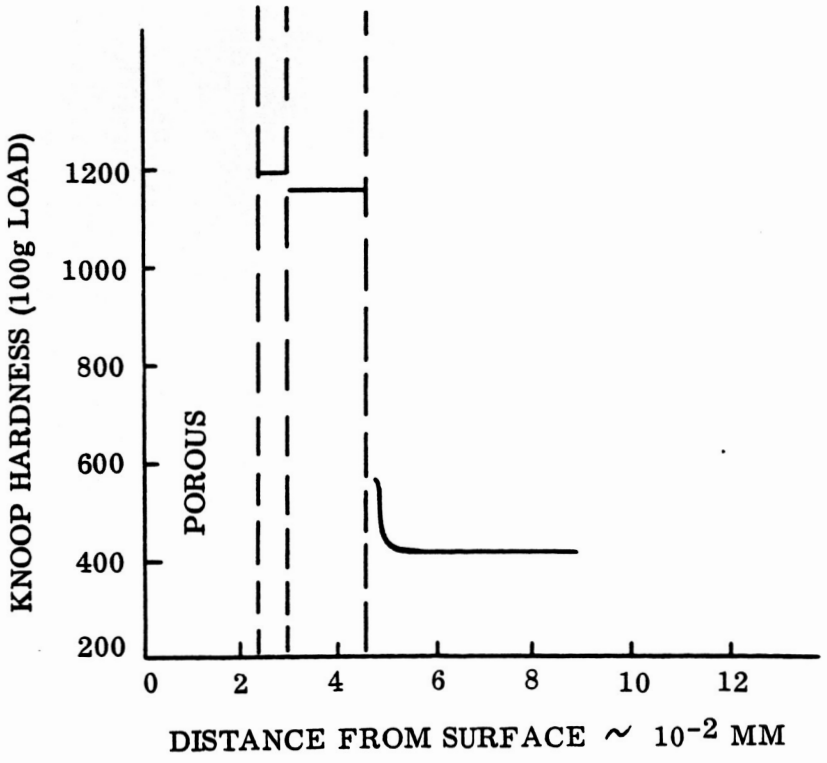

FIGURE 24

MICROSTRUCTURE OF HAYNES 25 COATED WITH MOLYBDENUM-SILICON, AFTER PERMEABILITY TESTING, REFRACTORY METAL
ETCH: 15% HF, 15% H_2SO_4, 8% HNO_3, 62% H_2O; 500 X

RDM 6391

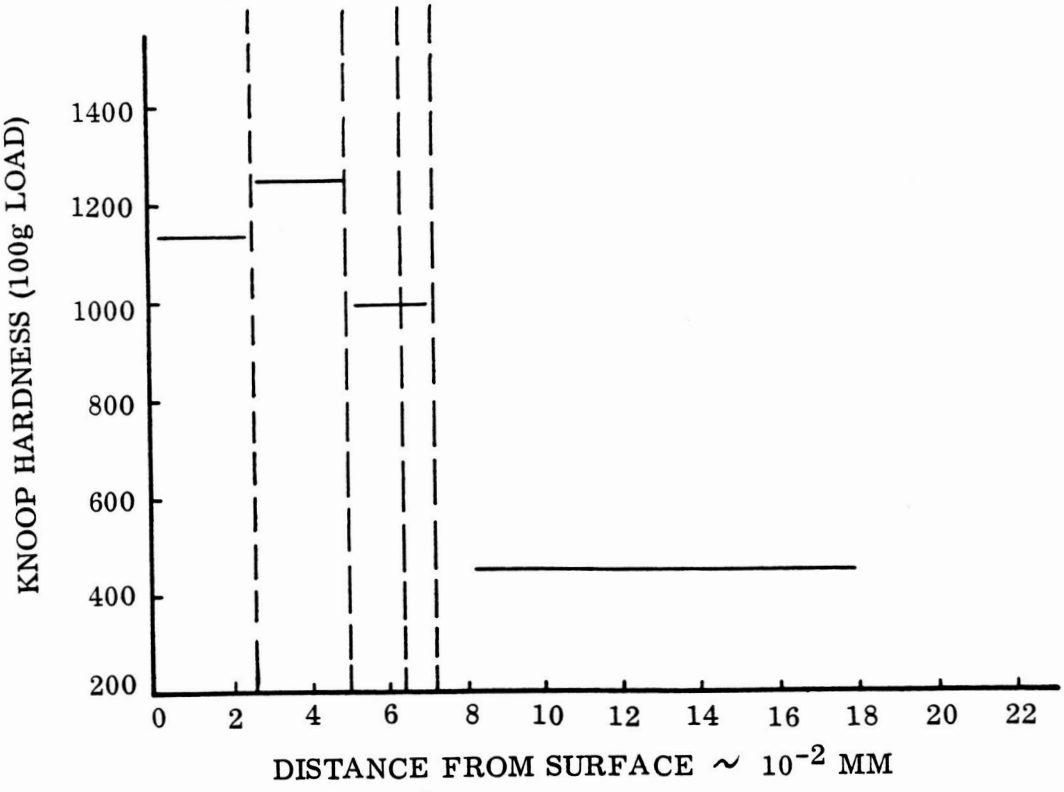

FIGURE 25

MICROSTRUCTURE OF HAYNES 25 COATED WITH TUNGSTEN-SILICON, ETCH: 15% HF, 15% H_2SO_4, 8% HNO_3, 62% H_2O; 500 X

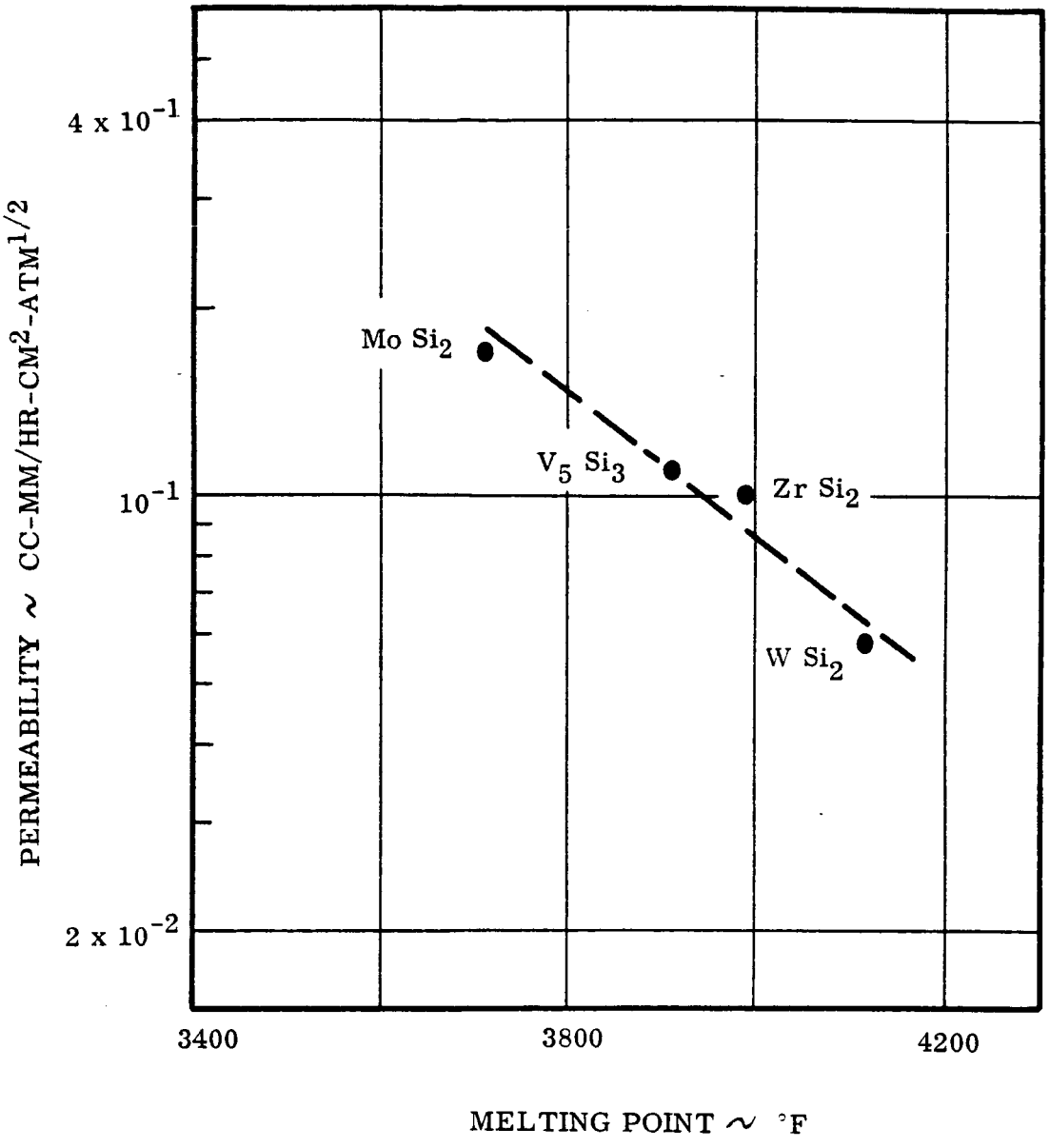

FIGURE 26

VARIATION OF PERMEABILITY OF SILICON-COATED HAYNES 25 WITH MELTING POINT OF THE SPECIFIC SILICIDES

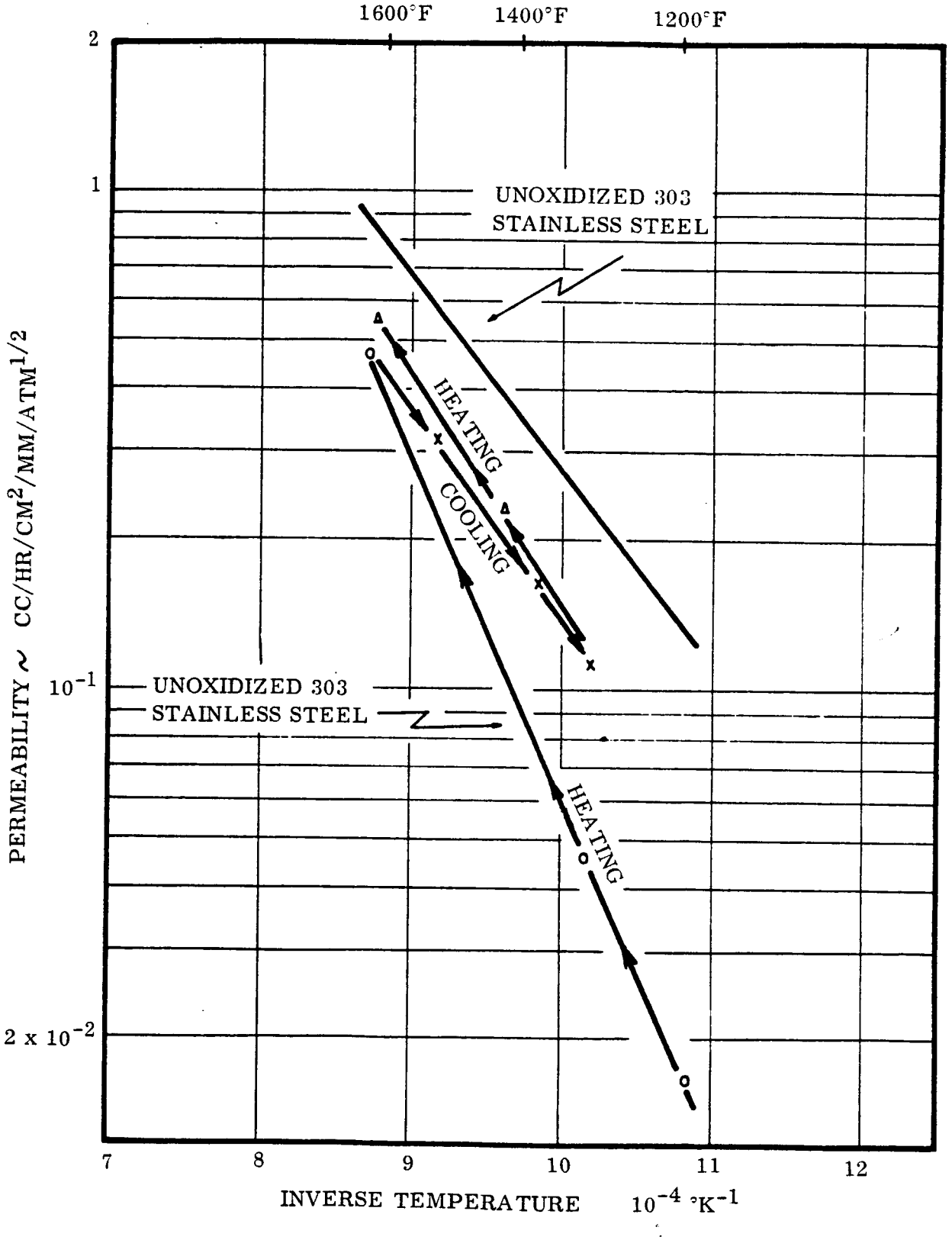

FIGURE 27

PERMEABILITY OF OXIDIZED 303 STAINLESS STEEL TO HYDROGEN

the diaphragm by an order of magnitude. As the test temperature was increased, the barrier effect was irreversibly reduced, indicating a steady deterioration of the oxide, presumably due to chemical reduction by the hydrogen. In the case of the oxidized Haynes 25 Alloy (see Figure 28), the oxide barrier was even less effective and less stable than that present on the stainless steel. Oxidizing treatments also were conducted in air and in atmospheres with low oxygen partial pressures, however, the permeability to hydrogen was comparable to that shown in Figures 27 and 28. In an effort to obtain more stability to the oxide coating, a 302B stainless steel containing 2.7% silicon was oxidized in air for two hours at 1800°F. As shown in Figure 29, silicon addition to the base 300 series composition did not produce a significant improvement in the ability of the oxidized diaphragm to retard hydrogen.

As previously discussed, an oxidation treatment applied to a Haynes 25 aluminized surface did not significantly alter the permeability of the diaphragm to hydrogen over that obtained with an unoxidized surface. A possible explanation for this effect was that the rate-determining step was flow through the intermetallic rather than the surface oxide. On this basis, oxidation applied to an aluminized 304 stainless steel which does not form an intermetallic should produce some variation in permeability. The results of tests conducted on the aluminized and oxidized 304 stainless steel are shown in Figure 30. The oxidation treatment reduced the permeability over the entire test temperature range, and this barrier effect was relatively stable during the entire test period.

D. Coated Metals - Glass Coatings

In evaluating the ability of glass coatings to retard hydrogen flow, some consideration has to be given to the orientation of the coating with respect to the inlet gas pressure. As shown in Figure 31, when the coated surface is on the inlet side, a compressive stress is placed on the glass coating, while the alternative method which involves placing the glass on the hign vacuum side (outlet side) exposes the coating to possible tensile stresses due to the effective hydrogen build-up at the glass-base metal interface. Since glass has poor tensile properties, the presence of the glass on the outlet side if unfavorable from a mechanical strength standpoint. This test condition, however, represents a more realistic approach from an application viewpoint since lithium hydride which is the hydrogen source in Sunflower is very corrosive to a glass liner.

The evaluation of glass coatings as hydrogen permeability barriers was conducted on a series of commercially-available coatings which, although not specifically designed as hydrogen barriers, at least had the capability to be used at temperatures up to 1600°F. The permeability results for glass coatings were obtained on the following coating systems:

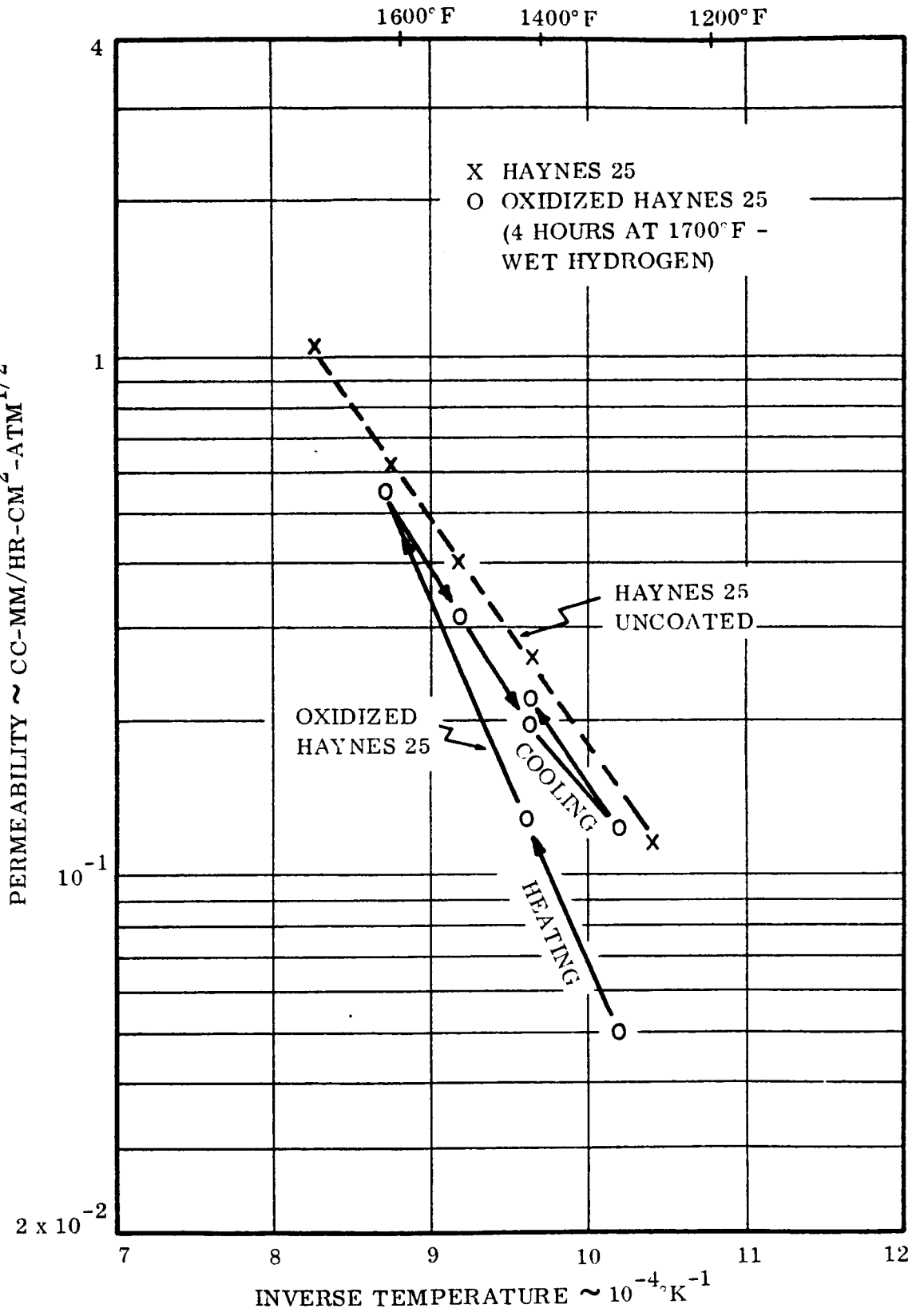

FIGURE 28

PERMEABILITY OF UNCOATED HAYNES 25 AND
OXIDIZED HAYNES 25 TO HYDROGEN

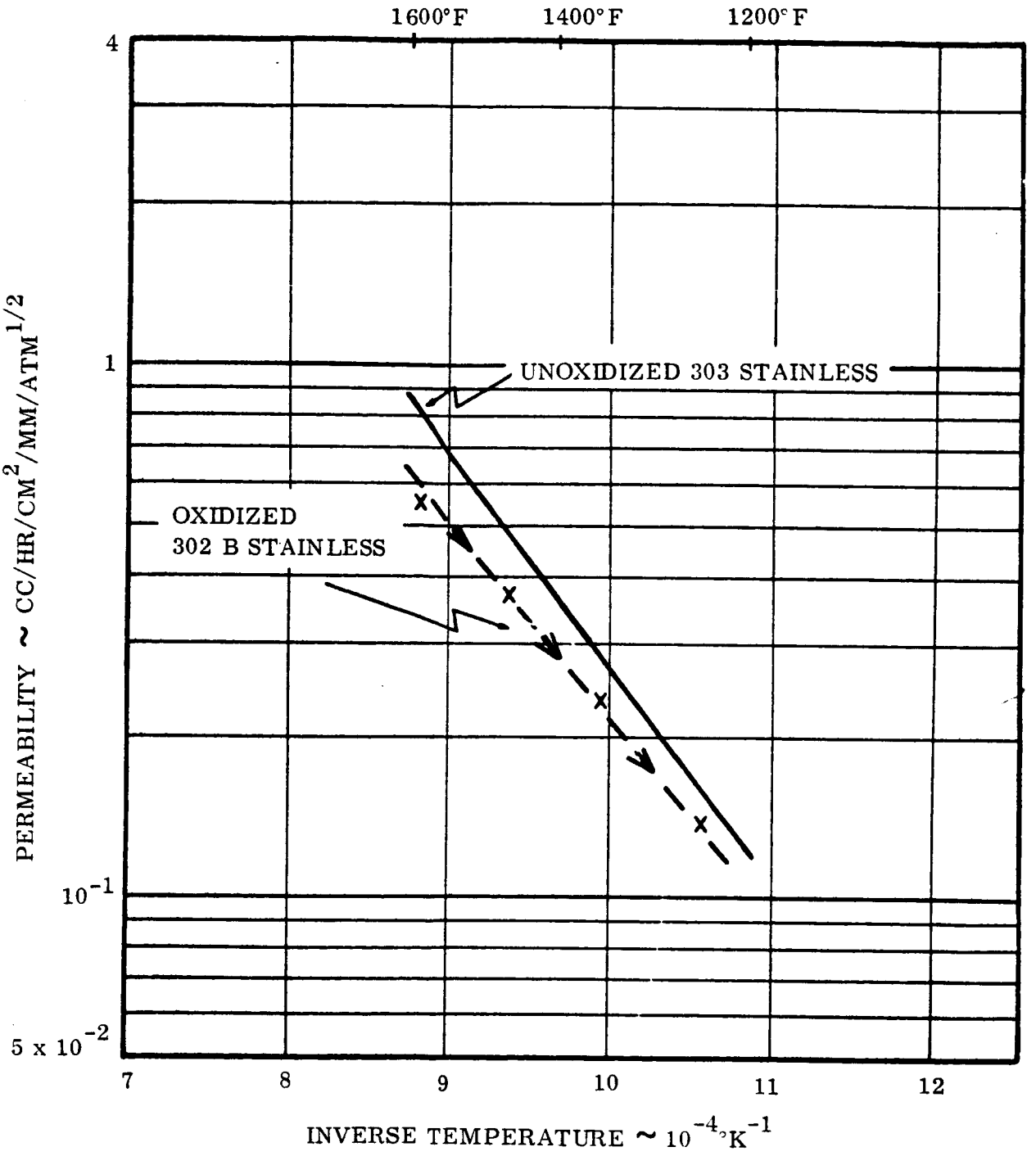

FIGURE 29

PERMEABILITY OF HYDROGEN THROUGH OXIDIZED
302 B STAINLESS STEEL

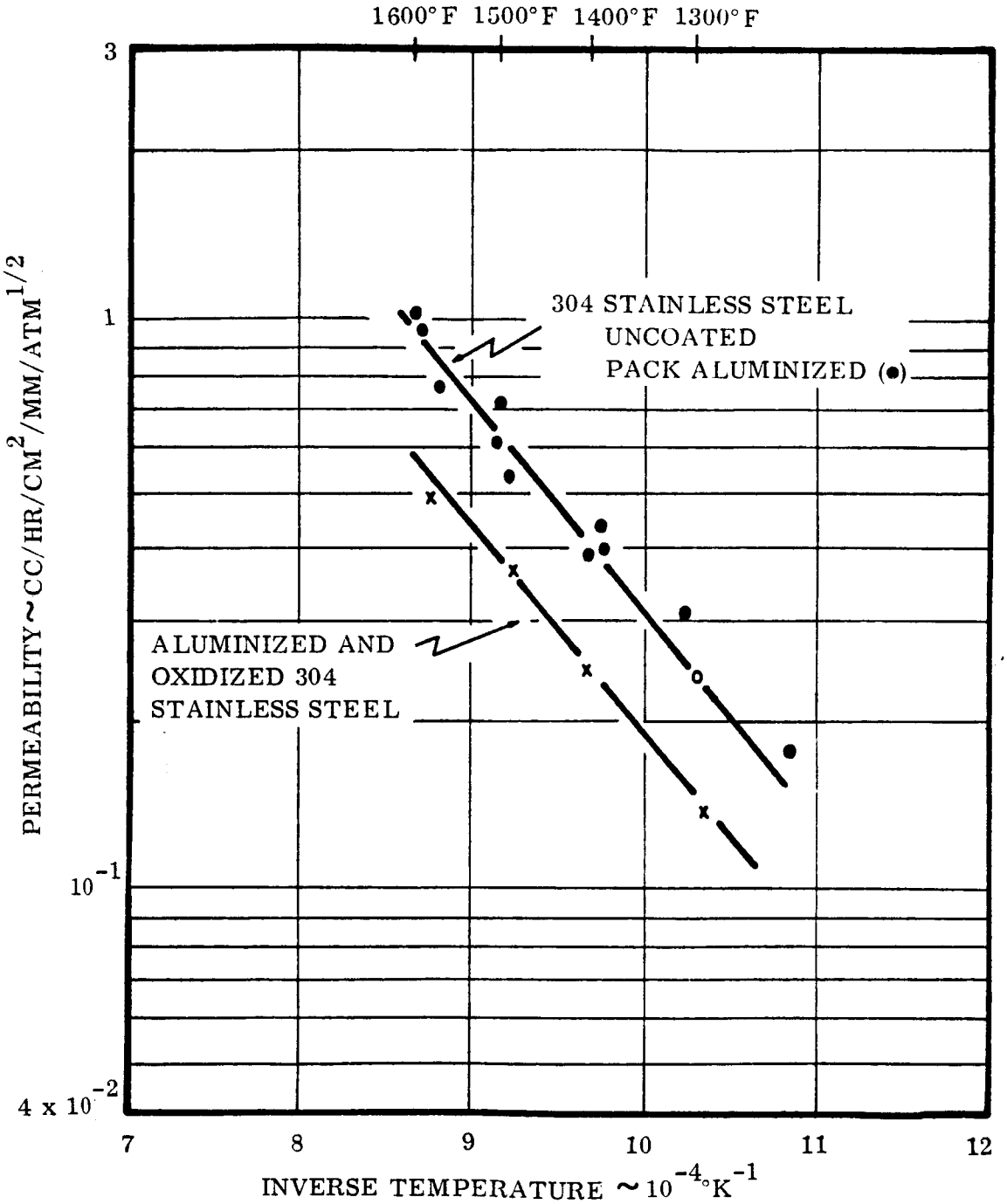

FIGURE 30

PERMEABILITY OF 304 STAINLESS STEEL AND ALUMINIZED 304 STAINLESS AS A FUNCTION OF TEMPERATURE

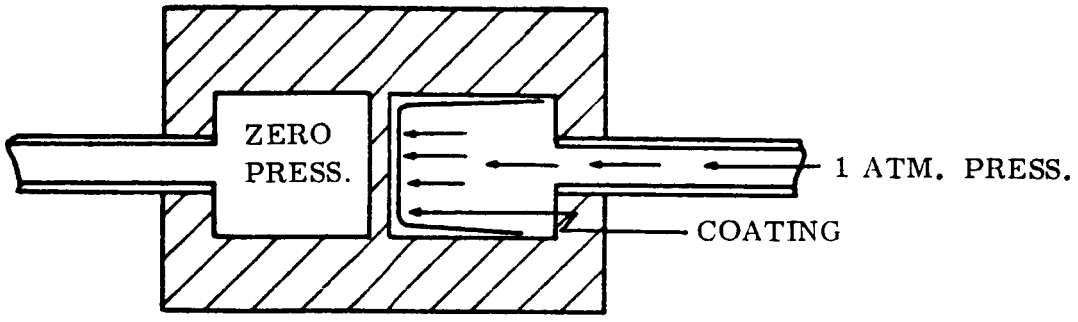

COATING ON INLET SIDE
DIAPHRAGM SUPPORTING COATING

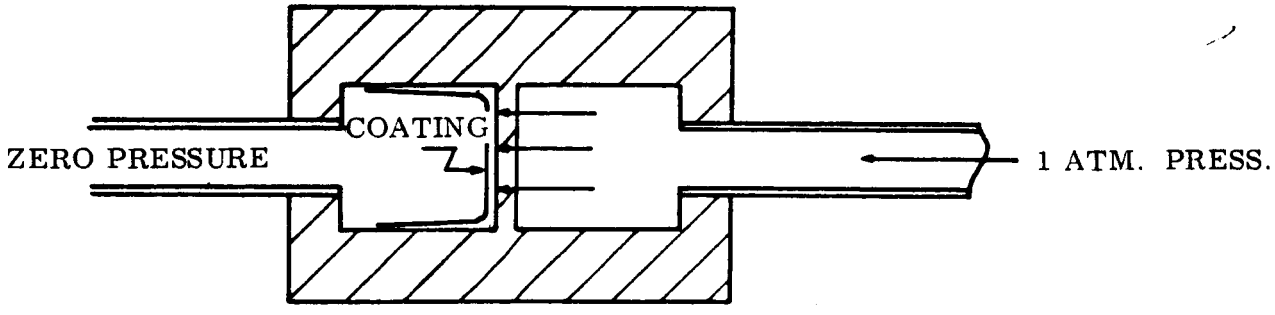

COATING ON OUTLET SIDE
NO DIAPHRAGM SUPPORT FOR BRITTLE COATING

FIGURE 31

POSSIBLE ORIENTATIONS OF COATING WITH RESPECT
TO DIFFUSING GAS PRESSURE

a. A. O. Smith

b. Nucerite

c. Bettinger

d. Engineered Ceramic, and

e. Solaramic.

a. A. O. Smith Coatings

The A. O. Smith #3308 glass coating recently was developed for operation at temperatures up to 1500°F. In this evaluation, emphasis was placed on the capabilities of this coating to retard hydrogen at temperatures up to 1600°F and under cyclic temperature conditions. The coating variables studied are summarized in Table VIII.

TABLE VIII

A. O. SMITH GLASS COATINGS EVALUATED

Chamber	Base Material	Thickness (in) Coating	Base Metal	Coating Type
1	304 SS	.004	.038	#3308
2	304 SS	.025	.040	#3308 plus NiO ground coat
3	Haynes 25	.040	.040	#3308 plus NiO ground coat
4	304 SS	.014	.025 + .009	Sandwich structure; #3308 between two metal layers.

The flow of hydrogen through the various A. O. Smith glass-coated chambers is presented in Figure 32. The thin A. O. Smith glass coatings which range in thickness from approximately 0.004 inch to 0.009 inch (chambers 1 and 4) exhibited higher rates of hydrogen passage than the diaphragms with the thicker coatings (chambers 2 and 3). This variation in hydrogen flux between the thick and thin coatings was eliminated after the specimens were exposed to approximately 140 hours of test time in the hydrogen permeability apparatus. As shown in Figure 33, the hydrogen flux for chamber #1 with the thin coating decreased as a function of test time and approached the values obtained for the thicker coating. This behavior was believed to be due to a general healing of small imperfections in the thin glass coating. Continuous imperfections of this type which pass through the coating are not generally found in the thicker barriers (12).

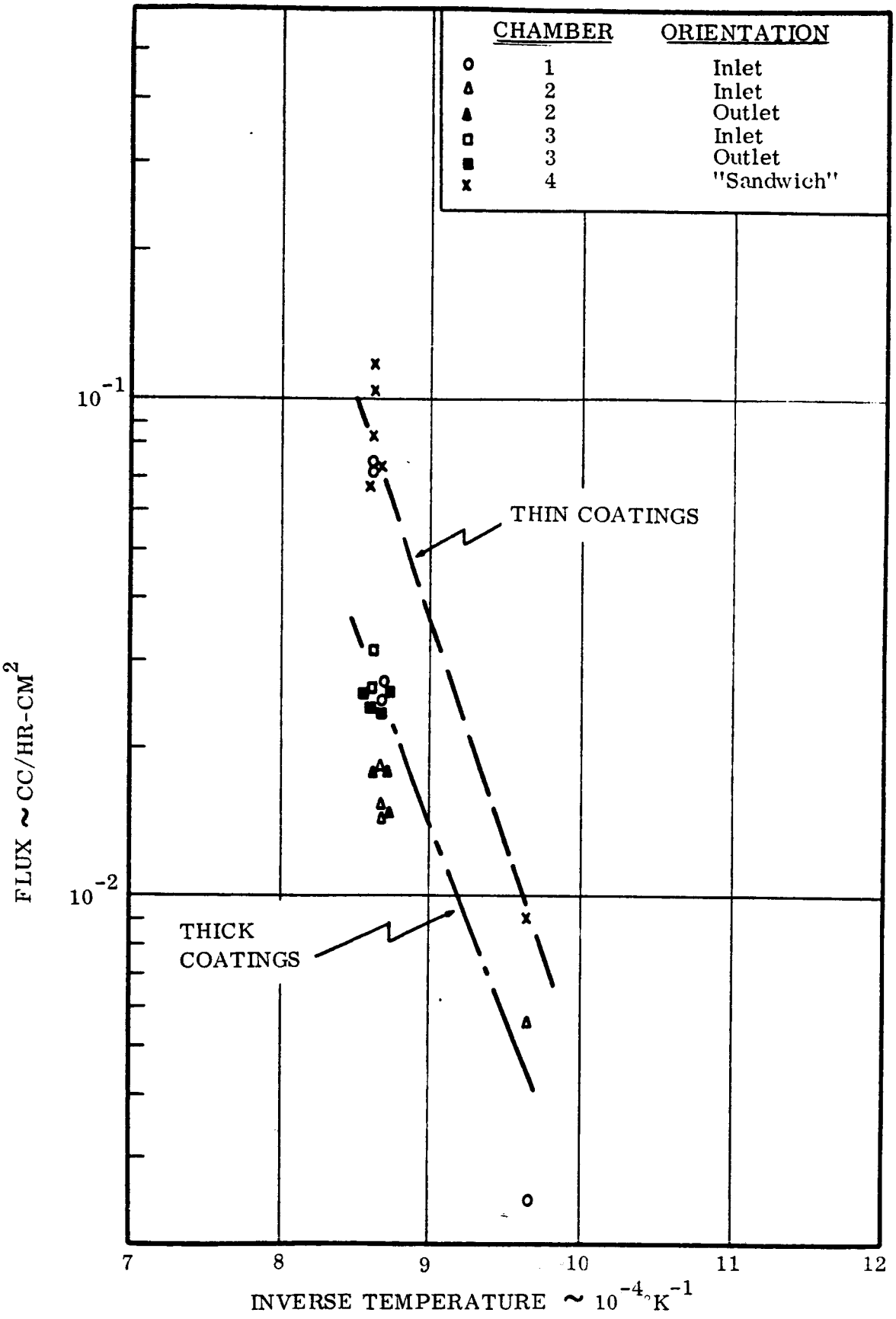

FIGURE 32

PERMEABILITY OF HYDROGEN THROUGH CHAMBERS
COATED WITH A. O. SMITH #3308 GLASS

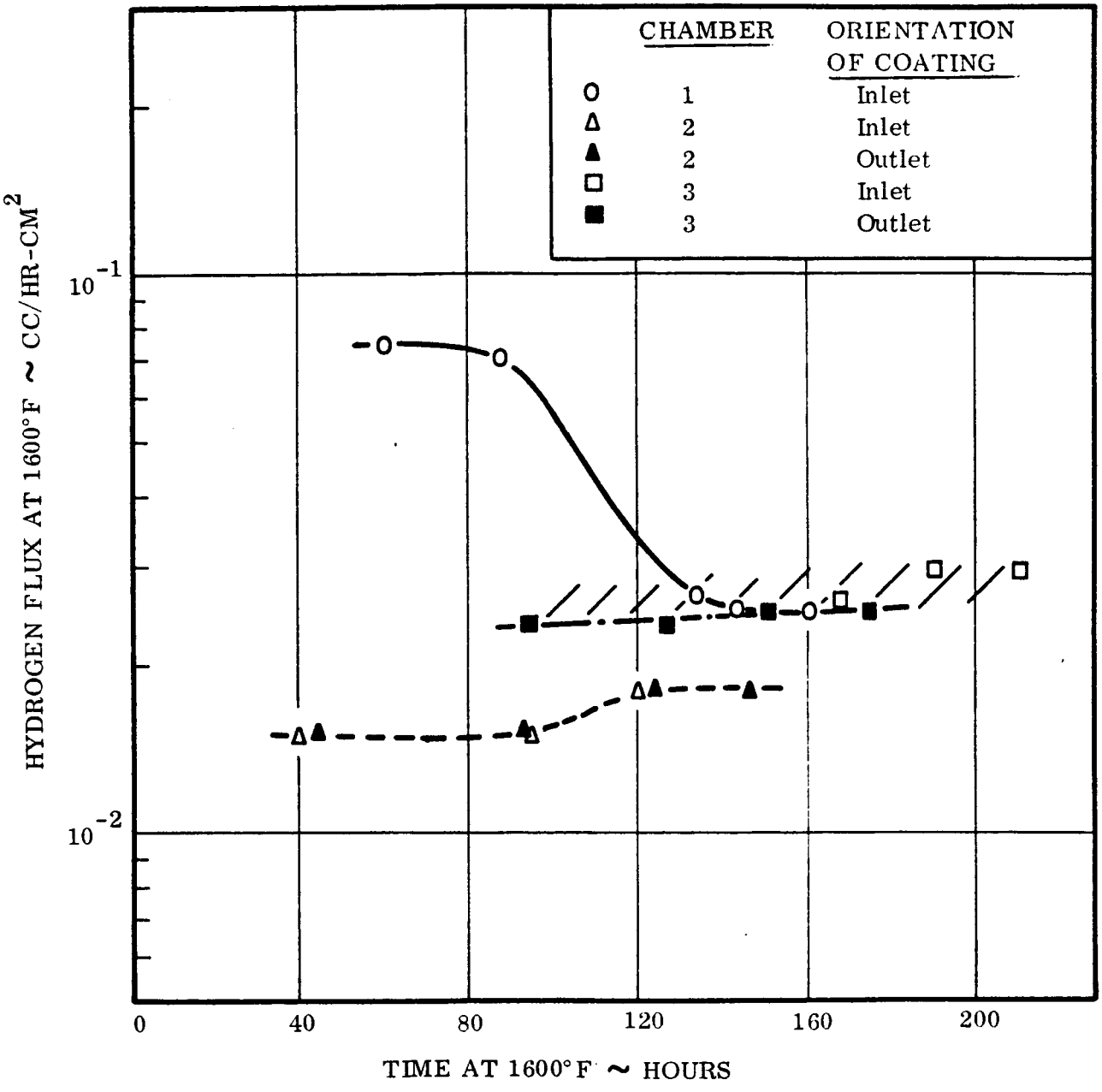

FIGURE 33

VARIATION OF HYDROGEN PERMEABILITY THROUGH CHAMBERS COATED WITH A. O. SMITH GLASS #3308

A NiO ground coat was applied on two of the diaphragms in an effort to increase the bondability of the coating and the mechanical stability during cyclic temperature conditions. The mechanical deterioration of the A. O. Smith #3308 with no precoat after cyclic exposure (325 cycles between 1200 and 1600°F) is shown in Figure 34. This treatment produced extensive fissuring and mechanical spalling. The use of NiO precoat minimized the degree of fissuring which occurred during cyclic testing but did not eliminate it (see Figure 35). This fissuring which occurred as a result of many temperature cycles produced almost complete elimination of the hydrogen barrier.

b. Nucerite* Coatings

Three types of Nucerite coatings were evaluated:

i) Nucerite SC-30 oriented on outlet side (chamber 1) and inlet side (chamber 2).

ii) Nucerite RD-30 oriented on outlet side.

iii) Nucerite Special oriented on inlet side.

In all cases when the coating was oriented on the outlet side (Nucerite SC-30, chamber 1 and Nucerite RD-30), considerable spalling occurred and the coating offered virtually no resistance to hydrogen flow. Permeability measurements obtained on the diaphragm coated with Nucerite SC-30 and oriented on the outlet side are presented in Figure 36. Marked deterioration of the barrier occurred with each measurement cycle. The appearance of the coating after testing is shown in Figure 37. The chamber coated with Nucerite RD-30 oriented on the outlet side showed virtually no barrier to hydrogen during the first test at 1600°F. The coating was extensively spalled after this short-time test (see Figure 38).

The Nucerite SC-30 coating oriented on the inlet side exhibited a very interesting type of behavior. As shown in Figures 39 and 40, the permeability decreased with increasing test time and the magnitude of the decrease was almost an order of magnitude. After initially testing the Nucerite SC-30 chamber #2 for approximately 250 hours with the coating on the inlet side, the specimen was reversed. Under these conditions, the permeability was slightly increased but was considerably below that previously experienced (compare Figures 36 and 39). Apparently the initial testing with the coating on the inlet side had stabilized the coating and improved its bondability so that it maintained its mechanical integrity and barrier properties when retested in the outlet position. The appearance of the coating changed from glossy to metallic, and these were some indications that certain coating constituents had melted.

*Nucerite is a trade name of a special glass coating developed by the Pfaudler Company. The coating composition and processing methods are proprietary.

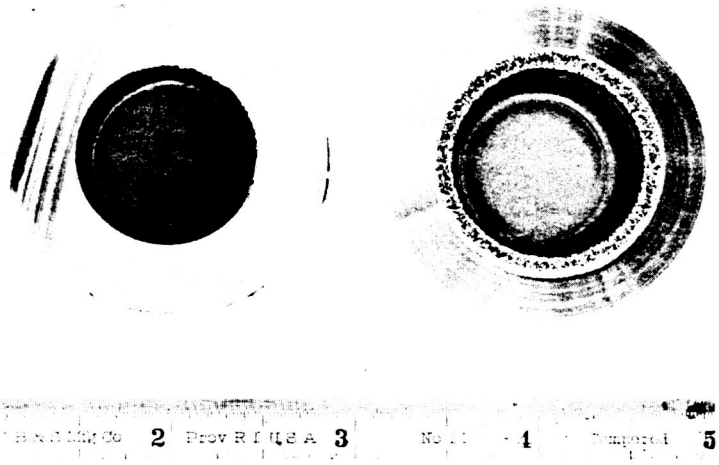

05716

AFTER TEST BEFORE TEST

FIGURE 34A

APPEARANCE OF A. O. SMITH GLASS COATING BEFORE AND AFTER PERMEABILITY TESTS, GLASS ON OUTLET SIDE

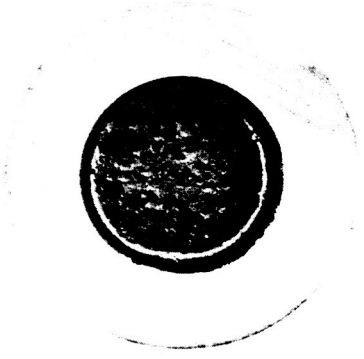

05783

FIGURE 34B

APPEARANCE OF A. O. SMITH GLASS COATING AFTER 325 CYCLES BETWEEN 1200°F AND 1600°F

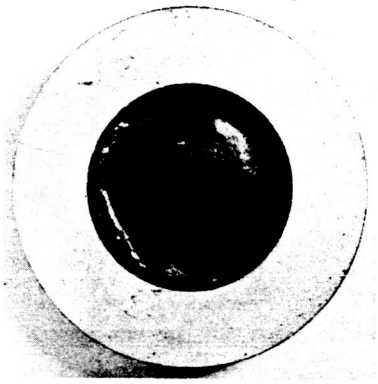

06953-1

CHAMBER #2, NiO PRECOAT
ON 304 STAINLESS STEEL

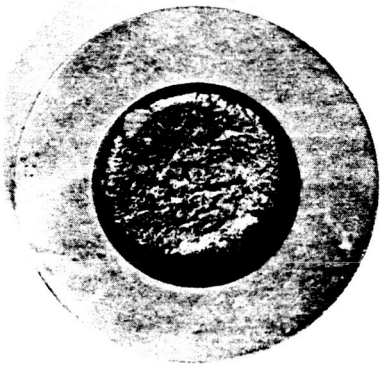

06953-3

CHAMBER #1, THIN COAT
ON 304 STAINLESS STEEL

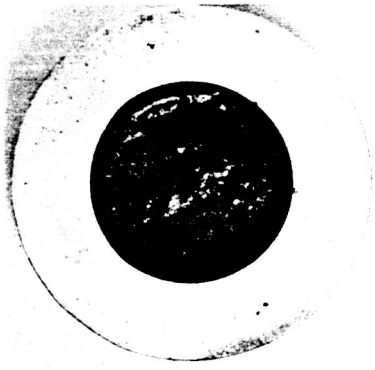

06953-2

CHAMBER #3, NiO PRECOAT
ON HAYNES 25

FIGURE 35

INFLUENCE OF NiO PRECOAT ON THE SPALLING TENDENCY OF A. O. SMITH GLASS COATING EXPOSED 103 CYCLES BETWEEN 1165°F AND 1600°F

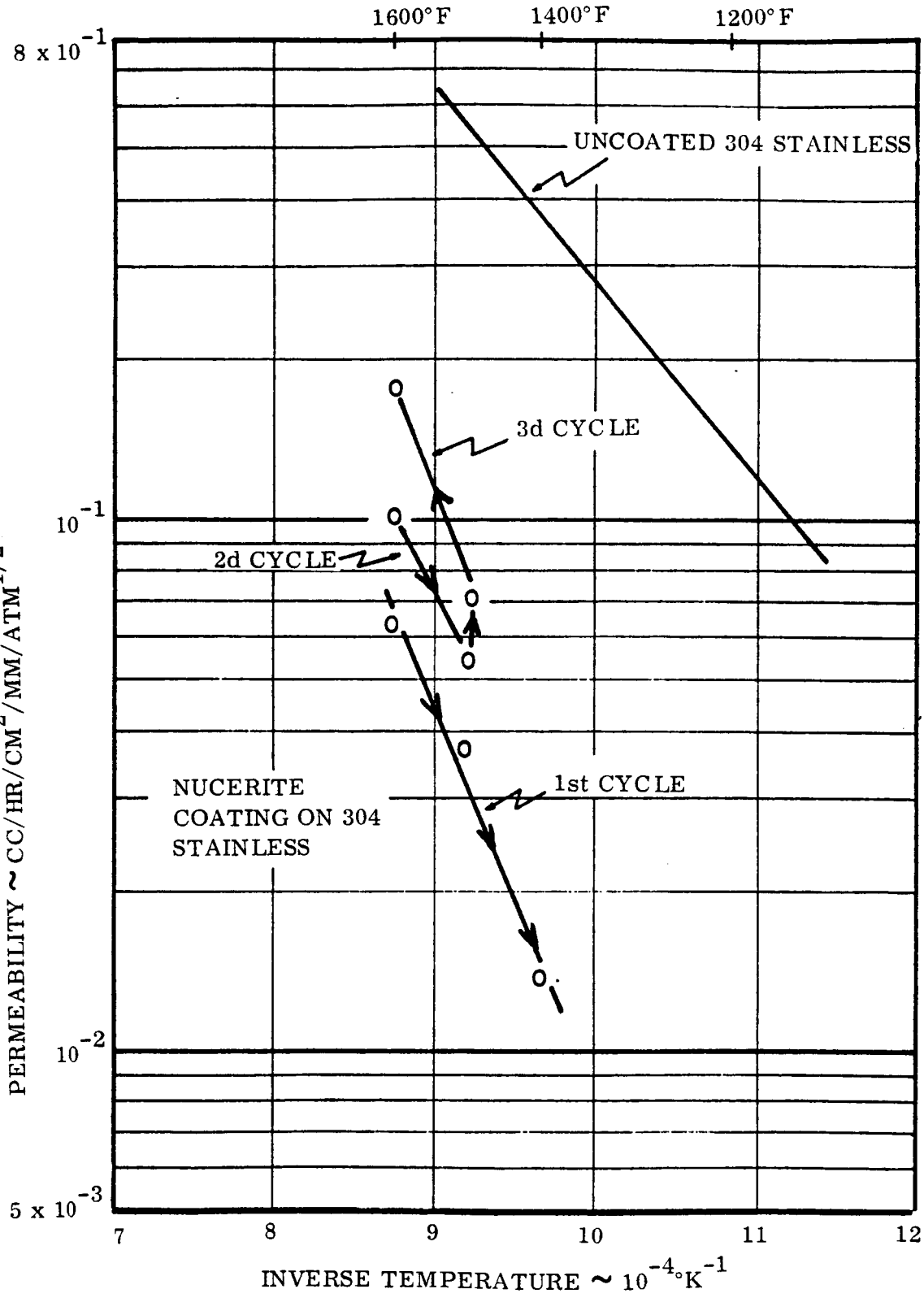

FIGURE 36

PERMEABILITY OF HYDROGEN THROUGH 304 STAINLESS STEEL COATED WITH NUCERITE SC-30, INITIALLY TESTED WITH COATING ON INLET SIDE

05843

FIGURE 37

APPEARANCE OF SPECIMEN COATED WITH NUCERITE SC-30 AFTER PERMEABILITY TESTING, COATING ORIENTED ON OUTLET SIDE

06459

FIGURE 38

APPEARANCE OF SPECIMEN COATED WITH NUCERITE RD-30 AFTER PERMEABILITY TESTING, COATING ORIENTED ON OUTLET SIDE. 2X

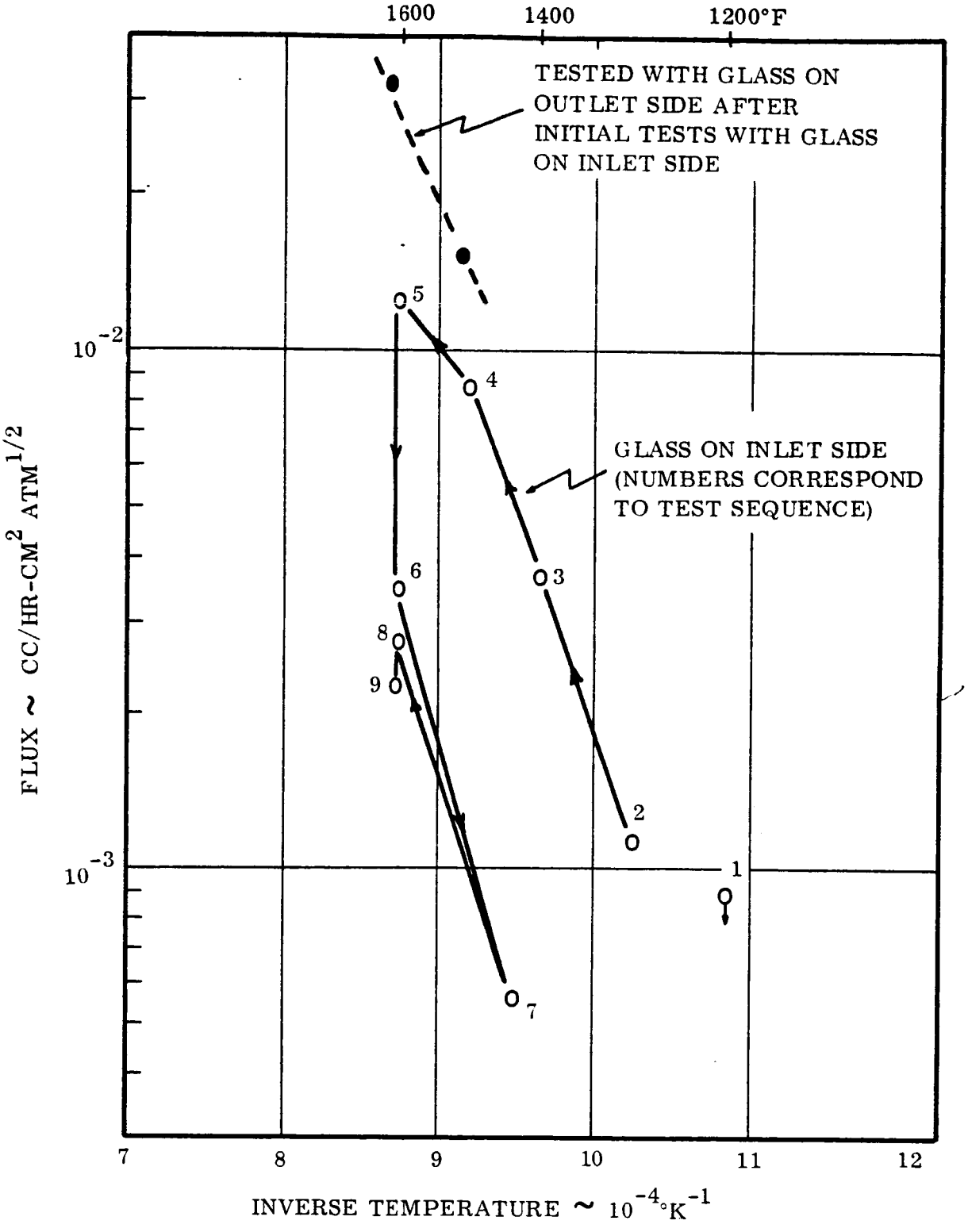

FIGURE 39

PERMEABILITY OF HYDROGEN THROUGH 304 STAINLESS STEEL COATED WITH NUCERITE SC-30, INITIALLY TESTED WITH COATING ON INLET SIDE

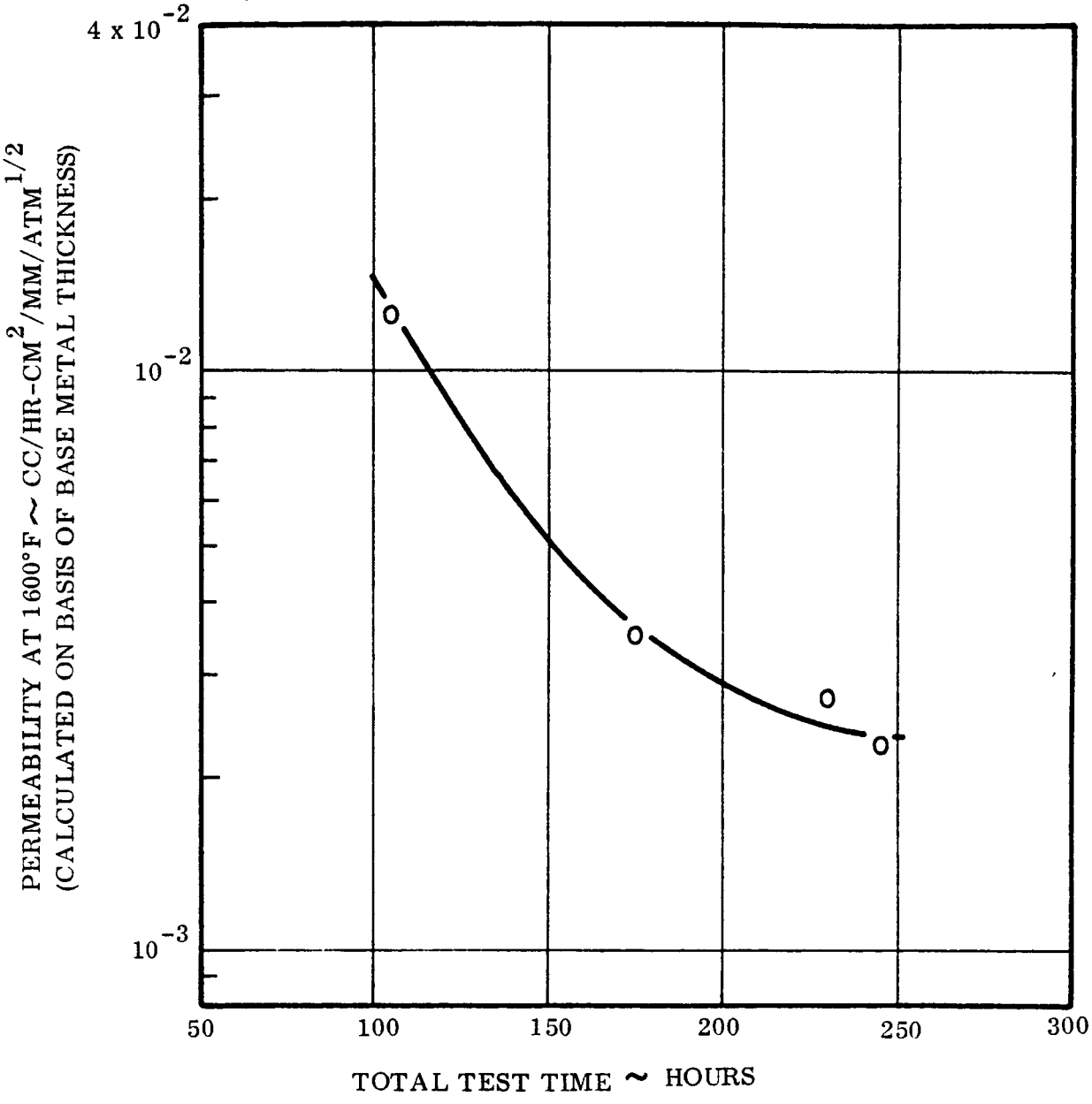

FIGURE 40

VARIATION OF PERMEABILITY WITH TIME.
NUCERITE SC-30 COATING, COATING ON INLET SIDE

The flow of hydrogen through the diaphragm coated with the Nucerite Special glass is summarized in Figure 41. The barrier properties did not increase with increasing test time, as was the case for the Nucerite SC-30. In addition, the overall hydrogen flux through the special coating was somewhat greater than in the tests on the Nucerite SC-30 coating.

c. Bettinger Glass Coatings

The hydrogen flow through two Bettinger glass coatings, designated as B-green and B-gray, applied to 304 stainless steel is summarized in Figure 42. The coatings were oriented on the outlet side. The B-gray coating produced slightly lower values of hydrogen flow than the B-green glass, however, this material exhibited a rather large degree of scatter and some deterioration in barrier properties. The variation of hydrogen flux through the chamber coated with the B-gray glass as a function on hydrogen pressure is presented in Figure 43. The hydrogen flow varied as a function of pressure to the 0.79 power. This exponent is higher than the square root dependence exhibited by metals and approximates the unity exponent which characterizes the molecular flow of hydrogen through glasses.

d. Engineered Ceramics Coating

The flow of hydrogen through a 304 stainless steel diaphragm coated with the Engineered Ceramics barrier is summarized in Figure 44. When the coating was oriented on the inlet side, the initial hydrogen flux at 1300°F was relatively low, however, at higher temperatures the flow increased and there appeared to be some degradation in the barrier properties as a result of exposing the coating to the 1600°F temperature. When the coating was oriented on the outlet side, its initial permeability to hydrogen was comparable to that obtained with the reverse orientation, however, a progressive deterioration of the barrier properties occurred as a function of increasing test time at 1600°F.

e. Solaramic Glass Coatings

The permeability of hydrogen through Solaramic-coated 304 stainless steel and Haynes 25 is shown in Figures 45 and 46. The time-temperature cycles which preceded each test run are shown in Figures 47 and 48. The permeability of hydrogen through the Solaramic-coated diaphragm fell within a well-defined scatter band. Gradual deterioration of the barrier properties of the coating occurred during the initial tests, however, the hydrogen flow eventually stabilized. Comparative permeability results obtained from other investigators (13) using a Hastelloy base metal are shown in Figure 49. In general, the results of the two sets of data are comparable and the barrier properties of the Solaramic coating appeared to be independent of coating orientation.

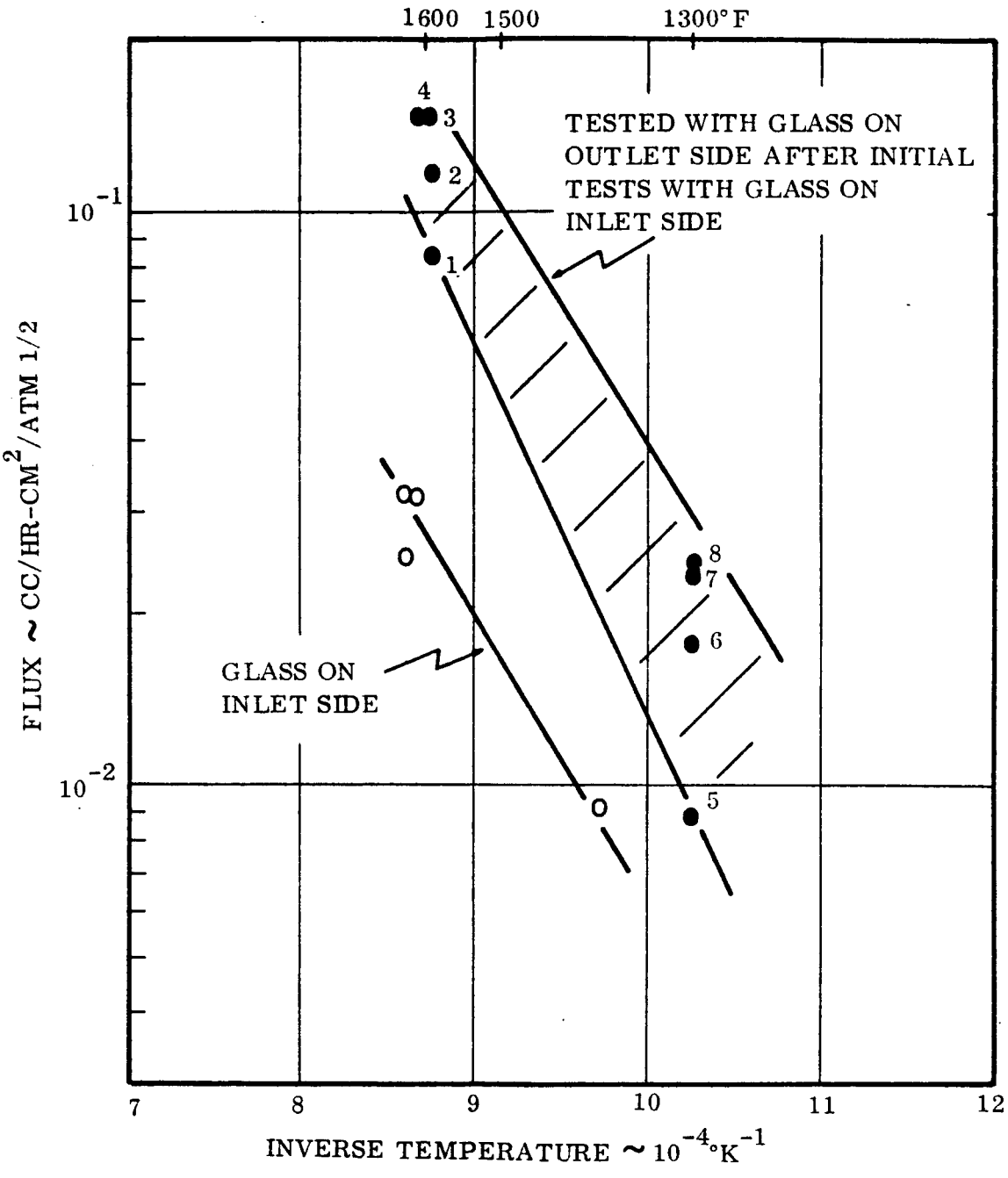

FIGURE 41

PERMEABILITY OF HYDROGEN THROUGH 304 STAINLESS STEEL COATED WITH NUCERITE SPECIAL GLASS. SPECIMEN INITIALLY TESTED WITH COATING ON INLET SIDE

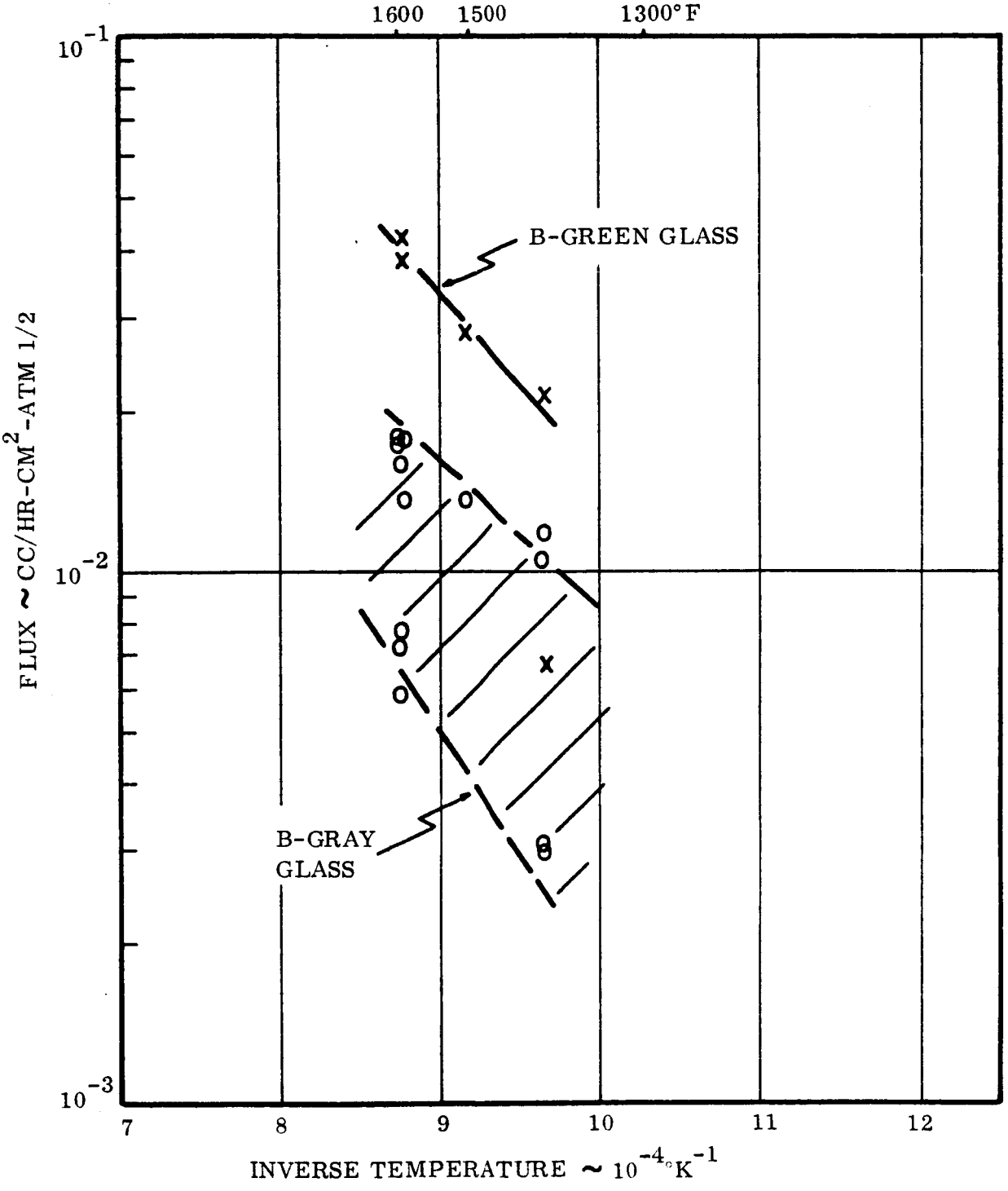

FIGURE 42

PERMEABILITY OF HYDROGEN THROUGH 304 STAINLESS STEEL COATED WITH BETTINGER GLASSES. COATINGS ORIENTED ON OUTLET SIDE

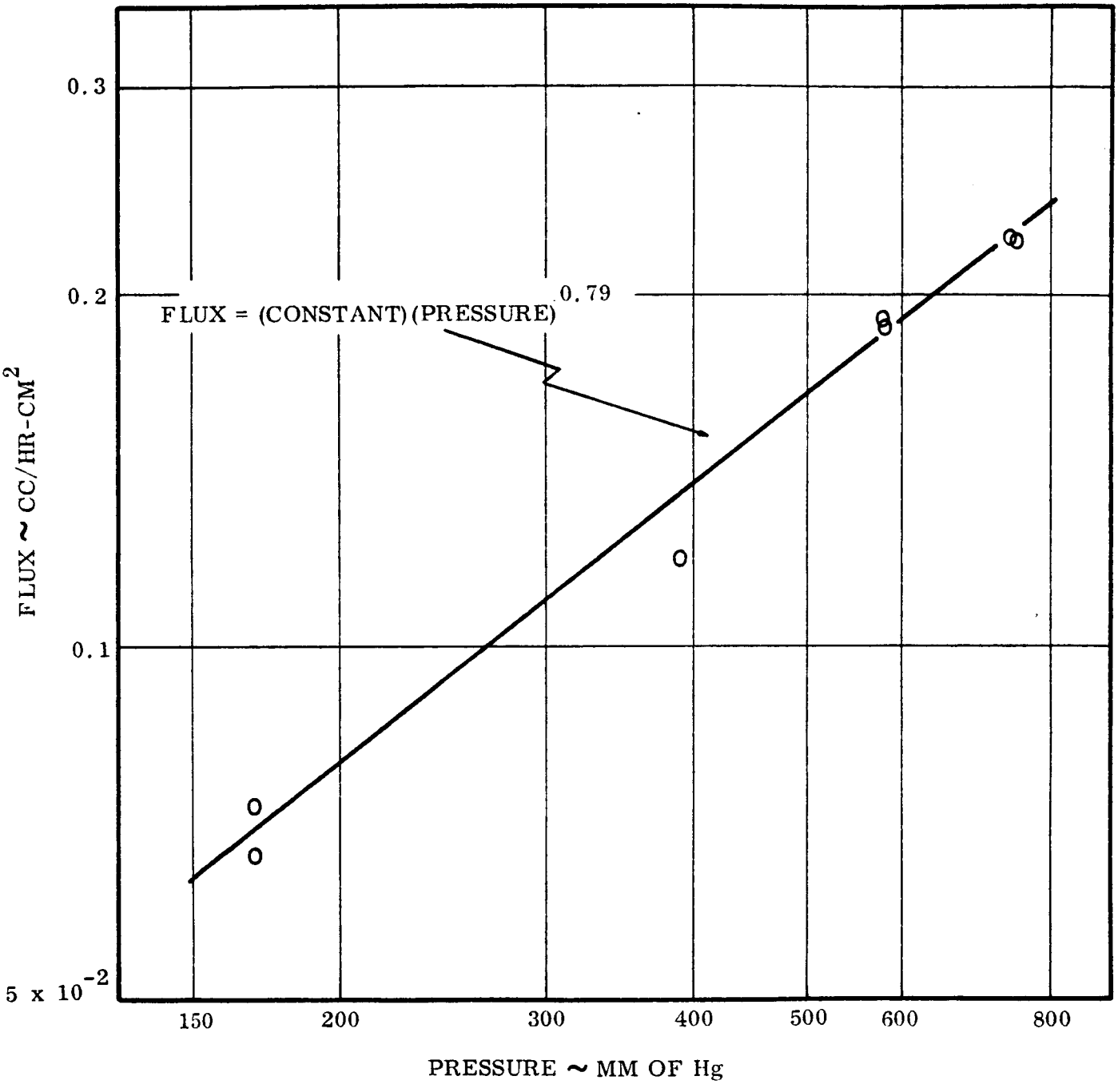

FIGURE 43

INFLUENCE OF PRESSURE ON HYDROGEN FLUX THROUGH
304 STAINLESS STEEL CHAMBER COATED WITH BETTINGER GRAY GLASS

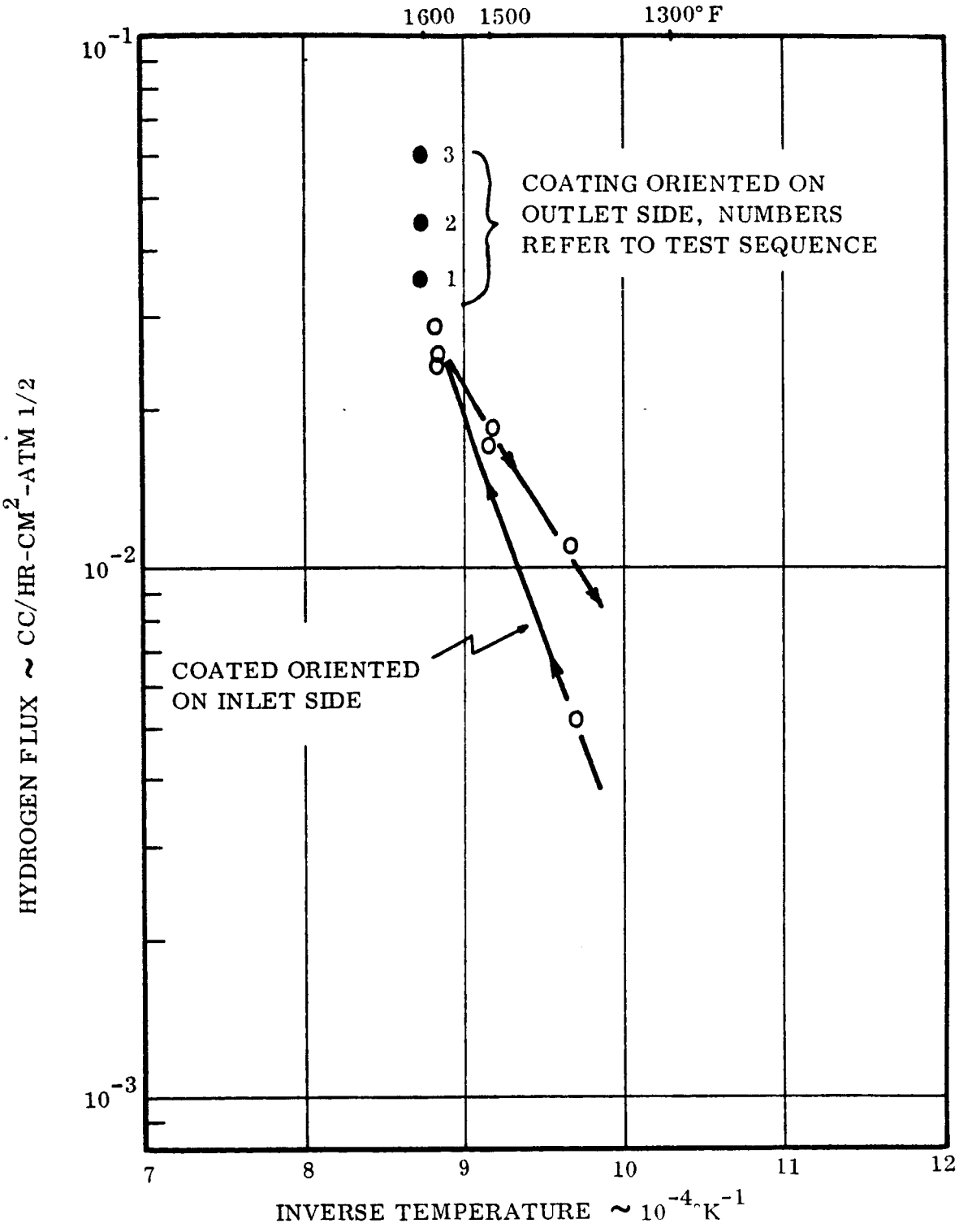

FIGURE 44

PERMEABILITY OF HYDROGEN THROUGH 304 STAINLESS STEEL COATED WITH ENGINEERED CERAMICS BARRIER

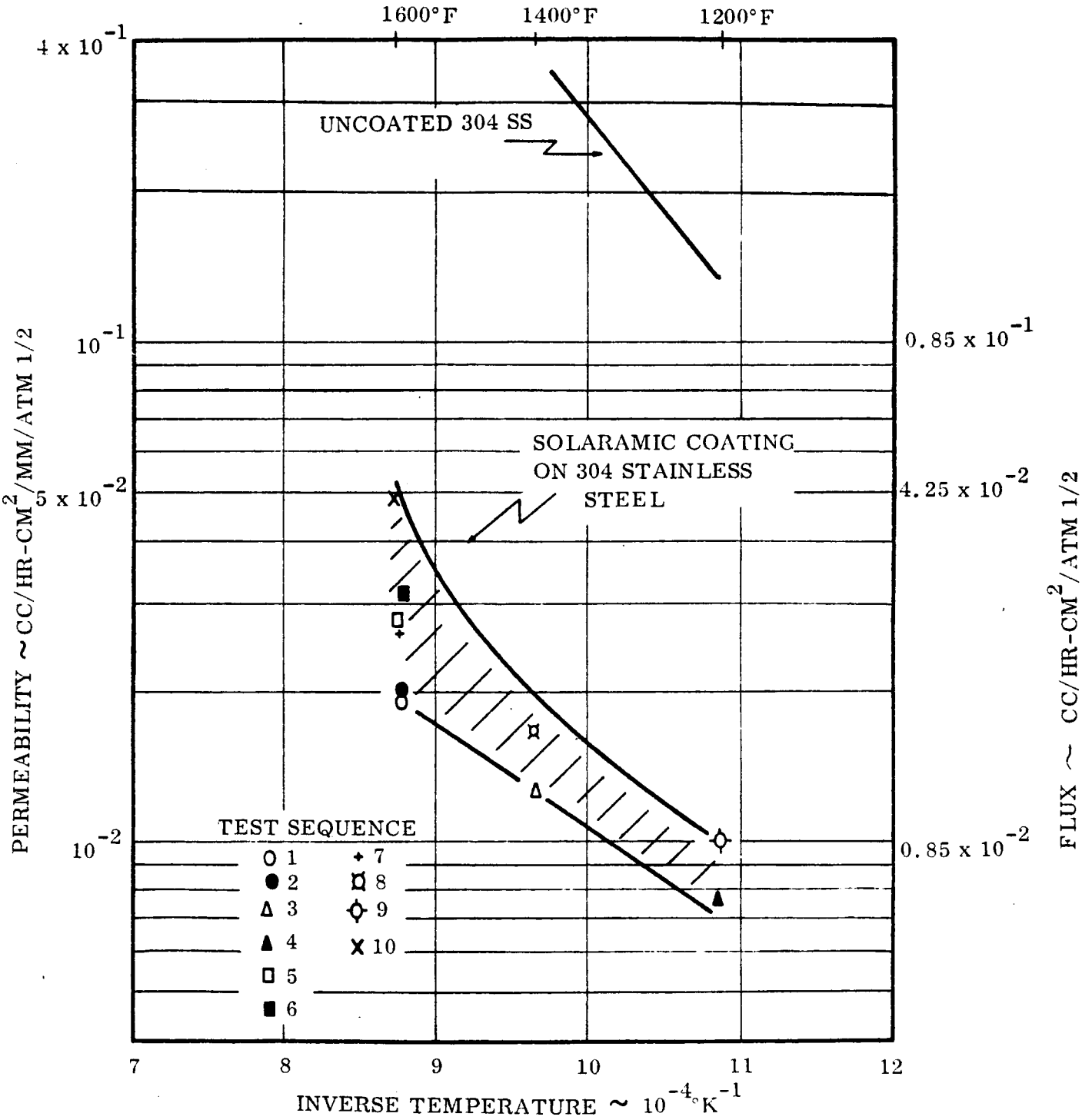

FIGURE 45

PERMEABILITY OF HYDROGEN THROUGH SOLARAMIC-COATED 304 STAINLESS STEEL. COATING ON OUTLET SIDE

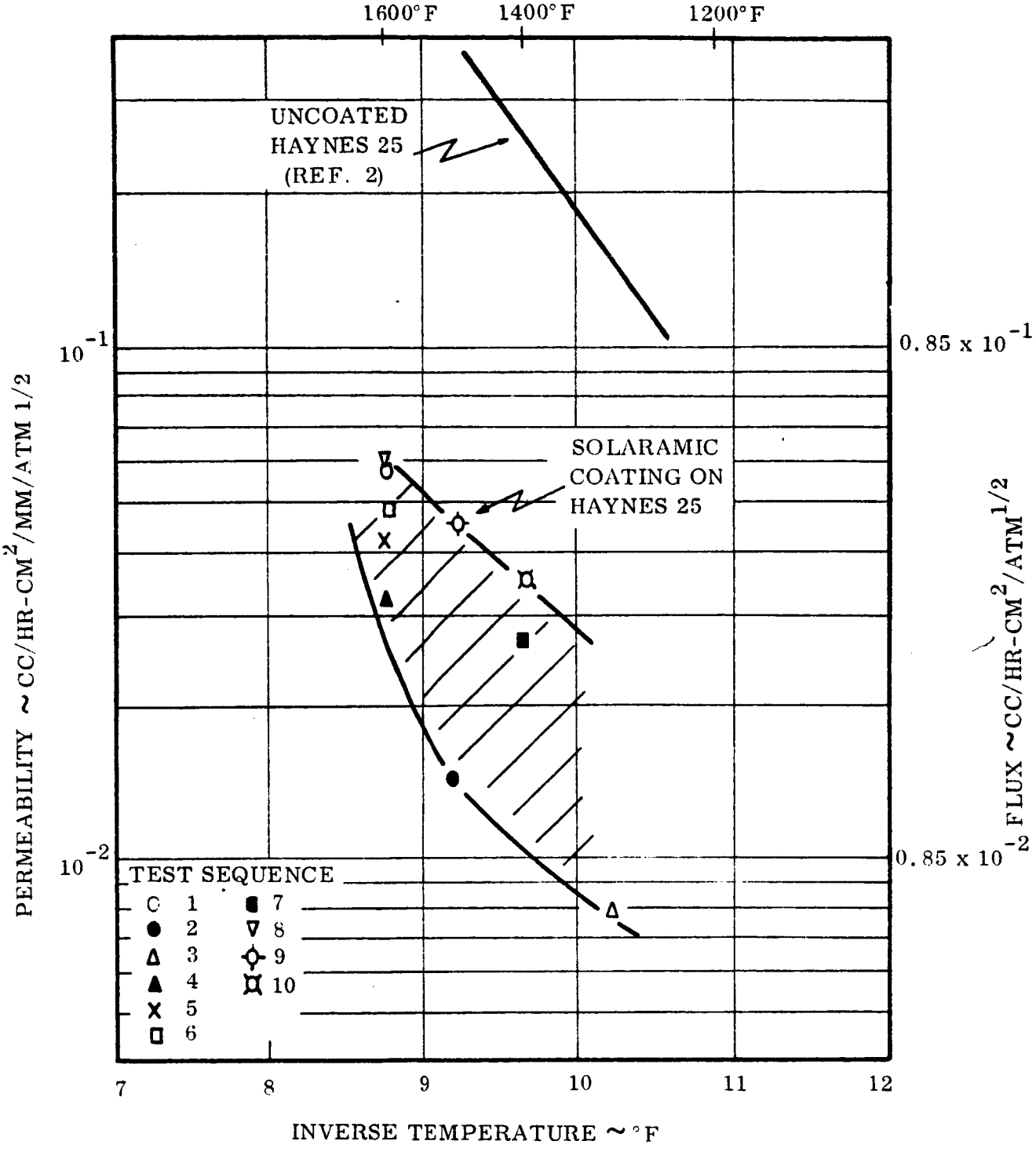

FIGURE 46

PERMEABILITY OF HYDROGEN THROUGH SOLARAMIC-COATED HAYNES 25. COATING ON OUTLET SIDE

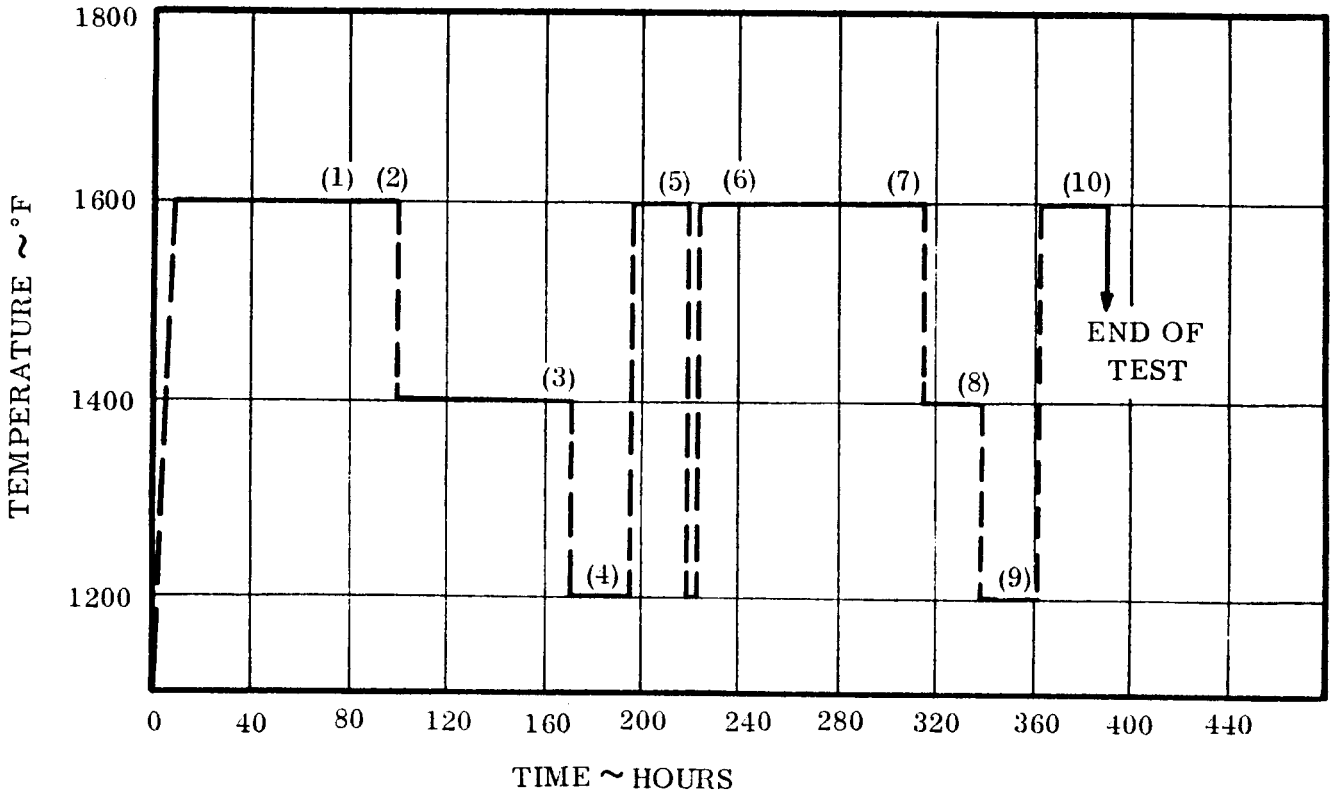

FIGURE 47

SEQUENCE OF TEST TIME AND TEMPERATURES USED TO EVALUATE PERMEABILITY OF HYDROGEN THROUGH SOLARAMIC-COATED 304 STAINLESS STEEL. NUMBERS IN PARENTHESES INDICATE EXPERIMENTAL RUNS AND CORRESPOND TO TEST POINTS IN FIGURE 45.

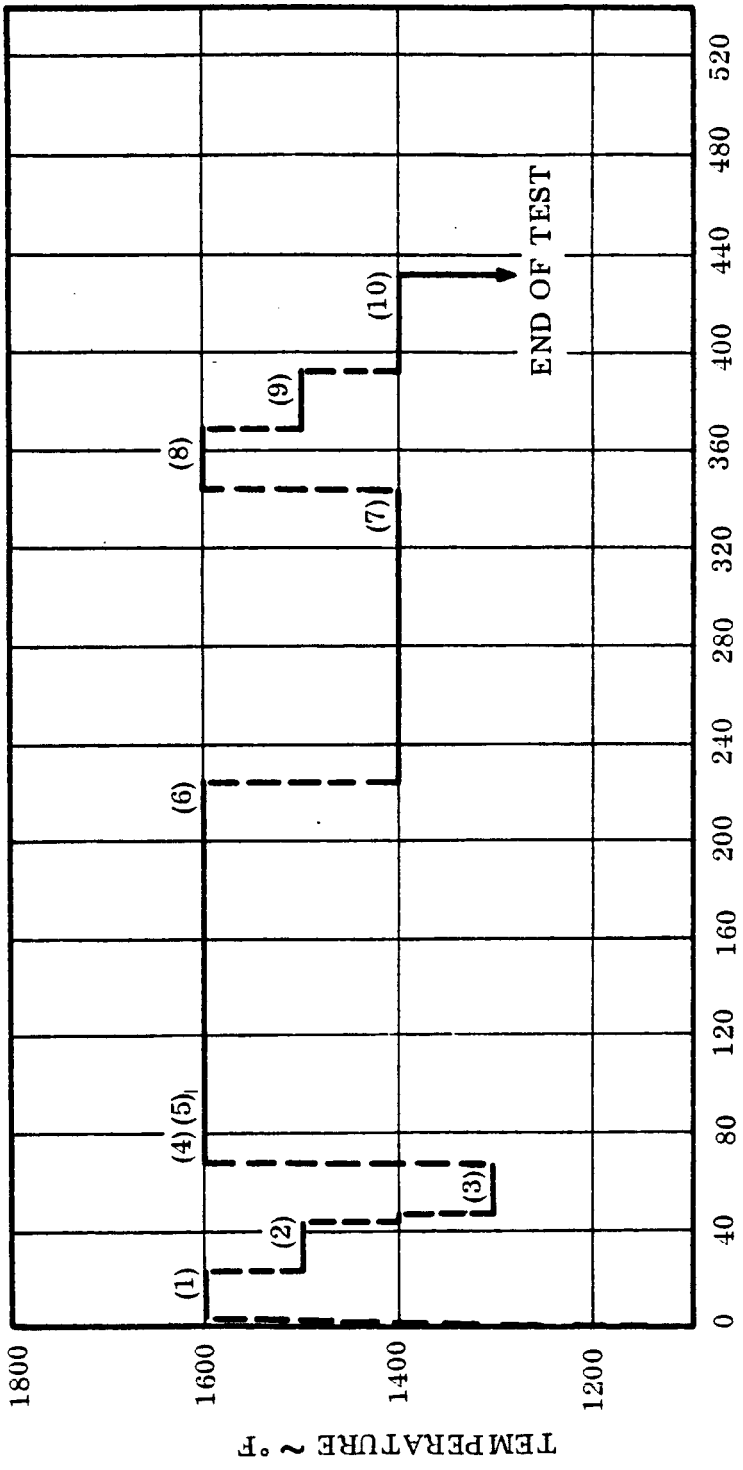

FIGURE 48

SEQUENCE OF TEST TIME AND TEMPERATURES USED TO EVALUATE PERMEABILITY OF HYDROGEN THROUGH SOLARAMIC-COATED HAYNES 25. NUMBERS IN PARENTHESES INDICATE EXPERIMENTAL RUNS AND CORRESPOND TO TEST POINTS IN FIGURE 46

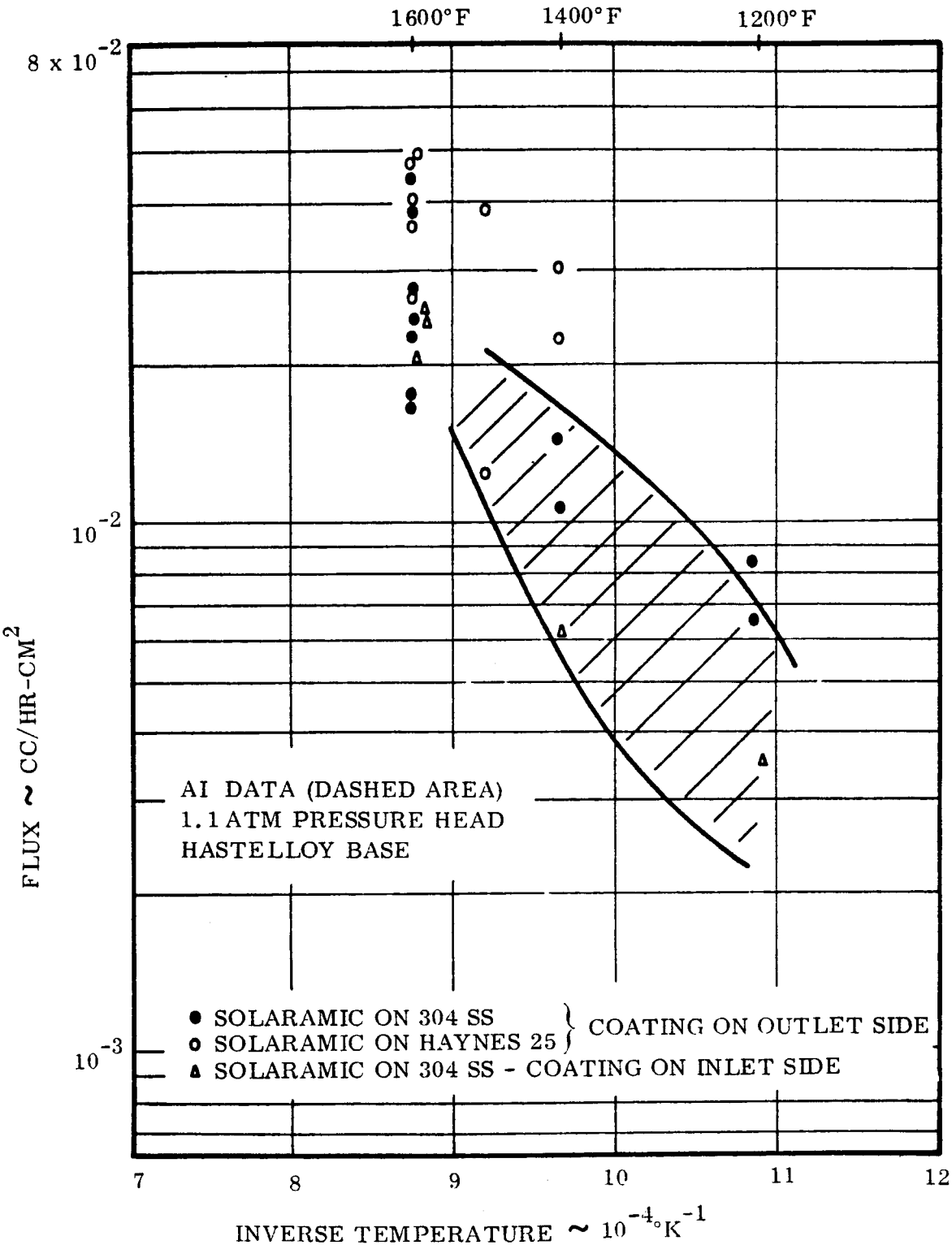

FIGURE 49

COMPARISON OF TRW HYDROGEN PERMEABILITY DATA FOR SOLARAMIC-COATED CHAMBERS WITH ATOMICS INTERNATIONAL DATA (REF. 13)

Studies conducted to determine the long-time stability properties of the Solaramic coating in a vacuum environment (1) indicated that a certain portion of the exterior section of the coating often spalls, but a well-bonded surface layer remains and this appears to provide the major portion of barrier properties. The variation of microstructures which occurs in the Solaramic coating as a result of 370 hours exposure at 1600°F is shown in Figure 50. The coating exhibited some change in microstructure as a result of exposure and an increase in the degree of bonding to the base metal.

The influence of hydrogen pressure on the permeability is shown in Figure 51. The hydrogen flux through the Solaramic coating was directly proportional to the square root of pressure. This interesting and somewhat unexpected result indicates that a dissociation process occurs at the surface of the coating and the hydrogen diffuses as an atom (or proton) rather than a molecule. In this respect, the Solaramic-coated specimen behaves more like a metal than a glass.

Although the Sunflower boiler has been designed for use at 1600°F, there was some interest in raising the operating temperatures to 1700°F to increase the heat input to the boiler. In an effort to obtain the hydrogen permeability and coating stability at this higher temperature, permeability tests were conducted on Solaramic-coated 304 stainless steel diaphragms. The results of this study are summarized in Figure 52. The hydrogen flux markedly decreased as a function of test time at 1700°F. In fact, after approximately 70 hours of exposure at 1700°F, the permeability was actually less than it had been for the 1600°F tests. Examination of the coating by X-ray diffraction indicated that considerable crystallization of the glass had occurred as a result of the 1700°F exposure. Although the degree of glass crystallization and the structure varied as a function of exposure temperature, no systematic relationship was noted between coating structure and permeability.

In an effort to determine whether a 1700°F age prior to testing would significantly decrease the hydrogen permeability, three Solaramic-coated stainless steel chambers were aged in air for 15 hours at 1900°F, in vacuum for 100 hours at 1700°F and in air for 68 hours at 1700°F. As shown in Figure 53, the tests conducted on the three specially-processed, Solaramic-coated diaphragms indicated that these treatments did not improve, but rather decreased, the barrier properties of the Solaramic coating. The exact reason for the fact that aging during a test decreased the permeability at 1700°F while aging under the same conditions prior to testing did not improve the permeability at 1600°F is not known. One possible explanation for this behavior is the formation of a viscous film at 1700°F which is defect-free and more resistant to hydrogen passage than the glass at 1600°F. The crystallization which is apparent after the 1700°F treatment may occur during cooling and may not be representative of the structure at 1700°F. Another possibility is that some micro-fissuring may have occurred during the cooling period after the long-time pretreatment and prior to testing. This fissuring would not have been present in the first test sequence where the testing and aging were performed concurrently.

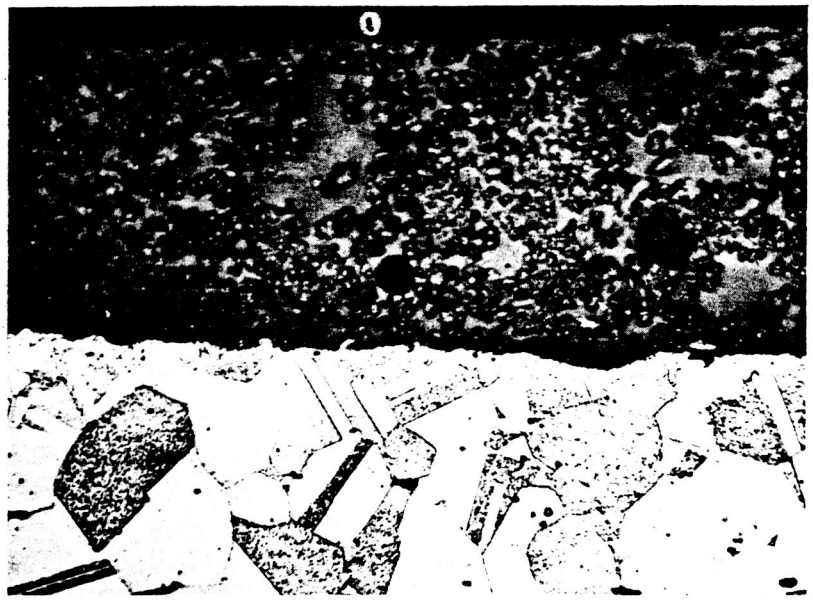

RDM 4791

A) MICROSTRUCTURE OF SOLARAMIC COATING BEFORE TESTING, 500X, CHROME REGIA + HF ETCH

RDM 4637

B) MICROSTRUCTURE OF SOLARAMIC COATING AFTER TESTING FOR 370 HOURS AT TEMPERATURES UP TO 1600°F

FIGURE 50
MICROSTRUCTURE OF SOLARAMIC-COATED STAINLESS STEEL BEFORE AND AFTER TESTING FOR HYDROGEN PERMEABILITY

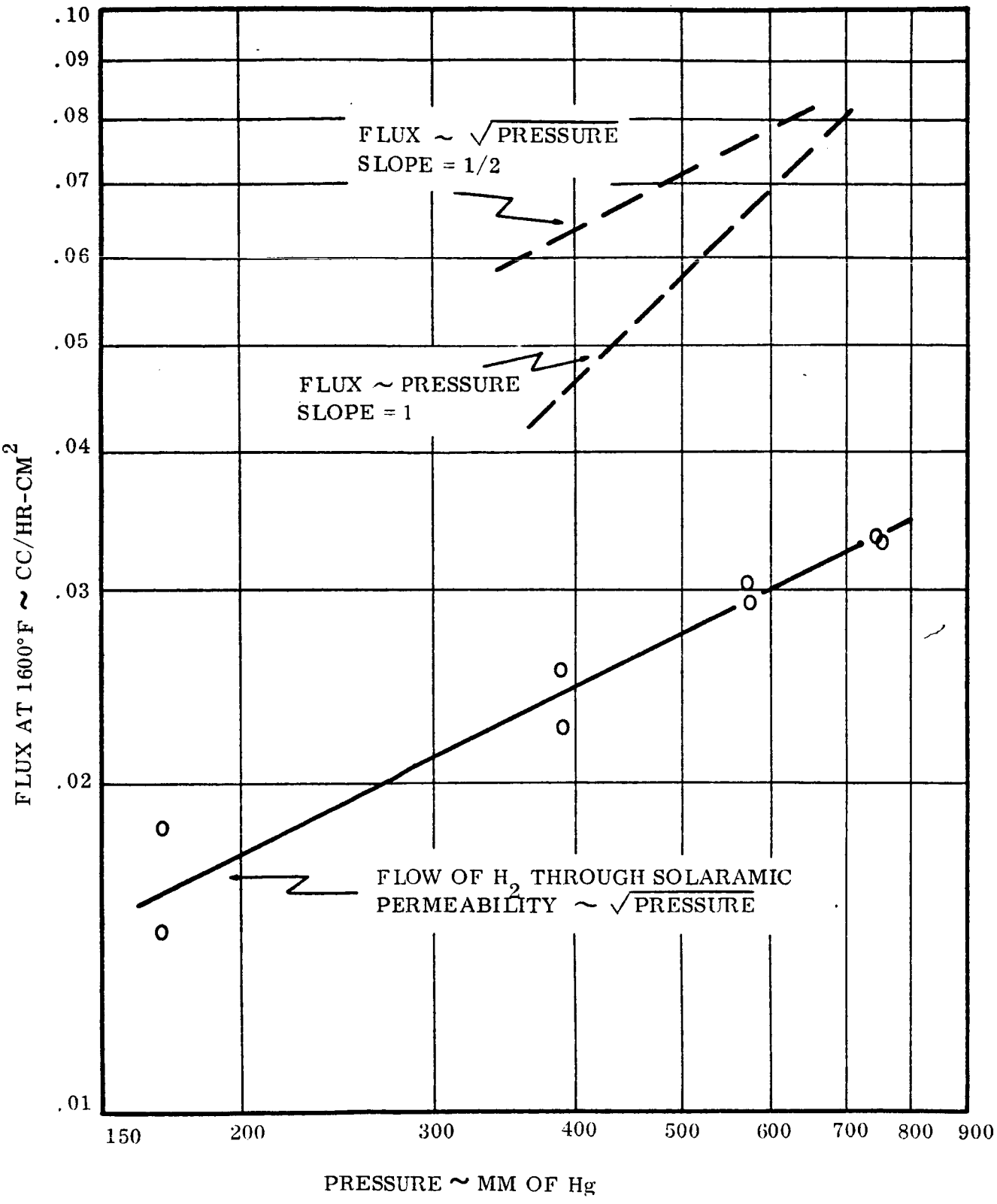

FIGURE 51
FLOW OF HYDROGEN THROUGH SOLARAMIC-COATED HAYNES 25 AT 1600°F

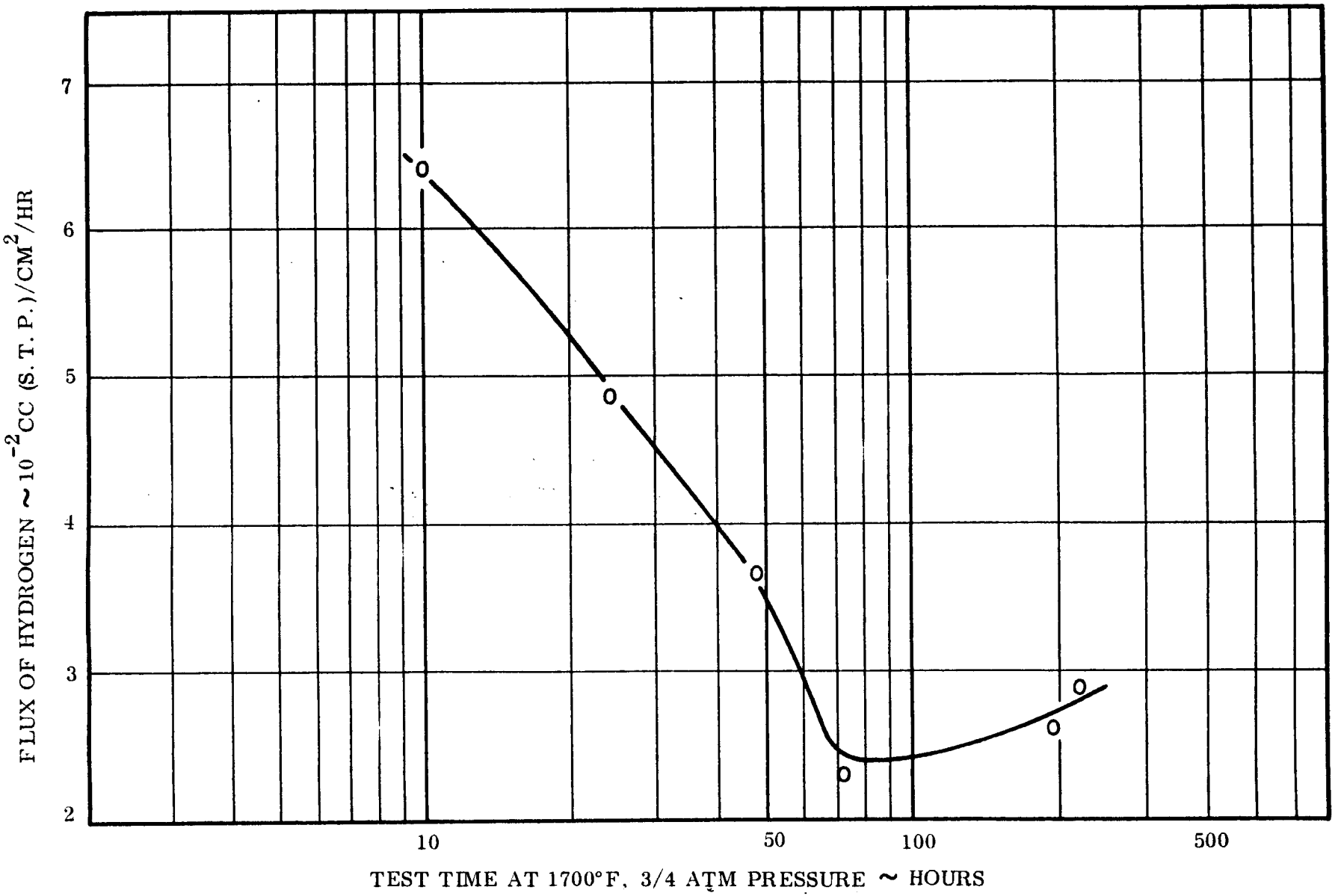

FIGURE 52

VARIATION IN HYDROGEN PERMEATION THROUGH SOLARAMIC-COATED CHAMBER AS A FUNCTION OF TEST TIME

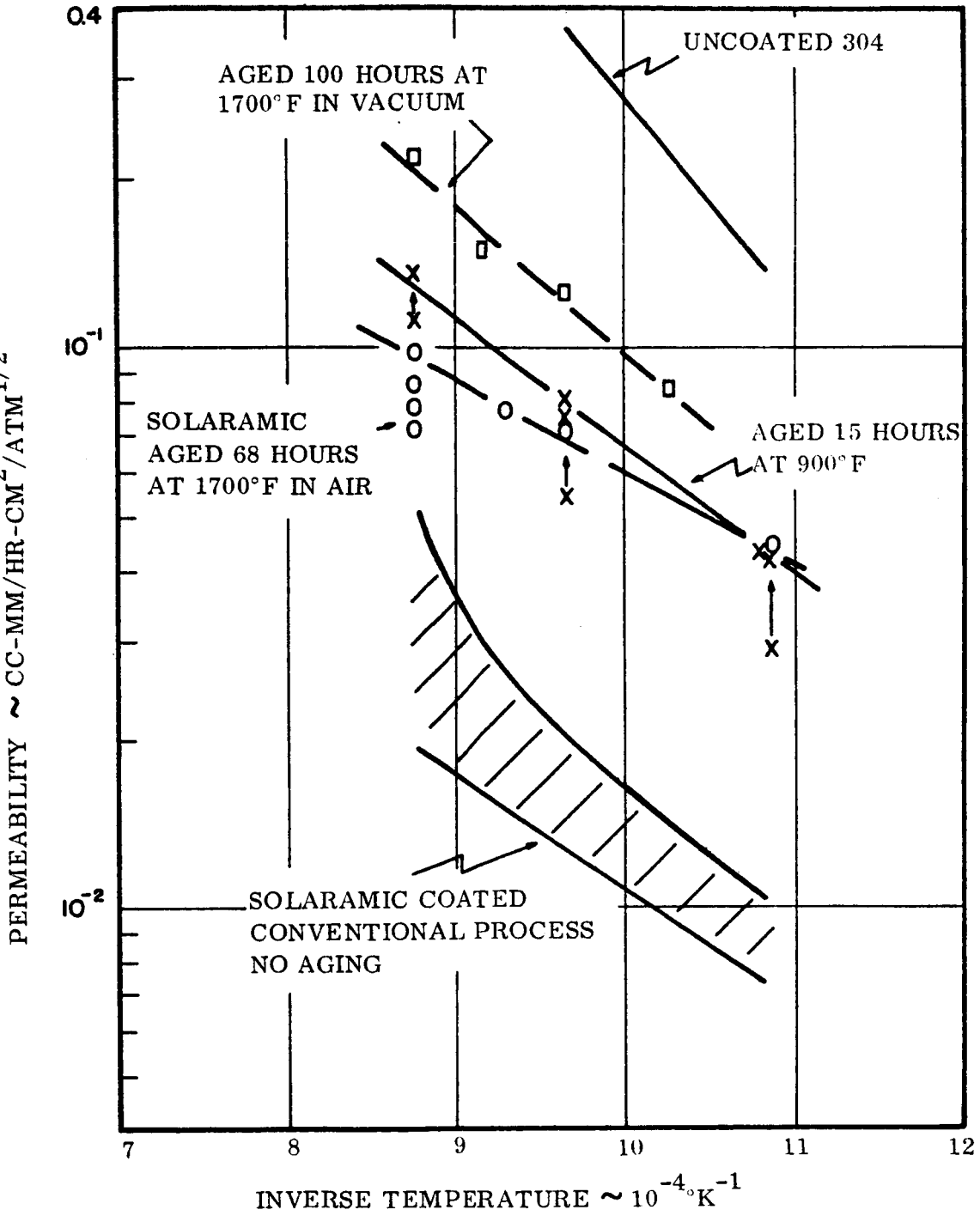

FIGURE 53

INFLUENCE OF VARIOUS PROCESSING TREATMENT ON THE PERMEABILITY OF HYDROGEN THROUGH SOLARAMIC-COATED 304 STAINLESS STEEL

The use of a refractory metal subcoat to improve the adherence of the glass coating on stainless steel was not evaluated. Preliminary attempts to coat the Solaramic glass on tungsten were not successful, presumably because the characteristics of the base metal oxide were not adequate to form a proper bond.

V SUMMARY AND CONCLUSIONS

The permeability of hydrogen through the optimum materials evaluated in this program are summarized in Figure 54. This figure indicates that tungsten has the lowest permeability, however, it is much too brittle to be used for constructional purposes. In the metallic coating area, the tungsten-silicon and alumunim coatings on Haynes 25 base metal represent significant barriers to hydrogen. Metallic coatings, however, show some limitation for long-time use at temperatures in the 1600°F range due to gradual coating diffusion into the base metal. The permeability of the oxide coatings examined in this program are not included in Figure 54, since none showed suitable stability properties.

Glass coatings provide excellent barriers to hydrogen flow, however, they show sensitivity to failure by mechanical spalling. The Nucerite SC-30 glass had a low permeability to hydrogen when oriented so that the coating was in compression during the early exposure stages. The Solaramic glass coating had the best overall properties from a general consideration of long-time stability, mechanical strength, hydrogen barrier effectiveness, ease of application and insensitivity to orientation.

The actual problem of hydrogen loss in the Sunflower system can be divided into three areas: the boiler inner shell, the boiler outer shell, and the boiler tubes. The majority of hydrogen loss through decomposition of the lithium hydride will occur through the inner shell of the boiler since this is at the highest operating temperature (approximately 1600°F). On the basis of the laboratory specimen test results, the optimum system for the boiler component (both inner and outer shell) is a Solaramic-coated metal, either Haynes 25 or austenitic stainless steel. This coating applied to the space side of the boiler provides a minimum loss of hydrogen and has acceptable long-time stability to insure efficient operation over the anticipated 10,000-hour life.

In the case of the boiler tubes which are exposed to a mercury environment on the inside and lithium hydride on the outer diameter, the selection of the optimum materials system is not obvious. The decrease in the quantity of lithium hydride as a result of hydrogen escaping through the boiler tubes is not a serious problem since the tubes operate at approximately 1200°F. The important consideration is the effect on pump performance of the hydrogen collecting in the system. One approach to minimizing hydrogen flow to the pump is to coat the boiler tubes. Since the operating temperatures are relatively low, metallic coatings as well as glass may be acceptable. There is, however, a very real fabrication problem in placing such coatings on the inner diameter of long tube lengths. In addition, preliminary work (14) has indicated that coatings may not be satisfactory since extremely-small quantities of hydrogen in the pump section can cause malfunction and the hydrogen can only be limited by providing a "vent" to insure that even small quantities of the gas do not build-up. Columbium with its extremely high permeability appears to be an excellent "window", however, it must be heated to above 1000°F to insure that surface reactions do not produce a drastic decrease in permeability.

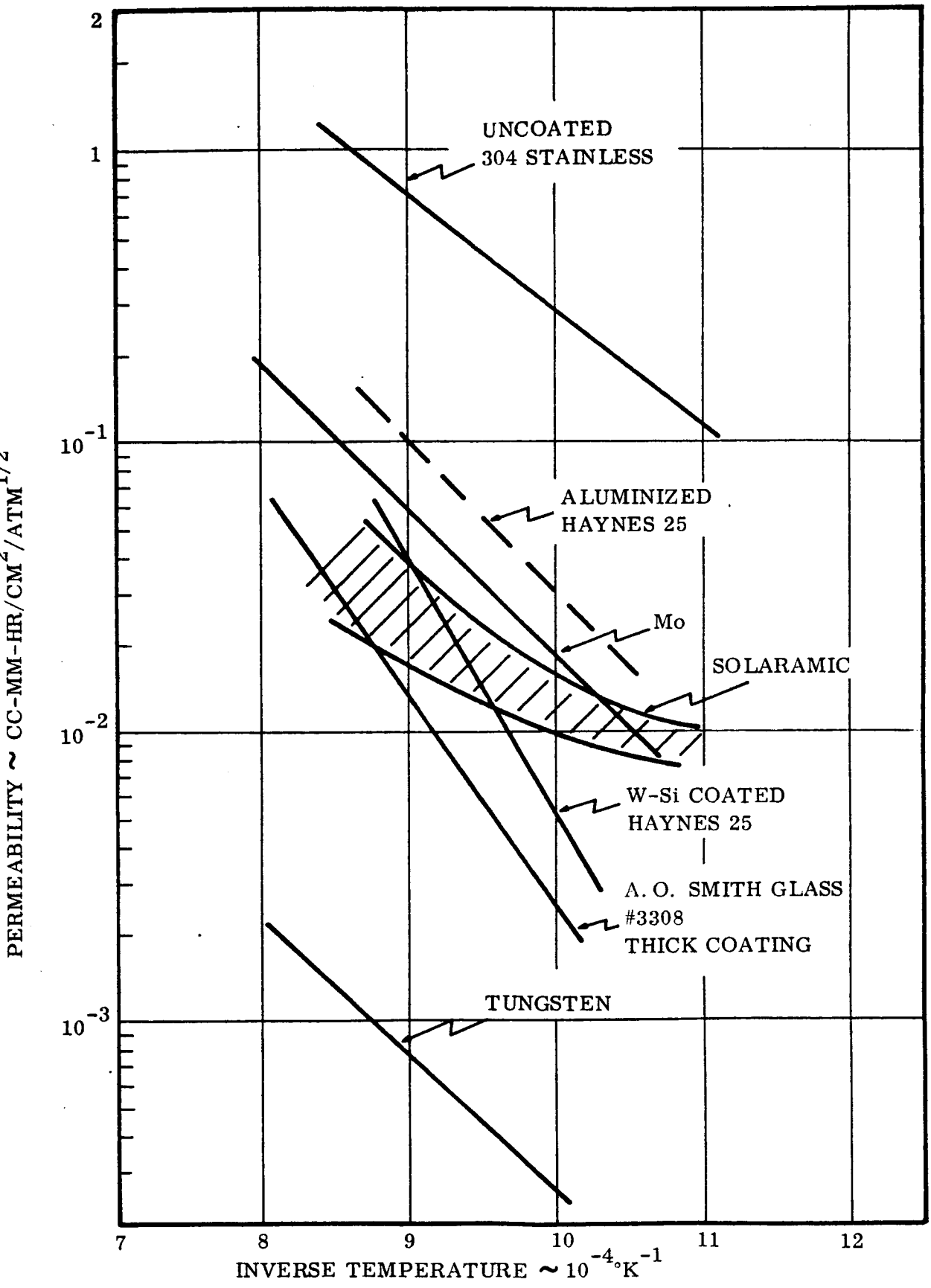

FIGURE 54

SUMMARY OF PERMEABILITY OF HYDROGEN THROUGH VARIOUS MATERIALS

VI BIBLIOGRAPHY

1. D. B. Cooper, E. A. Steigerwald and E. J. Vargo, "The Containment of Lithium Hydride for Space Power Generation", SAMPE, Philadelphia, Pa., (June 3, 1963).

2. S. Johnson, M. D. Barnes, and D. W. Vose, "Permeation of Hydrogen through Metals", 1st Metal Hydride Symposium, USAEC, Los Angeles, (January 30, 1958).

3. C. L. Huffine and J. M. Williams, "Hydrogen Permeation through Metals, Alloys, and Oxides at Elevated Temperatures," Corrosion, 16. 432t, (September, 1960).

4. S. Dushman, "Vacuum Technique," John Wiley and Sons Inc., New York, 608, (1949).

5. E. A. Steigerwald, "The Permeation of Hydrogen through Constructional Materials," TRW, ER-4776, (November 30, 1961).

6. R. M. Barrier, "Diffusion in and Through Solids," Cambridge, 145-238, (1951).

7. W. M. Albrecht, W. D. Goode, and M. W. Mallett, "Reactions in the Nb-H System", J1. Electrochem. Society, 981, (November, 1959).

8. D. W. Vose and S. Johnson, "The Permeation of Hydrogen through Columbium," Metal Hydrides Inc., Final Report Cont. No. AT (11-1) 229, (April 6, 1959).

9. P. S. Flint, "The Diffusion of Hydrogen through Materials of Construction," KAPL-659, (December 14, 1951).

10. A. Sawatzky and M. J. Rees, "The Permeability and Diffusion of Hydrogen in M-257 Aluminum Oxide Alloy." Atomic Energy of Canada Ltd., CRGM-995, Chalk River, Ontario, AECL-1252, (April, 1960).

11. P. Grieveson and C. B. Alcock, "The Thermodynamics of Metal Silicides and Metal Carbides," Special Ceramics, Edited by P. Popper, Academic Press Inc., New York, (1960).

12. F. W. Nelson, A. O. Smith Company, Private Communication.

13. D. W. Rudd, and J. B. Vetrano, "Permeability of Metals and Enameled Metals to Hydrogen," Atomics International Rep., No. NAA-SR 6109 (October 30, 1961).

14. Private Communications, E. J. Vargo and D. B. Cooper, Thompson Ramo Wooldridge Inc., (September, 1963).

APPENDIX I

Example Calculation of Permeability Constant of Hydrogen Through a Diaphragm Specimen (303 Stainless Steel)

The rate of hydrogen flow follows the relationship:

$$Q = \frac{KA}{d} \left(\sqrt{P_1} - \sqrt{P_o} \right)$$

where: Q = hydrogen flux in cc/hr (S. T. P.)

K = permeability constant

A = area of diaphragm

d = thickness of diaphragm

P_1 and P_o = inlet and outlet pressure respectively.

From Figure IA, the steady state rate of pressure increase at 1558°F is 0.126 mm/min. The volume of the collecting system was 304.2 cc and the temperature of the collecting chamber was 300°K, therefore:

$$Q = 0.126 \text{ mm/min.} \times \frac{304.2 \text{ cc}}{760 \text{ mm}} \times \frac{60 \text{ min.}}{\text{Hr.}} \times \frac{273°\text{K}}{300°\text{K}} = 2.75 \text{ cc (S. T. P.)/hr.}$$

$$K = \frac{Qd}{A \left(\sqrt{P_1} - \sqrt{P_o} \right)}$$

$d = 127$ mm

$A = 5.05 \text{ cm}^2$

$P_o = 0$

$P_1 = 1.01$ atm

$$K = 0.692 \text{ cc } \frac{\text{(S. T. P.)-mm}}{\text{cm}^2 - \text{hr} - \text{atm}^{1/2}}$$

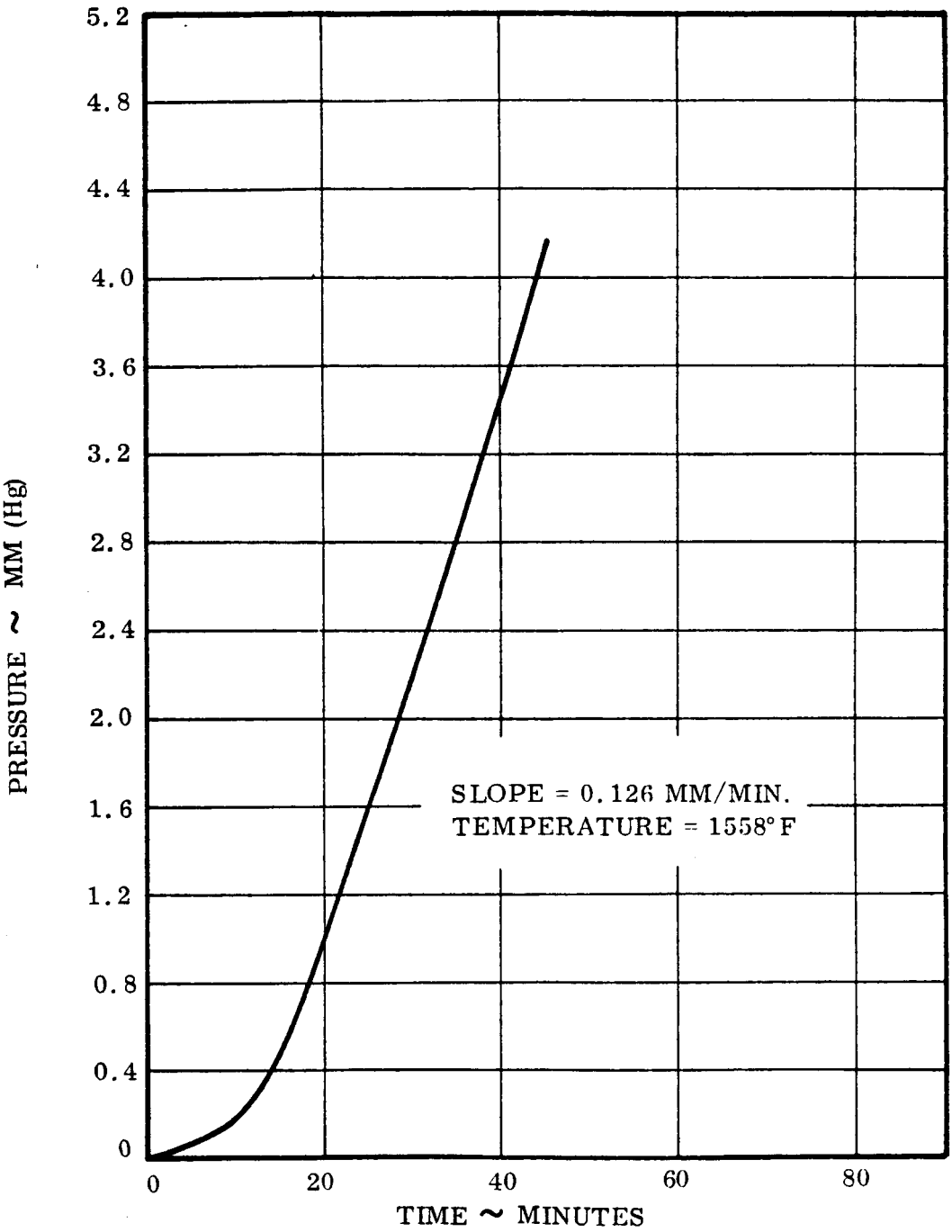

FIGURE IA

TYPICAL PRESSURE-TIME CURVE FOR HYDROGEN
FLOW THROUGH 303 STAINLESS STEEL DIAPHRAGM

APPENDIX II

Example Calculation of Permeability Constant of Hydrogen Through Tube Specimen (Tungsten)

For a tube specimen the hydrogen flux (ΔQ_i) that passes through a small tube element (Δl_i) can be expressed as:

$$\Delta Q_i = \frac{K\, 2\pi\, (\Delta l_i)}{\ln (b/a)} \left(\sqrt{P_1} - \sqrt{P_o} \right) \qquad (1)$$

where: ΔQ_i is the hydrogen flow per unit time through an element of tube length Δl_i.

K is the permeability constant,

b is the outside diameter of the tube,

a is the inside diameter of the tube, and

P_1 and P_o are the pressures of hydrogen on the inlet and outlet side, respectively.

In the current experiments $P_o = 0$.

The problem in using a refractory metal tube specimen is that a temperature gradient exists along a certain portion of the tube (See Figure IIA). The permeability K is dependent on temperature according to the equation:

$$K = K_o\, e^{-A/T} \qquad (2)$$

where: T is the absolute temperature, and

K_o and A are material constants.

Substituting equation 1 into equation 2 yields:

$$\Delta Q_i = \frac{2\pi\, K_o\, e^{-A/T_i}\, (\Delta l_i)}{\ln (b/a)} \left(\sqrt{P_i} \right) \qquad (3)$$

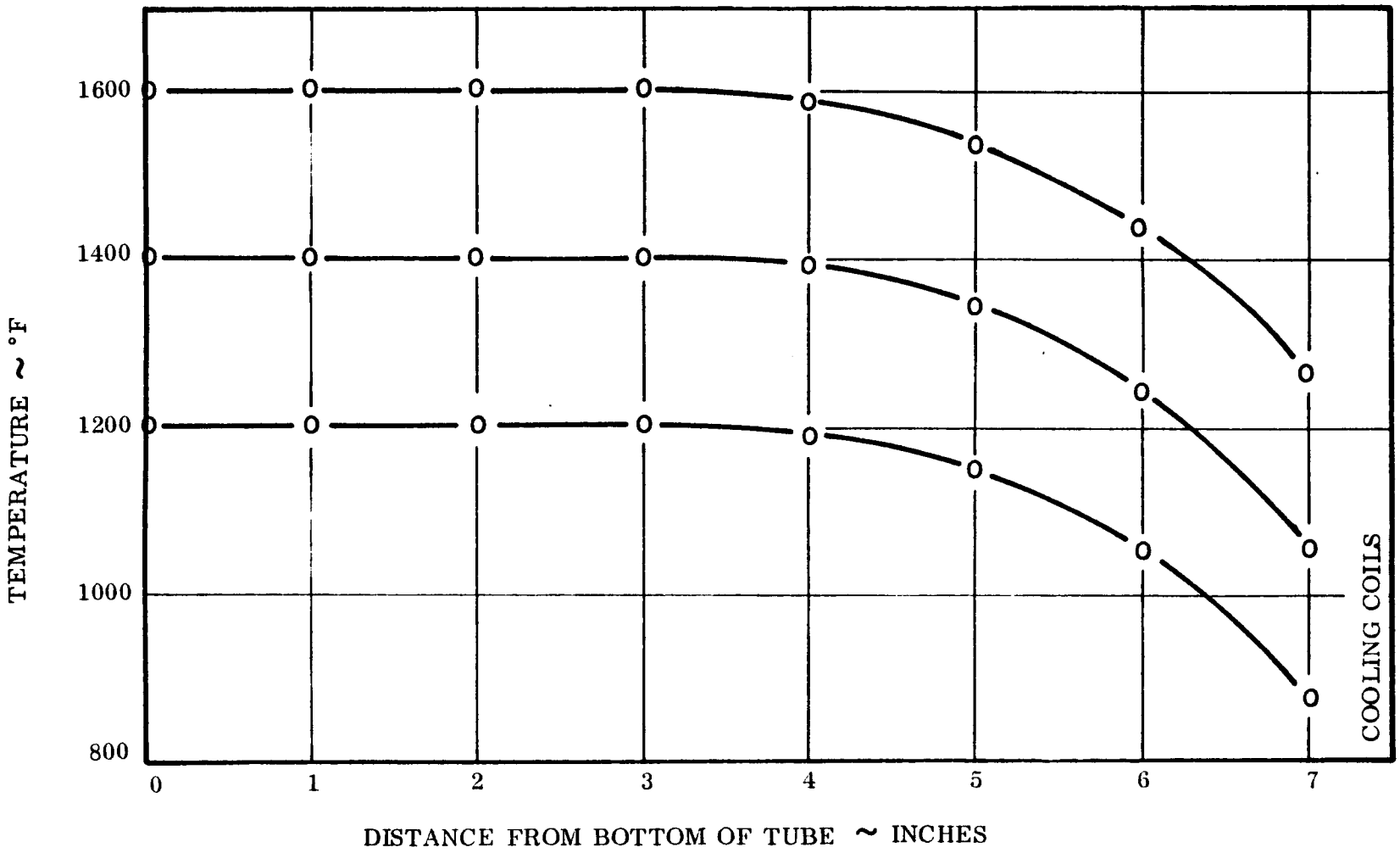

FIGURE IIA

TEMPERATURE DISTRIBUTION IN TUBE SPECIMENS

The total hydrogen flux (Q) through the tube can be expressed as the summation of the contribution of each element Δl_i. Expressed in integral form:

$$Q = \frac{2\pi K_o \sqrt{P_1}}{\ln (b/a)} \int_o^L e^{-A/T_i} \, dl_i \qquad (4)$$

The Integral can be evaluated graphically by using the temperature distribution plots shown in Figure IIA and obtaining the conatant A in equation 4 from a plot of the experimentally measured total hydrogen flux through the tube as a function of the reciprocal absolute temperature.

The total hydrogen flux can also be expressed as:

$$Q = \frac{K\, 2\pi}{\ln (b/a)} \, l_{eff} \, \sqrt{P_1} \qquad (5)$$

where: l_{eff} is a fictitious length which converts the effective temperature distribution from that shown at the top of Figure IIB to that shown in the bottom of the same figure.

K is the permeability constant for the temperature shown in the bottom of Figure IIB.

Equating equations (4) and (5):

$$l_{eff} = \frac{\int_o^L e^{-A/T_i} \, dl_i}{e^{-A/T_a}} \qquad (6)$$

For any given temperature, l_{eff} can be computed from equation (6) and then used in equation (5) to determine the permeability constant.

Representative calculations for the tungsten tube at a nominal temperature (Ta of 1600°F) are summarized in Table IIA. From the temperature distribution shown in Figure IIA, the integral equals 7.51×10^{-4} cm and $l_{eff} = 15.0$ cm.

Rearranging equation 5 and using the dimensions of the tungsten tube:

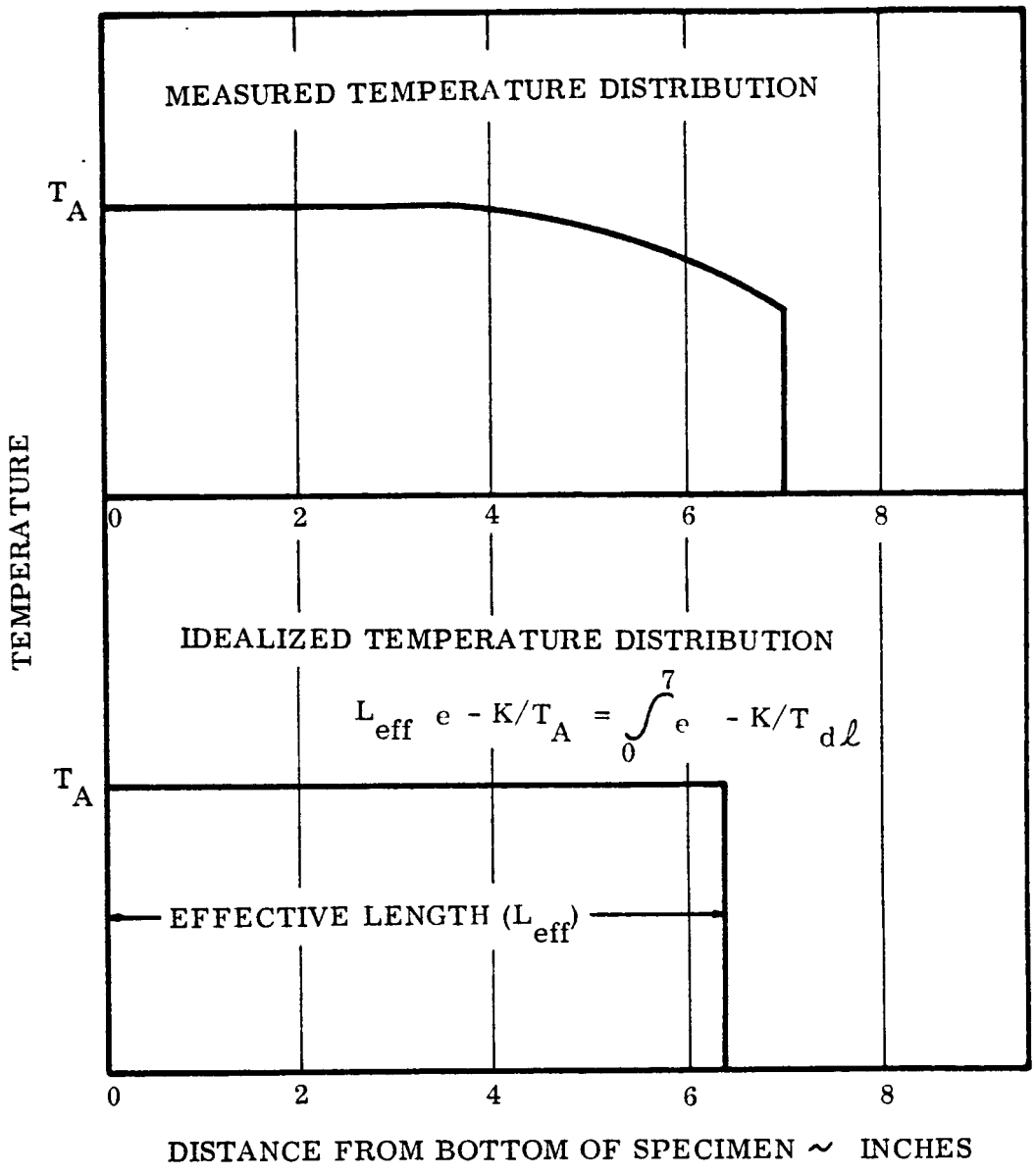

FIGURE II B

MEASURED AND IDEALIZED TEMPERATURE DISTRIBUTIONS
IN REFRACTORY METAL TUBE SPECIMENS

$$K \text{ (for W at } 1600°F) = \frac{Q \text{ meas}}{(1_{eff})\ P_1^2} \ln (b/a)$$

$$K_{1600} = \frac{0.258 \times 10^{-2} \ln \left(\frac{.368}{.250}\right)}{15.0 \quad .99 \quad 2} = 1.04 \times 10^{-4} \frac{\text{cc (S. T. P.)}}{\text{cm-hr-atm}^{1.2}}$$

$$K_{1600} = 1.04 \times 10^{-3} \frac{\text{cc(S. T. P.) - mm}}{\text{cm}^2\text{-hr-atm}^{1/2}}$$

TABLE IIA

Method Employed to Calculate the Permeability Constant of Refractory Metals from Tube Specimens

Distance From Bottom of Tube (Inches)	(cm)	T(°F)	T(°K)	e^{-K/T^*}
0	0	1590	1137	5.0×10^{-5}
1	2.54	1590	1137	5.0×10^{-5}
2	5.08	1590	1137	5.0×10^{-5}
3	7.62	1590	1137	5.0×10^{-5}
4	10.2	1575	1129	4.9×10^{-5}
5	12.7	1530	1104	4.2×10^{-5}
6	15.2	1435	1052	2.5×10^{-5}
7	17.8	1250	948	7.4×10^{-6}

*K = 11,250

$$\text{area} = \int_0^7 e^{-K/T}\, dl = 7.51 \times 10^{-4} \text{ cm}$$

$$e^{-K/T_A} \, l_{eff} = 7.51 \times 10^{-4}; \quad T_A = 1137°K$$

$$l_{eff} = \frac{7.51 \times 10^{-4}}{5.0 \times 10^{-5}} = 15.0 \text{ cm}$$

APPENDIX III

Summary of Coating Techniques

Coating	Base Metal	Technique of Application
Ag-plate	304 SS	Silver cyanide - potassium cyanide bath, current density 6 amps/ft^2. Plate applied after appropriate cleaning and striking operations, plating time = 3 hours, plate thickness = 0.003".
Cu-plate	304 SS	Copper cyanide, sodium cyanide, sodium hydroxide bath, current density 20 amps/ft^2. Plate applied after appropriate cleaning and striking operations, plating time = 1-1/4 hours, plate thickness = 0.003".
Chromium	303 SS	Proprietary coating process by Chromalloy Corp. Pack-type process.
Chromium	HS 25	Vacuum vapor pack deposition Chromium sponge, KF activator, 2200°F, for 16 hours.
Aluminum	304 SS and HS 25	Proprietary coating process by Chromalloy Corp. Pack-type process.
Aluminum	HS 25	Proprietary process by Alon Corp.
Aluminum	304 SS and HS 25	Spray aluminum slurry on diaphragm, flow aluminum for 1/2 hour at 1370°F in argon atmosphere, diffusion anneal for 1 hour at 1700°F in an argon atmosphere.
Tungsten	304	Flash nickel plated, approximately 0.0005" thick. Vapor plate by Alloyd Corp., plate approximately 0.006" thick, plated on one side, diffusion annealed in vacuum for 4 hours at 1800°F.
Tungsten	HS 25	Vapor plated by Alloyd Corp., plate approx. 0.006" thick, plated on one side, diffusion annealed in vacuum for 3-1/2 hours at 2030°F.

APPENDIX III (continued)

Summary of Coating Techniques

Coating	Base Metal	Technique of Application
Tungsten	HS 25	Flash nickel plate, vapor deposition of tungsten hexachloride at 1750°F for seven minutes, plate approximately 0.006" per side, plated on both sides.
Silicon	HS 25	Silicon sponge plus KS activator, applied at 1650°F for 1-3/4 hours, mechanical vacuum, vapor pack process.
Silicon	304	Silicon sponge plus KF activator, applied at 1650°F for 1-3/4 hours, mechanical vacuum, vapor pack process.
Tungsten-Silicon	HS 25	Tungsten powder plus KF activator, applied at approximately 1970°F for 5-1/2 hours; tungsten and silicon sponge plus KF activator, applied at approximately 1700°F for 5-1/2 hours. Both steps performed in mechanical vacuum vapor pack process.
Molybdenum-Silicon	HS 25	Molybdenum powder (25g) plus KF activator (2g) applied at 1900°F for 20 hours; molybdenum (12g), silicon (12g) and KF activator (2g) applied at 1620°F for 6 hours. Both steps performed in mechanical vacuum, vapor pack process.
Zirconium-Silicon	HS 25	Zirconium sponge (20g) plus KF activator (2g) applied at 1600°F for 5 hours; silicon sponge (20g) plus KF activator (2g) applied at 1600°F for 5 hours. Both steps performed in mechanical vacuum, vapor pack process.
Vanadium-Silicon	HS 25	Vanadium sponge (20g) plus KF activator (2g) applied at 1800°F for 5 hours; second step same as for zirconium silicon.
Solaramic 5210-2C	304 or HS 25	Anneal in air at 1200°F for 2 minutes, sandblast spray 5210-2C coating on designated area, fire at 1750°F in air for 20 minutes.

A. O. Smith, Bettinger, Nucerite, and Engineered Ceramic Coatings applied by vendors with proprietary processes.